IMPERIAL COLLEGE OF SCIENCE AND TECHNOLOGY

UNIVERSITY OF LONDON

"Laminar boundary layers with non-uniform fluid properties."

Vol. I

by

Woon Mo Pun, M.Sc., G.I.Mech.E.

A thesis submitted for the degree of Doctor of Philosophy of the University of London in the Faculty of Engineering.

Department of Mechanical Engineering,
Imperial College,
London, S.W.7.

ABSTRACT

The present work is concerned with laminar boundary layers when the fluid-properties are non-uniform. The non-uniformity of the properties may be caused either by large temperature differences and/or by variations of composition in the boundary layer.

The differential equations governing the preblem were briefly developed for the most general case, special emphasis being laid on the hitherto much neglected coupling effects of the energy and mass transport phenomena. The exact solutions to these equations available in the literature were collected and systematically tabulated. Based on these solutions the influences of the various parameters on the heat and mass transfer characteristics were discussed. A new procedure has been developed to correlate these solutions; the method does not require any details of property-variations and is simpler to use than the existing methods available; it is sufficiently accurate for engineering applications. Functions needed for the use of the new procedure are included.

Experiments were carried out at an axi-symmetric stagnation-flow region formed by an air jet impinging on a flat plate; and heat-transfer measurements made on a solid surface as well as on a porous plate with injection through the pores of the gases: hydrogen, helium, air, nitrogen, carbon-dioxide and "Arcton-13" ($CClF_3$). The results confirm the existence of large differences (up to $+102^{\circ}F$) between

the adiabatic-surface temperature and the main-stream stagnation temperature when the lighter gases of hydrogen and helium are injected into an air stream, even in the absence of any appreciable aerodynamic heating; much smaller temperature differences of the opposite sign (up to -20.5°F) were observed for the injection of carbon-dioxide and "Arcton-13". These temperature differences can be accounted for by the effects of thermal diffusion and of the coupling between diffusion and heat conduction.

All the results agree satisfactorily with the theoretical predictions; they also confirm the reliability of the correlation developed in the present work.

ACKNOWLEDGEMENT

The work reported here has been made possible by the financial support of the Department of Scientific and Industrial Research and the University Grants Committee.

The author wishes to thank his supervisor, Prof. D. B. Spalding, for his inspiration and patient guidance.

He also wishes to express his gratitude to the various members of the Technical Staff for their help in the manufacturing of the test apparatus.

CONTENTS

LIST OF FIGURES

List of tables

CHAPTER 1 INTRODUCTION

1.1 The problem considered and its practical relevance.

The thermodynamic properties and transport coefficients of gases are generally functions of the pressure, temperature and, in the case of mixtures, also composition. In boundary-layer flows the pressure variation across the boundary layer is very small, and the dependence of fluid properties on pressure can be ignored. However, in many instances the temperature and/or composition variations are quite large, and it is necessary to take into account the resulting variations in fluid properties.

We shall here restrict our attention to laminar flows. This type of flows occurs in many practical situations; and, in many other cases, is the desired alternative to turbulent flows, which give rise to higher drag as well as higher heat-transfer rates.

In the front portion of an aerofoil wing the flow is usually laminar; and if the aircraft is moving at high speeds the kinetic heating effect will cause a large temperature variation across the boundary layer. At the blunt nose of a high speed object the flow is again laminar. The nose may be fabricated from a porous material and transpiration-cooled by the injection of a light gas through the pores; here in addition to the temperature variation there is also a concentration gradient across the boundary layer, causing non-uniformity of fluid properties. Similar processes may also occur in the transpiration-cooling of gas turbine blades or combustion-chamber walls.

Although the process of mass injection is known to be destabilising, there are indications that the stabilising effect of cooling, enchanced by the much lower surface temperature attained by transpiration-cooling, can offset the initial instability associated with mass injection and thereby provides a higher transition Reynolds number than that obtained without injection [S31, S28, G36].

1.2 Outline of present state of knowledge

Many theoretical analyses to the problem have been made in the past thirty years; during the same period, relatively little experimental work has been done. These will be reviewed in some detail in sections 3.1 and 6.1.3 respectively. Although many theoretical solutions are available, the comparatively large number of the parameters prohibits an adequate coverage of all the ranges of interest to the designer-engineers. For most applications, a high degree of accuracy can be sacrificed for a simpler method of calculations. To answer the designers' need, engineering correlation methods have been devised. Of the methods available, Eckert's reference enthalpy method [G8] is the most widely used one for zero-mass-transfer; for the case with gas injections there are the methods of Cross-Hartnett-Masson-Gazley [G14] and Knuth [G19], both make use of a reference state. All these methods suffer from the drawback that details of property-variations are needed for their use; furthermore, they tend to give erroneous prediction for skin friction for flows with large pressure gradients.

Until recently the reciprocal phenomena of thermal diffusion and diffusional conduction or diffusion-thermo[#] in binary boundary layers have been ignored, apparently because of their supposedly negligible effects and mainly perhaps of the insufficient knowledge of the thermal diffusion factor, which governs these phenomena. The first of these, thermal diffusion- sometimes known as the Soret effect, is the tendency of a heat-flux through a gaseous mixture to cause proportionate gradients in the mass fractions of the mixture components; its existence was predicted theoretically by Enskog and Chapman, working independently, in the period 1911 - 1917. The second phenomenon, the diffusional conduction is the tendency of the diffusion of a particular component through a gas mixture to cause a proportionate temperature gradient; it was discovered experimentally by Dufour in 1873, and is thus somtimes known as the Dufour effect.

The realization of the practical importance of these coupling effects was prompted by the persistent discrepancies observed between the measured and the predicted adiabatic-surface temperatures when the surface was transpiration-cooled by the injection of helium into a high-speed air stream. Recent analyses indicate that even in the

---

Although the term "diffusion-thermo" has been used frequently in the literature, it does not readily convey the meaning it represents. Here we shall follow Prof. Spalding's suggestion [G37] and adopt the term "diffusional conduction" , which corresponds with "thermal diffusion" describing the opposite phenomenon. Sometimes the abbreviations are used: TD ≡ thermal diffusion; DT ≡ diffusional conduction .

absence of any aerodynamic heating, the coupling effects can cause an appreciable difference between the adiabatic-surface temperature and the main-stream stagnation temperature. The sign of this temperature difference can be either positive or negative, depending on the sign of the thermal diffusion factor α_T for the mixture concerned. Generally, the injection of a lighter gas, e.g. hydrogen or helium, into an air stream (α_T negative) produces an adiabatic-surface temperature higher than the main-stream stagnation temperature: the injection of a heavier gas, e.g. carbon-dioxide, into the air stream (α_T positive) tends to produce an adiabatic-surface temperature lower than the main-stream stagnation temperature. Experimental measurements were usually made at high speeds, consequently, the effect of aerodynamic heating could not be separated from these coupling effects. It is thus desirable to have some low-speed experimental data, which can bring the effects of thermal diffusion and diffusional conduction more into focus.

1.3 Purpose and scope of present work

It is one of the main aims of the present work to develop a simpler method for the correlation of the theoretical solutions than the ones mentioned above. The method will be checked against the theoretical solutions collected from the literature and will be seen to be of sufficient accuracy for engineering applications. The method is developed for two-dimensional flows with and without a pressure gradient. The flows for non-zero pressure gradients covered correspond

to the axi-symmetric and the two-dimensional stagnation flows.

A series of experiments at an axi-symmetric stagnation-flow region formed by a low-speed air jet impinging on a porous plate, through which were injected a range of gases, both lighter and heavier than air, provide data for checking the theoretical predictions. The absence of any appreciable aerodynamic-heating effect should allow these data to provide a clear demonstration of the coupling effects of thermal diffusion and diffusional conduction. The design of the apparatus allows the use of hydrogen as one of the injectants, providing the first results using this gas in forced-convection experiments.

Chapter 2 below contains a very brief development, with some discussion, of the general laminar boundary layer equations, emphasis being laid on the coupling effects between energy and mass transfer. In Chapter 3 the exact theoretical solutions to the preblem are surveyed and systematically tabulated; based on these, the influences of the various parameters on the characteristics of the solutions are discussed. Chapter 4 is concerned with the correlation methods: the methods available are first introduced and the development of the new procedure occupies the rest of the chapter. A summary of the conclusions about the theoretical solutions appear in Chapter 5. Chapter 6 is entirely concerned with the experimental part of the present work, in which is contained a survey of similar experiments, as well as details of the apparatus and various tests conducted; results and discussions are contained in section 6.4; the conclusions derived from these results appear in Chapter 7. In Chapter 8 is suggested a future extension of the present studies.

To facilitate reference, the thesis has been divided into two volumes. The main text is in this volume, Vol. I, and all the figures, tables, references, appendices and the section on nomenclature are contained in Vol. II.

CHAPTER 2 GOVERNING EQUATIONS

2.1 Introduction

In this chapter the governing equations to the problem under consideration are presented. While the main object is to provide equations as a basis for later discussions, it is also intended to introduce the equations in such a way that some insight to the problem may be gained.

Although the equations have been known for a long time now, in the literature invariably only particular forms of the equations, simplified under various assumptions, are given. The laminar boundary layer equations which take into account fully the effects of mass transfer, thermal diffusion, diffusional conduction, pressure gradient, kinetic heating and non-uniform fluid properties, have seldom been discussed in a single work. Hence, without extensive reading, one is often at a loss to grasp the various aspects of the problem. In this chapter, the laminar boundary-layer equations are introduced; emphasis is laid on highlighting the various stages through which the final equations are obtained, rather than on a thorough mathematicl derivation.

From the basic conservation equations for a continuum fluid, the boundary layer equations for both two-dimensional and axi-symmetric flows are obtained. In the most general case, the equations take into account the effects of mass transfer, thermal diffusion, diffusional conduction, pressure gradient, kinetic heating and non-uniform fluid properties. From these equations, equations applicable for a few simpler particular cases are deduced.

Finally, the more important class of the so-called "similar" solutions for the boundary layer equations is discussed.

2.2 Basic conservation equations

Some defintion. Before writing down the fundamental conservation equations, we introduce the following definitions in connection with the process of mass transfer. The formulation is essentially that of Spalding [G38] .

The partial density, ρ_i, is defined as the mass of substance i to be found instantaneously in a small volume surrounding the point in question divided by the magnitude of the volume. It is related to the local mixture density ρ, defined as the total mass of material per unit volume locally, by:

$$\rho = \sum_i \rho_i \tag{2.2-1}$$

The mass fraction m_i is simply defined as:

$$m_i \equiv \rho_i / \rho \quad . \tag{2.2-2}$$

This definition implies that

$$\sum_i m_i = 1 \quad . \tag{2.2-3}$$

Across any arbitrarily orientated surface in the medium, there is a net transfer of mass. And in the vicinity of any point a maximum mass flux exists for a particular orientation of a surface element. The magnitude and the associated direction of the normal of the surface of this maximum mass flux is represented by the "total mass

flux" $\underline{G}$, which is necessarily a vectorial quantity.

With $\underline{G}$ thus defined, a mean mixture velocity $\underline{v}$ can then be defined by:

$$\underline{v} \equiv \underline{G} / \rho \quad . \tag{2.2-4}$$

For a substance i we can similarly define a "total mass flux of i", $\underline{G}_{t,i}$. $\underline{G}$ and $\underline{G}_{t,i}$ are connected by:

$$\underline{G} = \sum_i \underline{G}_{t,i} \tag{2.2-5}$$

Similarly, a mean velocity for species i, $\underline{v}_i$, may be defined as:

$$\underline{v}_i \equiv \underline{G}_{t,i} / \rho_i \quad . \tag{2.2-6}$$

The total mass flux of i is often split into two parts, one, the convective mass flux, $\underline{G}_{c,i}$, is defined by:

$$\begin{aligned} \underline{G}_{c,i} &\equiv m_i \underline{G} \\ &= \rho_i \underline{v} \quad , \end{aligned} \tag{2.2-7}$$

and the other, the diffusive mass flux, $\underline{G}_{d,i}$, is the difference between $\underline{G}_{t,i}$ and $\underline{G}_{c,i}$, that is:

$$\begin{aligned} \underline{G}_{d,i} &\equiv \underline{G}_{t,i} - \underline{G}_{c,i} \\ &= \rho_i (\underline{v}_i - \underline{v}) \end{aligned} \tag{2.2-8}$$

Also:

$$\begin{aligned} \sum_k \underline{G}_{d,k} &= \sum_k \underline{G}_{t,k} - \sum_k \underline{G}_{c,k} \\ &= \underline{G} - \underline{G} = 0. \end{aligned} \tag{2.2-9}$$

Conservation equations. For a steady, non-reacting, binary fluid system of i and j components when the effects of external forces such as gravitational, magnetic etc. are excluded, application of the physical laws (conservation of mass, momentum and energy) yield the following equations, which may be readily found in standard text books or published papers, for example, Bird, Stewart and Lightfoot [G2], Hirschfelder, Bird and Curtiss [G17] , Aris [G1] , Merk [G22] , Hall [G16] . For compactness the equations are given in vectorial form#.

Conservation of mass for the mixture

$$\nabla \cdot \underline{G} = 0 \qquad (2.2\text{-}10)$$

Conservation of mass for species i

$$\underline{G} \cdot \nabla m_i + \nabla \cdot \underline{G}_{d,i} = 0 \qquad (2.2\text{-}11)$$

Conservation of momentum

$$\underline{G} \cdot \nabla \underline{v} = -\nabla p + \nabla \cdot \underline{\underline{\tau}} \qquad (2.2\text{-}12)$$

Conservation of energy

$$\underline{G} \cdot \nabla h + \nabla \cdot \underline{Q} = \underline{v} \cdot \nabla p + \underline{\underline{\tau}} : \nabla \underline{v} \qquad (2.2\text{-}13)$$

Vectorial quantities are singly underlined and tensorial quantities doubly underlined. The "del" operator, ∇ , is used, with:

$\nabla \cdot$vector $\equiv$ div ; ∇scalar $\equiv$ grad ; ∇vector = a tensor.

A "double dot product" of two tensors can be expressed as:

$$\underline{\underline{\tau}} : \nabla \underline{v} = \nabla \cdot (\underline{\underline{\tau}} \cdot \underline{v}) - \underline{v} \cdot (\nabla \cdot \underline{\underline{\tau}}) \ .$$

The shear stress tensor $\underline{\underline{\tau}}$ is given by:

$$\underline{\underline{\tau}} = (K - \tfrac{2}{3}\mu)\,\underline{\underline{U}}\,\nabla\cdot\underline{v} + \mu\left[\nabla\underline{v} + (\nabla\underline{v})^{+}\right] \qquad (2.2\text{-}14)$$

where $\underline{\underline{U}}$ is a unit tensor of the second order; $(\nabla\underline{v})^{+}$ is the transpose of the dyadic product $\nabla\underline{v}$. It should be noted that the sign of the shear stress tensor $\underline{\underline{\tau}}$ is so chosen that the right hand side of equation (2.2-12) represents the net force acting on the fluid element.

In the energy equation (2.2-13), $\underline{Q}$ is the total energy-flux vector relative to the mean velocity of the fluid mixture, and may be written as the sum of two terms:

$$\underline{Q} \equiv \underline{q} + \sum_k h_k \underline{G}_{d,k} \quad , \qquad k = 1,2 \qquad (2.2\text{-}15)$$

where $\underline{q}$ is sometimes called the "reduced" energy flux; and $\sum_k h_k \underline{G}_{d,k}$ is of course the energy flux caused by the interdiffusion of the species.

Since $$\nabla h_k = c_{p,k}\nabla T$$

and $$\nabla h = \sum_k m_k \nabla h_k + \sum_k h_k \nabla m_k \quad ,$$

the use of the mass conservation equation (2.2-11) gives us the following identity:

$$\underline{G}\cdot\nabla h + \nabla\cdot\left(\sum_k h_k \underline{G}_{d,k}\right) = c_p\underline{G}\cdot\nabla T + \sum_k c_{p,k}\,\underline{G}_{d,k}\cdot\nabla T \quad .$$

Hence, in terms of $\underline{q}$ and T, the energy equation may be written as:

$$\boxed{c_p\underline{G}\cdot\nabla T + \sum_k c_{p,k}\,\underline{G}_{d,k}\cdot\nabla T + \nabla\cdot\underline{q} = \underline{v}\cdot\nabla p + \underline{\underline{\tau}} : \nabla\underline{v}} \qquad (2.2\text{-}13a)$$

2.3 Flux laws

Although the basic conservation equations have been quoted for two-component systems, they can be readily adapted to multi-component systems by extending all the summations to n components. The main difference in the flow equations between a two-component system and a multi-component system lies in the expressions for the fluxes $\underline{G}_{d,i}$ and $\underline{q}$. While it is possible to deduce $\underline{G}_{d,i}$ and $\underline{q}$ for two-component system from the corresponding expressions for multi-component systems, we shall introduce the binary expressions directly. In this way, much simplification in presentation can be achieved.

According to kinetic theory, Chapman and Cowling [G4] , the energy flux $\underline{q}$ for a binary mixture of i and j components is given by:

$$\underline{q} = -k \nabla T + \frac{\rho \mathcal{R} T k_T}{M} (\underline{v}_i - \underline{v}_j) \qquad (2.3\text{-}1)$$

where k_T is the thermal diffusion ratio; and the diffusion velocity $(\underline{v}_i - \underline{v}_j)$ is given by:

$$\underline{v}_i - \underline{v}_j = -D_{ij}\left[\frac{1}{m_j}\nabla \ln m_i + \frac{M_j - M_i}{M}\nabla \ln p + \frac{M_i M_j k_T}{m_i m_j M^2}\nabla \ln T\right] \qquad (2.3\text{-}2)$$

For the binary mixture, we have:

$$\sum_k m_k = m_i + m_j = 1 \quad ; \qquad (2.3\text{-}3)$$

and from equations (2.2-8) and (2.2-9) we have:

$$\sum_k \underline{G}_{d,k} = \rho\left[m_i(\underline{v}_i - \underline{v}) + m_j(\underline{v}_j - \underline{v})\right] = 0. \qquad (2.3\text{-}4)$$

Now, $\underline{G}_{d,i} = \rho m_i (\underline{v}_i - \underline{v})$.

Thus, making use of euqations (2.3-3) and (2.3-4), we can write:

$$\underline{G}_{d,i} = \rho m_i \left[(m_i + m_j)(\underline{v}_i - \underline{v}) - m_i(\underline{v}_i - \underline{v}) - m_j(\underline{v}_j - \underline{v}) \right] \quad ;$$

thence we obtain:

$$\underline{G}_{d,i} = \rho m_i m_j (\underline{v}_i - \underline{v}_j) \qquad (2.3\text{-}5)$$

Combination of equations (2.3-2) and (2.3-5) then gives the following expression for the diffusive mass flux for the i species:

$$\boxed{\underline{G}_{d,i} = -\Gamma_i \left[\nabla m_i + \frac{m_i m_j (M_j - M_i)}{M} \nabla \ln p + \frac{M_i M_j k_T}{M^2} \nabla \ln T \right]} \qquad (2.3\text{-}6)$$

where Γ_i is the "exchange coefficient", $\equiv \rho D_{ij}$; and equation (2.3-1) may be written as:

$$\boxed{\underline{q} = -k \nabla T + \frac{\mathcal{R} k_T T}{M m_i m_j} \underline{G}_{d,i}} \qquad (2.3\text{-}7)$$

Equation (2.3-6) shows that the diffusive mass flux is made up of three contributions. The first one is associated with a concentration gradient and is known as "mass diffusion", or sometimes as "ordinary diffusion"; this is the term described by Fick's law. The second contribution is caused by a pressure gradient and is accordingly known as "pressure diffusion". The third contribution arises from a temperature gradient and is the "thermal diffusion", also known as the Soret effect.

The expression for the energy flux $\underline{q}$, equation (2.3-7), shows

that besides the familiar Fourier conduction term there is a term directly proportional to the diffusion mass-flux $\underline{G}_{d,i}$. This transport of energy through diffusion is termed the diffusional conduction or diffusion-thermo, it is also known as the Dufour effect.

As can be seen from equations (2.3-6) and (2.3-7), the phenomena of thermal diffusion and diffusional conduction are reciprocal effects; both are characterised by the same thermal diffusion ratio k_T[#]. In a constant pressure system, if two gases initially at the same temperature interdiffuse, then for a negative k_T, a positive $(\underline{v}_i - \underline{v}_j)$ is accompanied by a negative values of the concentration gradient ∇m_i, as can be seen from equation (2.3-2). Since initially the temperature is uniform, the diffusional conduction effect, equation (2.3-7), then produces a negative energy flux; this sets up a negative temperature gradient, as shown in the sketch. From equation (2.3-2) it is seen that due to this temperature gradient the reciprocal effect (thermal diffusion) tends to reduce the diffusion velocity and hence the diffusive mass-flux. The argument holds also for positive values of k_T. Thus we see that the direction of the temperature gradient is such that the thermal diffusion which results from it opposes the diffusion to which the gradient is due.

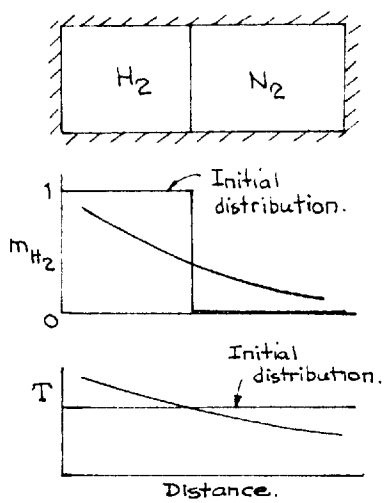

The sign of k_T (and hence α_T) deserves particular attention. For more detials., refer to section 2.7.3.

For example, if hydrogen diffuses into nitrogen (k_T negative) the temperature rises where hydrogen is in excess and falls where the nitrogen is in excess.

A more detailed account of the physical aspects of these phenomena may be found in the monograph by Grew and Ibbs [G15] .

2.4 Boundary layer equations for two-dimensional flows

This and the next two sections are devoted to the boundary layer equations, for two-dimensional as well as axi-symmetric flows, and the associated boundary conditions. For those who are not interested in the discussion of the equations, these may be skipped and turn their attention to p. 56 .

2.4.1 General case

The two-dimensional flow equations (Appendix 2.1), are seen to be quite complicated. However, if we assume that each of the various processes of mass transfer, momentum transfer and energy transfer takes place within a thin layer of thickness δ (the boundary layer), small compared with, for example, a characteristic dimension of the body L, some terms are seen to be much smaller than others and hence may be neglected.

By these order-of-magnitude considerations, it may also be seen that of the two components of the diffusive mass flux vector $\underline{G}_{d,i}$ only the y component, $(G_{d,i})_y$, is of significance; similarly for the energy flux vector $\underline{q}$, only q_y is of significance. As confusion is not likely to arise now, we shall drop the subscript y and write $G_{d,i}$ instead $(G_{d,i})_y$ and q instead of q_y.

The resulting simplified flow equations, the boundary-layer equations, can be written as follows:

Conservation of mass for the mixture

$$\frac{\partial(\rho u)}{\partial x} + \frac{\partial(\rho v)}{\partial y} = 0 \qquad (2.4.1\text{-}1)$$

Conservation of mass for species i

$$\rho u \frac{\partial m_i}{\partial x} + \rho v \frac{\partial m_i}{\partial y} = -\frac{\partial}{\partial y} G_{d,i} \qquad (2.4.1\text{-}2)$$

Conservation of momentum

x - component

$$\rho u \frac{\partial u}{\partial x} + \rho v \frac{\partial u}{\partial y} = -\frac{\partial p}{\partial x} + \frac{\partial}{\partial y}\left(\mu \frac{\partial u}{\partial y}\right) \qquad (2.4.1\text{-}3)$$

y - component

$$\frac{\partial p}{\partial y} = 0 \qquad (2.4.1\text{-}4)$$

Conservation of energy

$$\rho u c_p \frac{\partial T}{\partial x} + \rho v c_p \frac{\partial T}{\partial y} + (c_{p,i} - c_{p,j}) G_{d,i} \frac{\partial T}{\partial y} = u \frac{\partial p}{\partial x} - \frac{\partial q}{\partial y} + \mu \left(\frac{\partial u}{\partial y}\right)^2 \qquad (2.4.1\text{-}5)$$

Dropping the subscript y, we have from equation (A2.1 -9):

$$q = -k \frac{\partial T}{\partial y} + \frac{\mathcal{R} T k_T}{M m_i m_j} \cdot G_{d,i} \qquad (2.4.1\text{-}6)$$

As a consequence of equation (2.4.1-4), the pressure diffusion contribution to $(G_{d,i})_y$ vanishes, hence equation (A2.1-4) becomes

(with subscript y dropped):

$$G_{d,i} = -\Gamma_i \left[\frac{\partial m_i}{\partial y} + \frac{M_i M_j k_T}{M^2 T} \frac{\partial T}{\partial y} \right] . \qquad (2.4.1\text{-}7)$$

The boundary layer equations (2.4.1-1) to (2.4.1-5) together with the equations of state for the fluids constitute the set of equations to be solved. These equations are valid for the general case when the effects of mass transfer, thermal diffusion, diffusional conduction, kinetic heating, variable fluid-properties and pressure gradient are included.

Unless specifically stated we shall assume that the partial pressure of each component in the mixture is given by the following perfect gas relationship:

$$p_i = \frac{\mathcal{R}}{M_i} \rho_i T \qquad (2.4.1\text{-}8)$$

Consequently, the total pressure is similarly related to the mixture properties:

$$p = \frac{\mathcal{R}}{M} \rho T \quad . \qquad (2.4.1\text{-}9)$$

These are then the appropriate state equations.

2.4.2 Non-zero mass transfer, low-speed flow with constant fluid properties

Since the fluid properties are constant, i.e. independent of both temperature and composition, the phenomena of thermal diffusion and diffusional conduction do not arise. The heat flux q and the diffusive mass flux $G_{d,i}$ are then given by:

$$q = - k \frac{\partial T}{\partial y} \qquad (2.4.2\text{-}1)$$

and $$G_{d,i} = - \Gamma_i \frac{\partial m_i}{\partial y} \qquad (2.4.2\text{-}2)$$

The boundary layer equations (2.4.1-1) to (2.4.1-5) then reduce to:

Conservation of mass for the mixture

$$\frac{\partial u}{\partial x} + \frac{\partial v}{\partial y} = 0 \qquad (2.4.2\text{-}3)$$

Conservation of mass for species i

$$\rho u \frac{\partial m_i}{\partial x} + \rho v \frac{\partial m_i}{\partial y} = \Gamma_i \frac{\partial^2 m_i}{\partial y^2} \qquad (2.4.2\text{-}4)$$

Conservation of momentum

x - component

$$\rho u \frac{\partial u}{\partial x} + \rho v \frac{\partial u}{\partial y} = - \frac{\partial p}{\partial x} \qquad (2.4.2\text{-}5)$$

y - component

$$\partial p / \partial y = 0 \qquad (2.4.2\text{-}6)$$

Conservation of energy

$$\rho u \frac{\partial T}{\partial x} + \rho v \frac{\partial T}{\partial y} = \Gamma \frac{\partial^2 T}{\partial y^2} \qquad (2.4.2\text{-}7)$$

2.4.3 Non-zero mass transfer, high speed flow with non-uniform fluid properties but thermal-diffusional effects neglected

For this case the boundary-layer equations may be obtained from equations (2.4.1-1) to (2.4.1-5) with the thermal diffusion ratio k_T set equal to zero.

Conservation of mass for the mixture

$$\frac{\partial(\rho u)}{\partial x} + \frac{\partial(\rho v)}{\partial y} = 0 \qquad (2.4.3\text{-}1)$$

Conservation of mass for species i

$$\rho u \frac{\partial m_i}{\partial x} + \rho v \frac{\partial m_i}{\partial y} = \frac{\partial}{\partial y}\left(\Gamma_i \frac{\partial m_i}{\partial y}\right) \qquad (2.4.3\text{-}2)$$

Conservation of momentum

x - component

$$\rho u \frac{\partial u}{\partial x} + \rho v \frac{\partial u}{\partial y} = -\frac{\partial p}{\partial x} + \frac{\partial}{\partial y}\left(\mu \frac{\partial u}{\partial y}\right) \qquad (2.4.3\text{-}3)$$

y - component

$$\partial p / \partial y = 0 \qquad (2.4.3\text{-}4)$$

Conservation of energy

$$\rho u c_p \frac{\partial T}{\partial x} + \rho v c_p \frac{\partial T}{\partial y} - (c_{p,i} - c_{p,j}) \frac{\partial T}{\partial y}\left(\Gamma_i \frac{\partial m_i}{\partial y}\right) = u \frac{\partial p}{\partial x} + \frac{\partial}{\partial y}\left(k \frac{\partial T}{\partial y}\right) + \mu \left(\frac{\partial u}{\partial y}\right)^2 \qquad (2.4.3\text{-}5)$$

2.4.4 Zero mass transfer, high speed flow with non-uniform fluid properties

In this case the main stream fluid is the only fluid under consideration and the boundary layer equations may be obtained from equations (2.4.1-1) to (2.4.1-5) by neglecting any terms pertaining to mass transfer. The resulting equations are:

Conservation of mass

$$\frac{\partial(\rho u)}{\partial x} + \frac{\partial(\rho v)}{\partial y} = 0 \qquad (2.4.4\text{-}1)$$

Conservation of momentum

x - component

$$\rho u \frac{\partial u}{\partial x} + \rho v \frac{\partial u}{\partial y} = -\frac{\partial p}{\partial x} + \frac{\partial}{\partial y}\left(\mu \frac{\partial u}{\partial y}\right) \qquad (2.4.4\text{-}2)$$

y - component

$$\partial p / \partial y = 0 \qquad (2.4.4\text{-}3)$$

Conservation of energy

$$\rho u c_p \frac{\partial T}{\partial x} + \rho v c_p \frac{\partial T}{\partial y} = \frac{\partial}{\partial y}\left(k \frac{\partial T}{\partial y}\right) + u \frac{\partial p}{\partial x} + \mu \left(\frac{\partial u}{\partial y}\right)^2 \qquad (2.4.4\text{-}4)$$

2.5 Boundary layer equations for axi-symmetric flows

The basic conservation equations (2.2-10) to (2.2-13) can be adapted to different coordinate systems. For two-dimensional flows it has been found convenient to use the Cartesian coordinates, and the equations expanded in component form for this system accordingly, equations (A2.1-1, -2, -5 and -7). However, for axi-symmetric flows it is more convenient to choose a new set of curvilinear orthogonal coordinates; this has been discussed by, among others, Millikan [G23] and Rosenhead [G24] .

If dS is an element of length, then for an orthogonal coordinate system we have in general:

$$dS^2 = h_1^2\, dx_1^2 + h_2^2\, dx_2^2 + h_3^2\, dx_3^2 \qquad (2.5\text{-}1)$$

where x_1, x_2 and x_3 are the three axes of the orthogonal system and h_1, h_2 and h_3 are scale factors, which may be functions of x_1, x_2 and x_3.

Operations involving the differential operator ∇ may be expanded in terms of h_1, h_2 and h_3, x_1, x_2 and x_3 and the scalar quantity or components of the vector quantity, to be operated on#.

For axi-symmetric flows, we define an orthogonal coordinate system (x, θ, y)*, fig. 2.5-1, such that x measures, in the direction of flow, the distance along the body of revolution from the leading

---

For example, if ϕ is a typical scalar quantity, then

$$\nabla\phi = \frac{1}{h_1}\frac{\partial\phi}{\partial x_1}\,\underline{i}_{x_1} + \frac{1}{h_2}\frac{\partial\phi}{\partial x_2}\,\underline{i}_{x_2} + \frac{1}{h_3}\frac{\partial\phi}{\partial x_3}\,\underline{i}_{x_3} \quad .$$

* As it is not likely to cause any confusion here with the coordinates used for two-dimensional flows in previous sections, the same symbols x and y are used.

edge of the forward stagnation point (for a closed body); θ is the angle between the meridian plane through the axis of revolution and a fixed plane also through the axis; y is the normal distance from the surface. If we put $x_1 = x$, $x_2 = \theta$ and $x_3 = y$, then by letting $dx = dy = 0$, it can be seen from equation (2.5-1) that $h_2 = r$, where r is the distance from the axis of the point (x, θ, y). We are intereste only in the region within the thin boundary layer δ ; hence if the longitudinal centre of curvature of the boundary, C_r, is very much greater than δ , i.e. $C_r \gg \delta$, we can write:

$$ds^2 = dx^2 + (r\, d\theta)^2 + dy^2. \qquad (2.5\text{-}2)$$

By comparing this equation with equation (2.5-1) , it can be deduced that:

$$h_1 = h_3 = 1 .$$

Because of the symmetry there cannot be any flow across a meridian plane through the axis of symmetry. Hence, our chosen curvilinear system is specified by:

$$\left.\begin{aligned} &x_1 = x, \quad h_1 = 1, \\ &x_2 = \ , \quad h_2 = r(x,y), \quad \frac{\partial}{\partial\theta} = 0, \text{ this component of velocity} = 0, \\ &x_3 = y, \quad h_3 = 1. \end{aligned}\right\} (2.5\text{-}3)$$

With these relations and the appropriate formulae for changing the vectorial operations into equivalent component expressions, the basic conservation equations (2.2-10) to (2.2-13) may be expanded in terms of the coordinates (x, θ, y). On making the usual boundary-layer assumptions and the additional one that $r(x,y) \approx r_o(x)$, we obtain

the following boundary layer equations for axi-symmetric flows:

Conservation of mass for the mixture

$$\frac{\partial}{\partial x}(r_o \rho u) + \frac{\partial}{\partial y}(r_o \rho v) = 0 \qquad (2.5\text{-}4)$$

Conservation of mass for species i

$$\rho u \frac{\partial m_i}{\partial x} + \rho v \frac{\partial m_i}{\partial y} = -\frac{\partial}{\partial y} G_{d,i} \qquad (2.5\text{-}5)$$

Conservation of momentum

x - component

$$\rho u \frac{\partial u}{\partial x} + \rho v \frac{\partial u}{\partial y} = -\frac{\partial p}{\partial x} + \frac{\partial}{\partial y}\left(\mu \frac{\partial u}{\partial y}\right) \qquad (2.5\text{-}6)$$

y - component

$$\partial p / \partial y = 0 \qquad (2.5\text{-}7)$$

Conservation of energy

$$\rho u c_p \frac{\partial T}{\partial x} + \rho v c_p \frac{\partial T}{\partial y} + (c_{p,i} - c_{p,j}) G_{d,i} \frac{\partial T}{\partial y} = u \frac{\partial p}{\partial x} - \frac{\partial q}{\partial y} + \mu \left(\frac{\partial u}{\partial y}\right)^2 . \qquad (2.5\text{-}8)$$

And the fluxes are given by:

$$G_{d,i} = -\Gamma_i \left[\frac{\partial m_i}{\partial y} + \frac{M_i M_j k_T}{M^2 T} \frac{\partial T}{\partial y}\right] \qquad (2.5\text{-}9)$$

$$q = -k \frac{\partial T}{\partial y} + \frac{\mathcal{R} T k_T}{M m_i m_j} G_{d,i} \quad . \qquad (2.5\text{-}10)$$

As can be seen, except the mass conservation equation for the mixture, all equations are identical in form to those for two-dimensional flows, equations (2.4.1-1, -2, -3, -4, and -5).

2.6 Boundary conditions

What follows applies to both two-dimensional and axi-symmetric flows, and no distinction will be made between the different coordinate systems used. It will be assumed that the i component is the fluid injected into the boundary layer, and the j component is the main-stream fluid. While it is not necessary to specify what the main-stream fluid is, it is often helpful to have atmospheric air in mind.

Referring to fig. 2.6-1, we define the following quantites:

$\dot{m}''$ ≡ total mass-flux across the interface into the main stream, $lb_m/ft^2\ h$;

$\dot{q}''_S$ ≡ value at the S-surface of the normal component of the heat-flux vector $\underline{q}$, $Btu/ft^2\ h$.

In addition we define:

$\dot{m}''_i$ ≡ total mass-flux of the i species into the main stream, $lb_m/ft^2 h$;

and $m_{i,T} \equiv \dot{m}''_i / \dot{m}''$

= mass fraction of the transferred substance.

At the surface, only the normal components of $\underline{G}_{t,i}$ and $\underline{q}$ are of significance; hence we can drop the subscript y denoting the normal components and write:

$$\dot{m}''_i = m_{i,T} \cdot \dot{m}'' = (G_{t,i})_S \qquad (2.6\text{-}1)$$

and

$$\dot{q}''_S = - q_S \qquad (2.6\text{-}2)$$

where subscript S denotes conditions at the surface, and q is as given by equation (2.4.1-6).

For the general case, the following boundary conditions are seen to be appropriate :

i) at the surface, y = 0,

$$\left.\begin{aligned} u &= 0 \\ v &= v_S(x) \\ v_j &= v_{j,S} = 0 \\ T &= T_S(x) \quad \text{or} \quad \dot{q}''_S = 0 \text{ (adiabatic surf.)} \\ m_i &= m_{i,S}(x) \end{aligned}\right\} \qquad (2.6\text{-}3)$$

ii) at $y \to \infty$,

$$\left.\begin{aligned} u &= u_G(x) \\ m_i &= m_{i,G}(x) \\ T &= T_G(x) \end{aligned}\right\} \qquad (2.6\text{-}4)$$

The condition $v_{j,S} = 0$ implies that $(G_{t,j})_S = 0$. This is obviously valid when the surface material itself evaporates# or sublimes# and the surface is impermeable to the main stream component (j). When the surface is a porous one and the diffusing component (i) is injected through it, as in the case of transpiration-cooling, the existence of the conidtion $v_{j,S} = 0$ implies that there is no net flow of the main stream fluid into the coolant reservoir: the diffusion flow being just balanced by the convection flow.

We have from equation (2.2-5):

$$\underline{G} = \underline{G}_{t,j} + \underline{G}_{t,i} \quad ;$$

hence at the surface,

$$G_S = \dot{m}'' = (G_{t,j})_S + (G_{t,i})_S \qquad (2.6\text{-}5)$$

$$= \left[(G_{d,j})_S + (G_{d,i})_S\right] + (G_{c,j})_S + (G_{c,i})_S$$

In these cases the surface temperature will be controlled by the mass transfer rates and vice versa.

i.e. $$G_S = \dot{m}'' = [\ 0\ ] + (\rho_{j,S} + \rho_{i,S})\ v_S$$

or, $$\boxed{\dot{m}'' = \rho_S\ v_S} \qquad (2.6\text{-}6)$$

In terms of the diffusive and convective mass fluxes, equation (2.6-1) may be written as:

$$\begin{aligned} m_{i,T}\ \dot{m}'' &= (G_{d,i})_S + (G_{c,i})_S \\ &= (G_{d,i})_S + \rho_{i,S}\ v_S \end{aligned} \qquad (2.6\text{-}7)$$

Eliminating v_S between equations (2.6-6) and (2.6-7) gives:

$$m_{i,T}\ \dot{m}'' = (G_{d,i})_S + \dot{m}''\ m_{i,S} \ .$$

That is $$\boxed{\dot{m}'' = \frac{(G_{d,i})_S}{m_{i,T} - m_{i,S}}} \ . \qquad (2.6\text{-}8)$$

Combination of equations (2.6-6), (2.6-8) and (2.4.1-7) then gives:

$$\dot{m}'' = \rho_S\ v_S = \frac{-\Gamma_{i,S}}{m_{i,T} - m_{i,S}} \left(\frac{\partial m_i}{\partial y} + \frac{M_i M_j k_T}{M^2 T} \frac{\partial T}{\partial y} \right)_S$$

or $$\boxed{\dot{m}'' = \frac{-\Gamma_{i,S}}{m_{i,T} - m_{i,S}} \left(\frac{\partial m_i}{\partial y} + \frac{m_i (1-m_i)\,\alpha_T}{T} \frac{\partial T}{\partial y} \right)_S} \qquad (2.6\text{-}9)$$

$m_{i,T}$ is invariably a prescribed quantity. When the reservoir contains pure coolant only, $m_{i,T} = 1$.

Similarly, combination of equations (2.6-2), (2.6-8) and (2.4.1-6) gives:

$$-\dot{q}''_S = -\left(k \frac{\partial T}{\partial y} \right)_S + \left(\frac{\mathcal{R} T k_T}{M m_i} \right)_S \dot{m}''$$

or
$$\boxed{-\dot{q}''_S = -\left(k\frac{\partial T}{\partial y}\right)_S + \mathcal{R}\left[\frac{(1-m_i)\,T\alpha_T}{M_i + (M_j - M_i)\,m_i}\right]_S \dot{m}''} \qquad (2.6\text{-}10)$$

When T_S is prescribed, equation (2.6-9) suggests that either v_S or $m_{i,S}$, but not both, may also be prescribed; otherwise the problem becomes a trivial one: this may be seen easily for the case when k_T or α_T equals zero (thermal diffusion neglected) then equation (2.6-9) will yield $(\partial m_i/\partial y)_S$ immediately. Hence, although eight conditions, (2.6-3) and (2.6-4), are listed, we have only seven independent boundary conidtions. Usually, $m_{i,S}$ is prescribed v_S or $\dot{m}''$ is then computed from equation (2.6-9).

In the present work we shall consider mainly the following set of boundary conditions, which may be regarded as a particular case of those given by equations (2.6-3 and -4):

At $y = 0$,
$$\left.\begin{aligned} u &= 0 \\ v &= v_S(x) \\ T &= T_S = \text{constant, or } \dot{q}''_S = 0 \\ m_i &= m_{i,S} = \text{constant,} \end{aligned}\right\} \qquad (2.6\text{-}11)$$

At $y \to \infty$,
$$\left.\begin{aligned} u &= u_G(x) \\ m_i &= 0 \\ T &= T_G = \text{constant,} \end{aligned}\right\} \qquad (2.6\text{-}12)$$

It should be noted that the conidtion $v_{j,S} = 0$ has been taken into account in equation (2.6-9), which also provides a functional relationship between v_S and $m_{i,S}$.

The condition $m_{i,G} = 0$ implies that the main stream fluid is

composed entirely of the j species.

The same set of boundary conditions is also appropriate for the special case of constant fluid-properties considered in section 2.4.2.

For zero mass-transfer with either uniform or non-uniform fluid properties, the boundary conditions (2.6-11) and (2.6-12) then reduce to:

$$\left.\begin{aligned} &\text{at } y = 0, && u = 0 , \\ & && v = 0 , \\ & && T = T_S = \text{constant, or } \mathring{q}''_S = 0; \end{aligned}\right\} \qquad (2.6\text{-}13)$$

$$\left.\begin{aligned} &\text{at } y \to \infty , && u = u_G(x) , \\ & && T = T_G = \text{constant.} \end{aligned}\right\} \qquad (2.6\text{-}14)$$

2.7 "Similar" solutions

2.7.1 Transformation of boundary layer equations

The transformation of the boundary layer equations to a form suitable for obtaining "similar" solutions has been discussed, in one way or another, by many authors; but it appears that no single discussion is sufficiently general ~~enough~~ to embrace all the aspects of the problem. Here we shall try to provide such a discussion.

It has been seen that with the exception of the conservation equation for the mixture mass, the boundary-layer equations for two-dimensional and axi-symmetric flows are identical in form. However, the two forms of the conservation equation for the mixture mass may be represented by a single equation of the form:

$$\frac{\partial(\rho u r_o^{\epsilon})}{\partial x} + \frac{\partial(\rho v r_o^{\epsilon})}{\partial y} = 0 \quad . \qquad (2.7.1\text{-}1)$$

By letting $\epsilon = 0$, we have the equation for two-dimensional flows; and putting $\epsilon = 1$ we get the equation for axi-symmetric flows. This equation together with equations (2.4.1-2) to (2.4.1-5) are then the equations we shall now consider.

It must, however, be borne in mind that although we are dealing these equations in the same set of coordinate symbols, x and y, these coordinates should be differently interpreted according to whether they are used in the two-dimensional flows or in the axi-symmetric flows.

The mass conservation equation for the mixture is always satisfied if we introduce a stream function ψ such that

$$\rho u r_o^{\epsilon} = \frac{\partial(\psi r_o^{\epsilon})}{\partial y} \qquad (2.7.1\text{-}2)$$

and

$$\rho v r_o^{\epsilon} = \frac{-\partial(\psi r_o^{\epsilon})}{\partial x} \quad . \qquad (2.7.1\text{-}3)$$

In order to obtain "similar" solutions for the equations (2.4.1-2) to (2.4.1-5) we must change the (x,y) coordinates to some suitably "stretched" ones. For this the new coordinates (s, η) are defined:

$$s(x) \equiv \int_o^x \mu_G \rho_G u_G \left[\frac{r_o(x)}{L}\right]^{2\epsilon} dx \qquad (2.7.1\text{-}4)$$

and

$$\eta(x,y) \equiv \frac{\rho_G u_G (r_o/L)^{\epsilon}}{(2s)^{1/2}} \int_o^y Y(\eta)\, dy \qquad (2.7.1\text{-}5)$$

where L is a characteristic dimension and $Y = Y(\eta)$ is an as-yet-unspecified ratio of some fluid properties. The above are essentially combinations of the transformations used by Mangler [G21] , Illingworth [G18] , Dorodnitzyn [G5] and Lees [G20] .

The transformation from the (x,y) coordinates to the (s, η) coordinates can be accomplished via the following relations:

$$\frac{\partial}{\partial x} = \mu_G \rho_G u_G \, (r_o/L)^{2\epsilon} \frac{\partial}{\partial s} + \frac{\partial \eta}{\partial x} \frac{\partial}{\partial \eta} \qquad (2.7.1\text{-}6)$$

and

$$\frac{\partial}{\partial y} = \frac{\rho_G u_G \, (r_o/L)^{\epsilon}}{(2s)^{1/2}} \, Y \frac{\partial}{\partial \eta} \qquad (2.7.1\text{-}7)$$

It will become clear later that it is not necessary , for the present purpose, to express the function $(\partial \eta / \partial x)$ in terms of the new coordinates (s, η).

We now stipulate that the velocity, concentration and static temperature profiles in the boundary layer are similar, i.e. they are functions of the independent variable η only.

From equations (2.7.1-2) and (2.7.1-7) we have:

$$\rho u = \frac{Y \rho_G u_G}{(2s)^{1/2}} \frac{\partial}{\partial \eta} \left[\psi (r_o/L)^{\epsilon} \right] \qquad (2.7.1\text{-}8)$$

From this equation it is clearly seen possible to introduce, within the restriction of similar profiles, a dimensionless stream function $f(\eta)$ defined by:

$$f(\eta) \equiv \psi (r_o/L)^{\epsilon} / (2s)^{1/2} \, . \qquad (2.7.1\text{-}9)$$

In terms of this dimensionless stream function, equations (2.7.1-8) and (2.7.1-3) become respectively:

$$\rho u = \rho_G u_G f' \qquad (2.7.1\text{-}10)$$

and

$$\rho v = -\left[\frac{\mu_G \rho_G u_G (r_o/L)^{\epsilon} \cdot f}{(2s)^{1/2}} + \frac{(2s)^{1/2} f'}{(r_o/L)^{\epsilon}} \frac{\partial \eta}{\partial x}\right] \qquad (2.7.1\text{-}11)$$

where $(\ )'$ denotes differentiation with respect to η .

In terms of the dimensionless temperature θ ($\equiv T/T_G$), f and the similar coordinates, the boundary layer equations for two-dimensional flows and axi-symmetric flows are seen to acquire the following identical dimensionless form:

Conservation of mass for species i

$$\left(\frac{Z_\mu Y}{N_{Sc}} m_i'\right)' + f m_i' + \left(\frac{Z_\mu Y M_i M_j k_T}{M^2 N_{Sc}} \frac{\theta'}{\theta}\right)' = 0 \qquad (2.7.1\text{-}12)$$

Conservation of momentum

$$\left[Z_\mu Y \left(\frac{Y f'}{Z_\rho}\right)'\right]' + f \left(\frac{Y f'}{Z_\rho}\right)' - \beta\left[\frac{Y}{Z_\rho}(f')^2 - \frac{1}{Y}\right] = 0 \qquad (2.7.1\text{-}13)$$

Conservation of energy

$$\frac{1}{N_{Pr,G}} (Z_k Y \theta')' + Z_{c_p} f \theta' + Z_{c_{p,ij}} Z_\mu Y \frac{\theta' m_i'}{N_{Sc}} + \left[(\gamma_G - 1) N^2_{Ma,G}\right] Z_\mu Y \left[\left(\frac{Y f'}{Z_\rho}\right)'\right]^2 -$$

$$-\beta\left[(\gamma_G - 1) N^2_{Ma,G}\right] \frac{f'}{Z_\rho} = \left[\frac{\mathcal{R} Z_\mu Y k_T}{c_{p,G} N_{Sc} M m_i (1 - m_i)} (\theta m_i' + \theta')\right]' + \frac{Z_{c_{p,ij}} Z_\mu Y M_i M_j k_T}{N_{Sc} M^2} \frac{(\theta')^2}{\theta}$$

---- (2.7.1-14)

In the above equations,

$$\beta \equiv \frac{2s}{u_G} \frac{du_G}{dx} \qquad (2.7.1\text{-}15)$$

and Z denotes the ratio of some property quantity, local value to main stream value; the particular property concerned appears as a subscript, e.g. $Z_\mu \equiv \mu/\mu_G$, $Z_\rho \equiv \rho/\rho_G$ etc. $Z_{c_{p,ij}}$ has the special meaning of $(c_{p,i} - c_{p,j})/c_{p,G}$.

It may be noted that in deriving equations (2.1.1-12) to (2.7.1-14) the following conditions have been invoked: $\partial\theta/\partial s = 0 = \partial m_i/\partial s$, and the fluid properties μ, ρ, k, c_p etc. being functions of η only; all these conditions arise out of the stipulation of similarity in the various profiles. In addition, it has been assumed that for the main stream fluid the accoustic velocity "a" is given by the perfect gas relationship, viz.: $a = (\gamma RT)^{1/2}$; hence,

$$\frac{u_G^2}{c_{p,G} T_G} = (\gamma_G - 1) N^2_{Ma,G} \qquad (2.7.1\text{-}16)$$

where γ is the ratio of specific heats.

Boundary conditions

After transformation, the boundary conditions (2.6 -11) and (2.6-12) become:

$$\left.\begin{aligned} \text{at } \eta = 0, \quad f' &= 0 \ , \\ f &= f_o \ , \\ \theta &= \theta_S = \text{constant, or } \dot{q}''_S = 0, \\ m_i &= m_{i,S} = \text{constant.} \end{aligned}\right\} \qquad (2.7.1\text{-}17)$$

$$\text{at } \eta \to \infty , \qquad \left.\begin{aligned} f' &= 1 , \\ m_i &= m_{i,G} = 0 , \\ \theta &= \theta_G = 1 . \end{aligned}\right\} \qquad (2.7.1\text{-}18)$$

From equation (2.7.1-11) the mass-transfer parameter f_o may be expressed as follows:

$$f_o = - \frac{\rho_S v_S (2s)^{1/2}}{\mu_G \rho_G u_G (r_o/L)^{\epsilon}} = - \frac{\dot{m}'' (2s)^{1/2}}{\mu_G \rho_G u_G (r_o/L)^{\epsilon}} \qquad (2.7.1\text{-}19)$$

It should be noted that f_o takes different forms for two-dimensional flows and for axi-symmetric flows. Making use of equation (2.6-8), we obtain another expression for f_o:

$$f_o = \left[\frac{Z_\mu Y}{N_{Sc}} \frac{m_i' + m_i(1 - m_i)\alpha_T \theta'/\theta}{1 - m_i} \right]_S \qquad (2.7.1\text{-}20)$$

From equations (2.6-10) and (2.6-9), there is obtained:

$$\frac{\dot{q}_S'' (2s)^{1/2}}{\mu_G \rho_G u_G c_{p,G} T_G (r_o/L)^{\epsilon}} = \left[\frac{Y Z_k}{N_{Pr,G}} \theta' + \frac{\mathcal{R} Z_\mu Y M \alpha_T \theta}{c_{p,G} M_i M_j N_{Sc}} \left\{ m_i' + m_i(1 - m_i)\alpha_T \theta'/\theta \right\} \right]_S$$

----- (2.7.1-21)

Thus when $\dot{q}_S'' = 0$, i.e. adiabatic surface,

$$\boxed{\left[\theta' + \frac{N_{Pr,G} (\mathcal{R}/c_{p,G}) Z_\mu M \alpha_T \theta}{Z_k N_{Sc} M_i M_j} \left\{ m_i' + m_i(1 - m_i)\alpha_T \theta'/\theta \right\} \right]_S = 0 .}$$

----- (2.7.1-22)

Inspection of the transformed equations (2.7.1-12, -13 and -14) shows that some simplification may be effected by setting $Y(\eta) = 1/Z_\mu$

or $Y(\eta) = Z_\rho$. The latter has of course been used by Dorodnitzyn [G5]; the former was frequently adopted by Eckert and his co-workers [S37, S44, S50, S52, S53] .

2.7.2 Conditions for existence of "similar" solutions

In order to validate the stipulation of similar profiles, the transformed equations must be of single-variable ones. Inspection of equations (2.7.1-12) to (2.7.1-14) and boundary conditions (2.7.1-17) and (2.7.1-18) shows that this condition is satisfied only when:

a) $$\beta \equiv \frac{2s}{u_G}\frac{du_G}{dx} = \text{constant} \quad , \qquad (2.7.2\text{-}1)$$

b) $$(\gamma_G - 1)\, N^2_{Ma,G} = \text{constant} \quad , \qquad (2.7.2\text{-}2)$$

and c) the boundary conditions θ_S, $m_{i,S}$ and f_o are all constant.

Equations (2.7.1-12) to (2.7.1-14) then become a set of ordinary differential equations, of order seven; they are soluble with the seven boundary conditions, (2.7.1-17) and (2.7.1-18).

Instead of similarity in static temperature profiles we could have stipulated similarity in stagnation temperature profiles. In that case a slightly different set of conditions would have resulted. However, we shall confine our attention to the problem with similar static temperature profiles.

We now consider in greater detail condition (a). Integration of equation (2.7.2-1) gives:

$$u_G = c\, s^{\beta/2} \qquad (2.7.2\text{-}3)$$

where c is a constant.

For two-dimensional flows $\epsilon = 0$, differentiating equation (2.7.1-4) yields:

$$\frac{ds}{\mu_G \rho_G u_G} = dx \qquad (2.7.2\text{-}4)$$

Eliminating u_G between equations (2.7.2-3) and (2.7.2-4) and integrating the resulting equation, we obtain for constant μ_G and ρ_G:

$$s = c_1 \; x^{2/(2-\beta)} \qquad (2.7.2\text{-}5)$$

where c_1 is a constant. Combination of equations (2.7.2-3) and (2.7.2-5) then gives:

$$\boxed{u_G = \text{constant} \cdot x^{\beta/(2-\beta)}} \qquad (2.7.2\text{-}6)$$

This external velocity distribution belongs to the well-known Falkan-Skan "wedge flow" [G13] ; $\beta/(2-\beta)$ is the Euler number, Eu. Physically, $\beta\pi$ is simply the included angle of the "wedge". Hence except for $\beta = 0$, the main stream velocity u_G will vary with x; for this reason β is often referred to as the "pressure gradient parameter". This means that for $\beta \neq 0$, the second condition for "similar" solutions, viz. $(\gamma_G - 1)N^2_{Ma,G} = \text{constant}$, can be realized only when T_G varies in such a way that $(c_{p,G}T_G) \propto u_G$. Clearly, for constant T_G and $\beta \neq 0$ the conditions (2.7.2-1) and (2.7.2-2) can only be simultaneously satisfied if $N_{Ma,G} \to 0$ or $N_{Ma,G} \to \infty$.

From the expression, $u_G^2 = \dfrac{(\gamma_G - 1)c_{p,G}T_{stagn,G}N^2_{Ma,G}}{1 + \frac{1}{2}(\gamma_G - 1)N^2_{Ma,G}}$, it is seen that as $N_{Ma,G}$ approaches infinity, u_G takes a constant finite

value of $(2c_{p,G}T_{stagn,G})^{\frac{1}{2}}$. However, since $1/\delta$ (Knudsen number) is proportional to $N_{Ma}/(N_{Re})^{\frac{1}{2}}$, for very large Mach number, the boundary layer thickness δ becomes comparable with the molecular mean free path 1 and the continuum theory, based on which the conservation equations have been derived, ceases to be valid. Consequently, the boundary layer equations do not apply to these situations. For this reason, we shall exclude the case when $N_{Ma,G} \to \infty$.

For $\beta = 0$, i.e. u_G = constant, both conditions (b) and (c) can be satisfied at the same time for arbitrary constant values of $N_{Ma,G}$ and T_G.

In summary, we note that for constant T_G, "similar" solutions exist in two-dimensional flows for the following combinations of conditions:

$$\left.\begin{array}{ll} 1) & \beta = 0 \text{ and } N_{Ma,G} = \text{constant} \geqslant 0; \\ 2) & \beta \neq 0 \text{ and } N_{Ma,G} \to 0. \end{array}\right\} \qquad (2.7.2\text{-}7)$$

Similarly, for axi-symmetric flows that correspond to two-dimensional flows under the above conditions, "similar" solutions exist.

2.7.3 Parameters and fluid properties

Parameters

From equations (2.7.1-12) to (2.7.1-14) and the associated boundary conditions (2.7.1-17) and (2.7.1-18) it may be seen that the solutions to the equations in general depend on the following parameters:

1) β - "pressure gradient" parameter;

2) $N_{Ma,G}$ ($N_{Ma,G} \to 0$ for $\beta \neq 0$);

3) T_G ;

4) T_S/T_G if $\dot{q}''_S \neq 0$, or $\dot{q}''_S = 0$ i.e. adiabatic surface ;

5) Fluid property values;

and 6) $m_{i,S}$ or f_o.

When there is no mass transfer, only the first five are relevant parameters.

Fluid-property values

In order to solve the boundary layer equations, we need to know as a pre-requisite the variations with temperature and/or composition of: density ρ, molecular weight M, specific heat c_p, viscosity μ, thermal conductivity k, binary coefficient of diffusion D_{ij} and thermal diffusion factor α_T.

With the exception of α_T all these properties have been discussed in one way or another by many investigators concerned with boundary layer flows, and no more need be said about them here. We shall, however, discuss in some detail the thermal diffusion factor α_T, as this is a less familiar property.

As has been seen in equations (2.3-6) and (2.3-7), the thermal diffusion ratio k_T is the quantity governing the phenomena of thermal diffusion and diffusional conduction. k_T is defined by:

$$k_T \equiv D_T/D_{ij} \quad , \qquad (2.7.3\text{-}1)$$

where D_T is the coefficient of thermal diffusion and D_{ij} is the binary coefficient of ordinary diffusion .

k_T usually varies quite considerably with concentration, and assumes a value of zero when either of the two mass fractions becomes zero. For this reason, it is sometimes more convenient to use instead the thermal diffusion factor α_T defined by:

$$\alpha_T \equiv k_T/(n_i\, n_j) \qquad (2.7.3\text{-}2)$$

where n_i is the mole fraction of the mixture component i. So defined, α_T varies less with concentration than k_T, and it assumes finite values even at very low concentrations.

The mole fraction n_i and the mass fraction m_i are connected by:

$$n_i = m_i M/M_i \quad . \qquad (2.7.3\text{-}3)$$

The sign of α_T deserves some attention. In the relevant literature [e.g. G15, G17] , this quantity is invariably given as positive. This implies that the following convention is adopted: if i is used to refer to the heavier component in a binary mixture comprising of i and j components, positive values of α_T (or k_T) always implies that thermal diffusion causes the i molecules to diffuse down the temperature gradient, i.e. to a cooler region. If, however, i is chosen to refer to the lighter component, then the sign reverses. In boundary layer flows concerned here we shall adopt i to denote the transpiring gas and j the main stream fluid, which is, without exception, air. Hence, the i component may be lighter or heavier than the j component; this will be reflected through the sign of α_T. As a general rule, when the i component is lighter than the j component (air), e.g. H_2-air, α_T is negative; when the i component is the

the heavier, e.g. CO_2-air, α_T is positive.

Experimental data for α_T are very scarce [G15] ; and there seem to be no data at all for mixtures with air as one of the components. Hence most of the investigators concerned with the problem of thermal diffusion and diffusional conduction in boundary layers rely on a theoretical method in calculating this quantity. The method used is invariably the first approximation of Hirschfelder [P7] . In Appendix 2.2 is contained an outline of Hirschfelder's first approximation to the thermal diffusion factor, which is a complex function of both temperature and composition.

Fig. 2.7 -1 shows some plots of α_T versus m_i for six mixtures as calculated by various authors; on the figure are also shown some experimental data.

2.7.4 Conductances, driving forces and recovery factors

The quantities that are of particular importance in engineering applications are the values at the surface of heat-transfer coefficient, skin friction and mass fraction as well as the recovery factors. The first three quantities can usually by embodied in various forms of dimensionless groups; here we shall adopt Spalding's concept of conductances and driving forces [G27, G28] .

Following Spalding, we introduce the "Ohm's law" relationship between a conductance g and the driving force B through:

$$\boxed{\dot{m}'' = g.B} \qquad (2.7.4\text{-}1)$$

and the conductance is then defined by:

$$g \equiv \dot{m}''/B \quad . \qquad (2.7.4\text{-}2)$$

Of particular interest are the following driving-force expressions:

$$B_h \equiv \frac{h_{GS,ad} - h_{GS}}{\dot{q}''_S / \dot{m}''} \quad , \tag{2.7.4-3}$$

$$B_u \equiv \dot{m}'' u_G / \tau_S \quad , \tag{2.7.4-4}$$

and

$$B_f \equiv \frac{f_G - f_S}{f_S - f_T} \quad , \tag{2.7.4-5}$$

where the subscript GS denotes fluid of G-state composition reduced to the temperature of the S-state; the subscript "ad" denotes adiabatic surface condition; τ_S is the shear stress at the surface and $f^{\#}$ is the mixture fraction. As far as the present work is concerned f can be treated as identical to m_i; hence

$$B_f = \frac{m_{i,G} - m_{i,S}}{m_{i,S} - m_{i,T}} \tag{2.7.4-6}$$

$$= \frac{m_{i,S}}{1 - m_{i,S}} \quad \text{for } m_{i,G} = 0 \text{ and } m_{i,T} = 1$$

\# In [G28] Spalding defined f as:

$$f \equiv (P - P_V)/(P_U - P_V)$$

in which P is a conserved extensive property, and subscripts U and V represent two reference "streams". In the present work, all the systems considered have air as the main stream fluid; so by choosing the injected fluid (the i component) as our "father" reference stream and air (the j component) as the other reference stream we have for the conserved property m_i:

$$f = \frac{m_i - 0}{1 - 0} = m_i \ .$$

Thus f has the same value and significance as the mass fraction for the injected fluid.

In transpiration-cooling problems, the surface heat flux $\dot{q}''_S$ can be conveniently related to the mass-transfer rate $\dot{m}''$ and the supply conditions of the coolant (denoted by the subscript T) by applying the Steady Flow Energy equation to a control volume bounded by the S-surface and by a control surface crossing the coolant-supply stream. When lateral heat conduction is neglected there results:

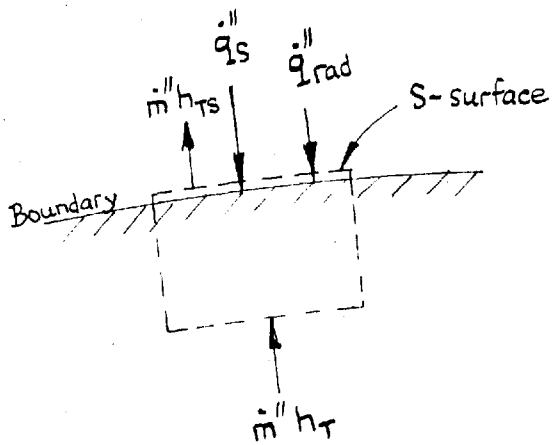

$$\dot{q}''_S = \dot{m}''(h_{TS} - h_T) - \dot{q}''_{rad} \quad .$$

Hence the driving force B_h may also be written as:

$$B_h = \frac{h_{GS,ad} - h_{GS}}{h_{TS} - h_T - \dot{q}''_{rad}/\dot{m}''} \qquad (2.7.4\text{-}3a)$$

The corresponding conductances can be obtained through equation (2.7.4-2). For "similar" flows the following dimensionless forms of the various conductances are independent of the variable x :

$$\frac{g_h}{(\mu_G \rho_G u_G / x)^{1/2}} \equiv \frac{\dot{q}''_S}{(h_{GS,ad} - h_{GS})(\mu_G \rho_G u_G / x)^{1/2}} , \qquad (2.7.4\text{-}7)$$

$$\frac{g_u}{(\mu_G \rho_G u_G / x)^{1/2}} \equiv \frac{\tau_S}{u_G (\mu_G \rho_G u_G / x)^{1/2}} , \qquad (2.7.4\text{-}8)$$

$$\frac{g_f}{(\mu_G \rho_G u_G / x)^{1/2}} \equiv \frac{\dot{m}''}{B_f (\mu_G \rho_G u_G / x)^{1/2}} . \qquad (2.7.4\text{-}9)$$

In a way entirely analogous to the case of constant-property solutions, in presenting solutions in later chapters we shall incorporate in the conductances the Prandtl number, Schmidt number and the pressure-gradient parameter β in the following form to reduce their influences on the conductances:

$$\left.\begin{aligned} (G_h)_G &\equiv (N_{Pr,G})^{2/3} (2-\beta)^{1/2} g_h / (\mu_G \rho_G u_G / x)^{1/2} \\ (G_u)_G &\equiv (2-\beta)^{1/2} g_u / (\mu_G \rho_G u_G / x)^{1/2} \\ (G_f)_G &\equiv (N_{Sc,G})^{2/3} (2-\beta)^{1/2} g_f / (\mu_G \rho_G u_G / x)^{1/2} \end{aligned}\right\} \qquad (2.7.4\text{-}10)$$

In the limiting case when $B \to 0$ (i.e. $\dot{m}'' \to 0$), the corresponding quantities are denoted by the superscript $(\quad)^*$, e.g. g_h^*, α^*, $(\dot{q}''_S)^*$, $h^*_{GS,ad}$ etc.

The local Nusselt number, Stanton number, skin friction factor and Reynolds number are connected to the conductances through the following relations:

$$\frac{N_{Nu,G}}{(N_{Re,G})^{1/2}} \equiv \frac{\alpha x/k_G}{(\mu_G \rho_G u_G/x)^{1/2}} = \frac{N_{Pr,G}(h_{GS,ad}-h_{GS})}{c_{p,G}(T_{S,ad}-T_S)} \cdot \frac{g_h}{(\mu_G \rho_G u_G/x)^{1/2}} ,$$

---- (2.7.4-11)

where the heat-transfer coefficient $\alpha \equiv \dot{q}''_S/(T_{S,ad} - T_S)$.

$$N_{St,G}(N_{Re,G})^{1/2} \equiv \frac{\alpha}{\rho_G u_G c_{p,G}} \left(\frac{u_G x \rho_G}{\mu_G}\right)^{1/2}$$

$$= \frac{h_{GS,ad} - h_{GS}}{c_{p,G}(T_{S,ad} - T_S)} \frac{g_h}{(\mu_G \rho_G u_G/x)^{1/2}} , \qquad (2.7.4\text{-}12)$$

$$c_f (N_{Re,G})^{1/2} \equiv \frac{2\tau_S}{\rho_G u_G^2} \left(\frac{u_G \rho_G x}{\mu_G}\right)^{1/2} = \frac{2 g_u}{(\mu_G \rho_G u_G/x)^{1/2}} . \qquad (2.7.4\text{-}13)$$

Recovery factors

Two recovery factors are defined:

(I) Temperature recovery factor, $N_{RF,T}$,

$$N_{RF,T} \equiv \frac{T_{S,ad} - T_G}{u_G^2/(2 g_o J)} . \qquad (2.7.4\text{-}14)$$

If the accoustic velocity "a" is given by the perfect gas relation $a = (\gamma R T)^{1/2}$, then,

$$N_{RF,T} = \frac{T_{S,ad} - T_G}{\frac{1}{2}(\gamma_G - 1) N_{Ma,G}^2 \cdot T_G} . \qquad (2.7.4\text{-}14a)$$

(II) Enthalpy recovery factor, N_{RF} ,

$$N_{RF} \equiv \frac{h_{GS,ad} - h_G}{c_{p,G}\, u_G^2/(2g_o J)} \quad . \qquad (2.7.4\text{-}15)$$

Again, if the accoustic velocity is given by the perfect gas law then:

$$N_{RF} = \frac{h_{GS,ad} - h_G}{\tfrac{1}{2}(\gamma_G - 1) N_{Ma,G}^2\, c_{p,G} T_G} \quad . \qquad (2.7.4\text{-}15a)$$

2.7.5 Relationship between two-dimensional flows and axi-symmetric flows

Since s, η and f (Section 2.7.1) are variables in the transformed common equations (2.7.1-12) to (2.7.1-14), their respective values for corresponding two-dimensional and axi-symmetric flows must be identical. To distinguish the two types of flow we shall in this section denote the two-dimensional flow by single-barred quantities and the axi-symmetric flow by double-barred quantities. Hence, we have:

$$\bar{\bar{s}} = \bar{s} \; ; \quad \bar{\bar{\eta}} = \bar{\eta} \; ; \quad \bar{\bar{f}} = \bar{f} \; .$$

Similarity of profiles holds, thus u is a function of η only. It then follows:

$$\bar{\bar{u}} = \bar{u} \; .$$

It is also assumed that all the fluid properties are identical for the two systems, i.e. $\bar{\bar{\mu}} = \bar{\mu}$, $\bar{\bar{\rho}} = \bar{\rho}$ etc. As confusion will not arise it is not necessary to distinguish these by bars.

From the definition of s, equation (2.7.1-4), we have for constant μ_G and ρ_G :

$$\bar{\bar{s}} = \mu_G \rho_G \int_0^{\bar{\bar{x}}} \bar{\bar{u}}_G \left[\frac{r_o(\bar{\bar{x}})}{L}\right]^2 d\bar{\bar{x}}$$

and $$\bar{s} = \mu_G \rho_G \int_0^{\bar{x}} \bar{u}_G \, d\bar{x} \quad .$$

But $\bar{\bar{s}} = \bar{s}$ and $\bar{\bar{u}}_G = \bar{u}_G$, thus:

$$d\bar{x} = \left[\frac{r_o(\bar{\bar{x}})}{L}\right]^2 d\bar{\bar{x}} \text{ , i.e. } \boxed{\bar{x} = \int_0^{\bar{\bar{x}}} \left[\frac{r_o(\bar{\bar{x}})}{L}\right]^2 d\bar{\bar{x}}} \quad (2.7.5\text{-}1)$$

From the definition of η, equation (2.7.1-5), we have:

$$\bar{\bar{\eta}} = \frac{\rho_G \bar{\bar{u}}_G \, (r_o/L)}{(2\bar{\bar{s}})^{1/2}} \int_0^{\bar{\bar{y}}} Y \, d\bar{\bar{y}} \text{ , and } \quad \bar{\eta} = \frac{\rho_G \bar{u}_G}{(2\bar{s})^{1/2}} \int_0^{\bar{y}} Y \, d\bar{y} \quad .$$

But $\bar{\bar{\eta}} = \bar{\eta}$, $\bar{\bar{u}}_G = \bar{u}_G$ and $\bar{\bar{s}} = \bar{s}$, thus:

$$\frac{r_o(\bar{\bar{x}})}{L} \cdot d\bar{\bar{y}} = d\bar{y} \text{ , i.e, } \boxed{\bar{y} = \frac{r_o(\bar{\bar{x}})}{L} \bar{\bar{y}}} \quad (2.7.5\text{-}2)$$

Relations (2.7.5-1) and (2.7.5-2) are of course the well-known Mangler's transformation. Using these, we easily obtain the following ratios, two-dimensional flow quantities to axi-symmetric flow quantities:

$$R_{2D/3D} \equiv \frac{\sqrt{\overline{Eu}}}{\sqrt{\overline{\overline{Eu}}}} = \frac{\overline{\dot{m}}''/(\mu_G \rho_G \bar{u}_G/\bar{x})^{1/2}}{\overline{\overline{\dot{m}}}''/(\mu_G \rho_G \overline{\bar{u}}_G/\overline{\bar{x}})^{1/2}} = \frac{\bar{g}_h/(\mu_G \rho_G \bar{u}_G/\bar{x})^{1/2}}{\overline{\bar{g}}_h/(\mu_G \rho_G \overline{\bar{u}}_G/\overline{\bar{x}})^{1/2}} =$$

$$= \frac{\bar{g}_f/(\mu_G \rho_G \bar{u}_G/\bar{x})^{1/2}}{\overline{\bar{g}}_f/(\mu_G \rho_G \overline{\bar{u}}_G/\overline{\bar{x}})^{1/2}} = \frac{\bar{g}_u/(\mu_G \rho_G \bar{u}_G/\bar{x})^{1/2}}{\overline{\bar{g}}_u/(\mu_G \rho_G \overline{\bar{u}}_G/\overline{\bar{x}})^{1/2}} = \left[\frac{\int_0^{\overline{\bar{x}}} \left(r_o(\bar{\bar{x}})/L\right)^2 \, d\bar{\bar{x}}}{\left(r_o(\bar{\bar{x}})/L\right)^2 \, \overline{\bar{x}}} \right]^{1/2}$$

------- (2.7.5-3)

where the Euler number Eu is connected to β by $Eu = \beta/(2 - \beta)$. It thus follows that:

$$\overline{\overline{B}}_h = \overline{B}_h \; ; \quad \overline{\overline{B}}_f = \overline{B}_f \; ; \quad \overline{\overline{B}}_u = \overline{B}_u \qquad (2.7.5\text{-}4)$$

For an axi-symmetric stagnation-point flow, we have:

$$\overline{\overline{u}}_G \propto \overline{\overline{x}}, \quad \text{i.e} \quad \overline{\overline{Eu}} = 1 \qquad \text{and} \qquad r_o = \overline{\overline{x}} \; . \qquad (2.7.5\text{-}5)$$

Equation (2.7.5-3) then gives:

$$R_{2D/3D} = 1/\sqrt{3} \qquad (2.7.5\text{-}6)$$

Thus: $\overline{Eu} = 1/3$

and $\overline{\beta} = 1/2$. (2.7.5-7)

Hence, solutions obtained for two-dimensional flows with $\beta = 1/2$ are applicable, after suitable modifications, to the axi-symmetric stagnation-point flows; and vice versa.

CHAPTER 3 "SIMILAR" SOLUTIONS TO THE BOUNDARY-LAYER EQUATIONS

3.1 Survey of exact solutions available in the literature

As the heading of this section suggests, only exact "similar" solutions to the boundary layer equations will be considered. The qualifying word "exact" is used here mainly to distinguish the solutions that satisfy exactly the differential equations from those which only satisfy the integral equations across the whole boundary layer thickness.

Without exception all the exact solutions that are available in the literature were obtained by a numerical method. Though here we are concerned more with the solutions themselves than the actual methods used to obtain them, it should be noted that the form of the differential equations for "similar" flows as presented in section 2.7.1 is not the only one; other variants are possible. However, the form chosen is the most generally used one. Once again, we shall not discuss the particular form each author adopted in obtaining the solutions.

As far as possible the solutions have been collected from the literature and tabulated in Tables 3.1-1 to 3.1-28 (pp.275-291). The tabulated solutions include the dimensionless conductances $(G_u)_G \equiv (2-\beta)^{1/2} g_u/(\mu_G \rho_G u_G/x)^{1/2}$, $(G_f)_G \equiv (N_{Sc})_G^{2/3}(2-\beta)^{1/2} g_f/(\mu_G \rho_G u_G/x)^{1/2}$ and $(G_h)_G \equiv (N_{Pr})_G^{2/3}(2-\beta)^{1/2} g_h/(\mu_G \rho_G u_G/x)^{1/2}$, and the enthalpy recovery factor N_{RF} or the temperature recovery factor $N_{RF,T}$. Where applicable the dimensionless mass-transfer rate $\dot{m}''/(\mu_G \rho_G u_G/x)^{1/2}$ and the driving forces B_u, B_f and B_h are also included. It may be noticed that in

the above groups the fluid property values in the main stream (the G state) have been used.

With each set of solutions is a summary of the particular property-variations which have been used in the solving of the boundary layer equations. Very often the difference between two sets of solutions lie only in the choice of slightly different property-variations.

Examination of these solutions reveals that for the zero-mass-transfer case the great majority of the solutions were obtained explicitly for air as the fluid; and for the non-zero mass-transfer case air was invariably the main stream fluid. This contrasts with the many constant-property solutions available for a wide variety of fluids, as characterized by the Prandtl number ranging from zero to infinity for the zero-mass-transfer case and from 0.0001 to 20 for the non-zero mass-transfer case [G12, G31] .

For convenience further discussions will be divided into two groups, viz. $\beta = 0$ and $\beta \neq 0$.

3.1.1 $\beta = 0$

From equation (2.7.2-6) it can be seen that $\beta = 0$ corresponds to an external flow with zero pressure-gradient, i.e. uniform main stream velocity. One of the most common situation for the realization of this flow is when a fluid flows over a flat plate at zero incidence. For this type of flow "similar" solutions exist for a main stream Mach number, $N_{Ma,G}$, of any finite constant value, greater than or approaching to zero, as has been discussed in section 2.7.2.

(a) $B \to 0$, i.e. zero-mass-transfer

The first solutions for variable fluid properties obtained for this case were for property-values varying with temperature according to power laws, e.g. $\mu \propto T^{\omega}$ where the index ω was invaribly chosen as a constant. Solutions were obtained by Busemann [S1], Karman and Tsien [S2], Hantzsche and Wendt [S3], Emmon and Brainerd [S4, S5] and, most extensive of all, Crocco [S7]. All these solutions are for constant Prandtl numbers and constant c_p with $\mu \propto T^{\omega}$ (ω varies between 0.5 to 1.25); temperature ratios T_S/T_G from 1/4 to adiabatic-surface conditions and Mach number from 0 to 12.5. Crocco [S7] in addition presented skin friction results for viscosity variations following Sutherland's formula; van Driest [S14] also used Sutherland's formula and obtained solutions for a constant N_{Pr} of 0.75 for T_S/T_G from 1/4 to 6 and $N_{Ma,G}$ from 0 to 20.

As a departure from the power-law variations, Klunker and McLean [S12, S17], Young and Janssen [S15], Moore [S16], Romig and Dore [S19] and van Driest [S20] obtained solutions explicitly for air with actual property-variations taken from tables. For these solutions the main-stream temperature T_G appears as an explicit parameter. Moore's results are for air in dissociation equilibrium. However, as pointed out by Hansen [P13] the Prandtl number for dissociated air as used by Moore is in error. Following Hansen's suggestion on the calculation of Prandtl number for dissociated air, Romig and Dore [S19] obtained "improved" solutions for air in dissociation equilibrium. This provides the most extensive results for a dissociated, laminar boundary-layer.

(b) B > 0, i.e. with gas injection

Smith [S22] considered the diffusion laminar boundary layer with variable fluid properties. As one of the boundary conditions for the momentum equation he assumed that the normal convective velocity at the plate surface is zero, i.e. $v_S = 0$. Eckert and Schneider [S30] pointed out that Smith's choice of this boundary condition is not a realistic representation of the actual situation at porous surfaces. Instead they allowed a non-vanishing v_S and stipulated that none of the main stream fluid passes through the surface (cf. section 2.6). All subsequent investigators seem to adopt this as one of the constrains to the boundary-layer equations.

Low [S28] presented results for an air-air system; Baron [S29] considered both the cases of helium and carbon-dioxide injection into an air stream. Under certain simplifying assumptions these results are independent of Mach number and temperature ratio T_S/T_G.

Sziklas [S31] reported results for a comprehensive range of mixtures: air-air, H_2O-air, He-air and H_2-air. He assumed that the value of mixture Prandtl number (= 0.72) was independent of both the temperature and composition; this produced the unexpected increase in recovery factor with blowing rates for helium and hydrogen injections. To improve on this, Sziklas and Banas [S32] obtained solutions for the same mixtures with Prandtl number allowed to vary with both the temperature and composition. Though the temperature ratio T_S/T_G was confined to unity, a range of main stream Mach number between 0 and 6 was considered. The case of helium injection was again considered by Baron and Scott [S41] for $T_S/T_G = 0.8$ and $N_{Ma} \to 0$; in addition to the

flat plate case results for $\beta = 1/2$ and $\beta = 1$ were also reported.

Eckert et al [S37, S44] considered the case of hydrogen injection. Solutions were reported for a wide range of parameters: T_G from 123° to 2000°R, T_S/T_G from 0.5 to 6 and $N_{Ma,G}$ from 0 to 12. These represent the most extensive results for the H_2-air system.

Gross [S49] studied the stability of laminar, binary boundary-layers on a flat plate and obtained solutions for skin friction and mass-fraction for three isothermal binary mixtures: H_2-air, CO_2-air and I_2-air (Iodine-air).

Baron [S48] conducted a searching discussion into the discrepancies between measured and theoretical recovery temperatures, and presented recovery factor solutions for helium injection with the hitherto neglected reciprocal effects of thermal diffusion and diffusional conduction fully accounted for; up to now these appear to be the only solutions obtained with these effects included for $\beta = 0$.

3.1.2 $\beta \neq 0$

With the exception of a few for vanishing mass-transfer rates ($B \to 0$) all the available solutions for non-zero β values are for β equal to either 1/2 or 1. Some solutions were explicitly obtained for an axi-symmetric stagnation point. However, through Mangler's transformation (section 2.7.5) these solutions can be readily converted to two-dimensional results for $\beta = 1/2$, and vice versa. The case of $\beta = 1$ corresponds to the plane stagnation flow.

As have been discussed in section 2.7.1, for constant T_G and T_S "similar" solutions for $\beta \neq 0$ exist only for $N_{Ma,G} \to 0$; hence the

Mach number does not explicitly appear as a parameter for these cases.

(a) $B \to 0$

Solutions for property-values varying according to power laws were obtained by Brown and Livingood [S13] , Ito [S18] , Levy [S21], Li and Nagamatsu [S24] , Cohen and Reshotko [S25] and Bade [S47] . While Bade restricted consideration to the $\beta = 1/2$ case, all the others covered a wide range of β values. Mark [S23] and Fay and Riddell [S35] provided results for $\beta = 1/2$ for air in dissociation equilibrium; they both covered a wide range of temperature levels.

(b) $B > 0$

All the solutions available for $B \neq 0$ are for β values of 1/2 and 1 only. Furthermore, among the hundreds of points only four are for $B < 0$, hence we shall concentrate our attention on the $B > 0$ case.

For air injection into an air stream solutions were obtained by Brown and Livingood [S13] for $\beta = 1$, and by Howe and Mersman [S38] and Libby [S45] for $\beta = 1/2$. All these authors used power-law variations of fluid properties. The case of helium injection was considered by Hoshizaki and Smith [S36] and Fox and Libby [S46] for $\beta = 1/2$, by Baron and Scott [S41] for both $\beta = 1/2$ and 1, and by Eckert et al [S50] for $\beta = 1$. Hayday [S39,S40] presented results for hydrogen injection for $\beta = 1/2$ and 1. Hurley [S42] reported solutions for $\beta = 1$ for isothermal binary mixtures of H_2-air, He-air, H_2O-air and CO_2-air.

So far, all the above mentioned solutions were obtained with the effects of both thermal diffusuon and the coupling between diffusion and heat conduction neglected. It was Baron [S48] who first

took full account of these effects and obtained results of adiabatic surface temperature with helium injection for $\beta = 1/2$. In a later publication [S51] he presented further results with helium and Freon-13 ($CClF_3$) injections, again for $\beta = 1/2$. The contrasting thermal diffusional properties of the He-air and $CClF_3$-air mixtures provide an informative comparison between the results.

The influences of the coupling between energy and mass transfer on the heat-transfer and skin-friction characteristics of laminar binary boundary-layers received more detailed consideration by Sparrow et al [S52, S53, S54] . They presented solutions for $\beta = 1/2$ and 1 for a wide range of binary mixtures with contrasting properties: H_2-air, He-air, H_2O-air, CO_2-air and Xe-air (Xenon-air). Particularly important are some results which permit a comparison to be made of the isolated effects of thermal diffusion and diffusional conduction on the boundary-layer characteristics.

3.2 Characteristics of the laminar boundary-layer solutions

The complexity of the boundary-layer equations makes it quite impossible to obtain from examination of the equations alone the influences of the various parameters on the solutions. However, as many solutions are available, it is possible, and profitable, to deduce from them the qualitative trends of the influence of such parameters as T_S/T_G, $N_{Ma,G}$, β , molecular weight ratio M_G/M_T etc. For this purpose some of the collected solutions (extracted from Tables 3.1-1 to 3.1-28) are plotted in figs. 3.2-1 to 3.2-10; based on these plots the following discussions are made. Once again we remark here that

the great majority of the solutions are explicitly obtained with air as the main stream fluid. The validity of the discussions following should be viewed bearing this in mind.

3.2.1 Effects of temperature ratio, T_S/T_G

In order to exclude as far as possible other parameters we shall examine the data for zero mass-transfer with $N_{Ma,G} \to 0$. On fig. 3.2-1 are shown the variations of the shear conductance ratio $(G_u^*)_G/(G_u^*)_{c.p.}$ with T_S/T_G for $\beta = 0$, ½ and 1; the subscript c.p. signifies that the quantity it attaches to is that for constant — properties ($T_S/T_G = 1$ in this case). As can be seen, variations of this skin-friction ratio differ according to β value . For $\beta = 0$ (flat plate) the skin friction decreases only slightly with T_S/T_G, while for $\beta = 1/2$ and 1 it increases rather rapidly with T_S/T_G. The rate of change appears to increase with β value ; the plot in diagram (a) of fig. 3.2-2 accords with this view. Physically, the increase of skin friction or the conductance $(G_u^*)_G$ with both β and T_S/T_G can be explained as follows.

As can be seen from equation (2.7.2-6), between 0 and 2 the "pressure gradient" parameter β characterize an accelerating main-stream flow; the accelerating pressure-gradient increases with increasing β values. For boundary-layer flows the same pressure gradient will be impressed by the main-stream flow on the fluid in the boundary layer. If the density of the fluid in the boundary layer is lower than that of the main-stream fluid, as in the case of $T_S/T_G > 1$, the acceleration of the boundary layer will be enhanced, producing a "steeper"

profile with higher skin friction. Obviously, higher values of the temperature ratio T_S/T_G and the parameter β will produce higher skin friction. Sometimes the acceleration of boundary layer fluid is enhanced so much that it may exceed the main stream velocity and produce an "overshoot" in the velocity profile (i.e. u/u_G first increases with distance from the surface to a value greater than 1, then decreases with increasing distance until unity is approached at infinity). This overshoot phenomenon was first discussed by Brown and Livingood in reference [S13] . By the same reasoning one can also expect this overshoot to occur when a light fluid is injected into an accelerating flow of a heavier fluid, providing T_S/T_G is not too small compared with unity. Hurley [S42] and Eckert et al [S50] do indeed provide this evidence for $\beta = 1$ with the binary systems of H_2-air, He-air and H_2O-air. Conversely, a denser fluid in the boundary layer ($T_S/T_G < 1$ and/or injection of a heavier gas) results in a lower skin friction.

On diagrams (a) to (c) in fig. 3.2-3 are plotted $(G_h^*)_G/(G_h^*)_{c.p.}$ versus R_T ($\equiv T_S/T_G$ or h_S/h_G) for $\beta = 0$, 1/2 and 1; in accordance with established practice the h_S/h_G ratio is used for dissociation data. As can be seen, the influence of R_T on the heat-transfer rates is not large. No precise trend can be detected; it, however, appears that the enthalpy conductance $(G_h^*)_G$ increases with decreasing R_T for $\beta = 0$ and 1/2, the rate of change being slightly higher for $\beta = 0$ than for $\beta = 1/2$, as can also be seen from diagram (b) of fig. 3.2-2. For $\beta = 1$ the available data show little influence of T_S/T_G; and no definite trend can be spotted.

Taking the $\beta = 1/2$ case, one notices that for the same T_S/T_G

range of 0.01 to 4, approximately, $(G_u^*)_G/(G_u^*)_{c.p.}$ varies between 0.8 and 1.7, while $(G_h^*)_G/(G_h^*)_{c.p.}$ varies only between 1.16 and 0.98.

3.2.2 Effects of main-stream Mach number, $N_{Ma,G}$ — $\beta = 0$

Once again we shall examine data for zero mass-transfer. On figs. 3.2-4a are plotted the data of $(G_u^*)_G/(G_u^*)_{c.p.}$, the abscissa being $N_{Ma,G}$. As can be seen, for a given T_S/T_G the skin friction decreases with increasing $N_{Ma,G}$; the rate of change decreases with increasing T_S/T_G. The same data are also plotted in fig. 3.2-4b, this time with T_S/T_G as the abscissa. Here it is seen that for a given $N_{Ma,G}$ the skin friction decreases with increasing T_S/T_G, the rate of decrease being higher at lower value of $N_{Ma,G}$. It appears that at very high Mach numbers the skin friction tends to become independent of T_S/T_G.

The effects of $N_{Ma,G}$ on $(G_h^*)_G$ are similar to those described above, as may be inferred from figs. 3.2-5a and 3.2-5b.

The variations of zero-mass-transfer recovery factors with Mach number are shown in figs. 3.2-6a and 3.2-6b. The temperature recovery factors, $N_{RF,T}^*$, are contained in fig. 3.2-6a; as can be seen there, when N_{Pr} and c_p are both constant, $N_{RF,T}^*$ is almost independent of $N_{Ma,G}$. However, if both N_{Pr} and c_p vary with temperature, then $N_{RF,T}^*$ decreases with increasing $N_{Ma,G}$. For a given $N_{Ma,G}$ the values of $N_{RF,T}^*$ can differ quite appreciably, according to the variations of the fluid properties. This is evident from the distinct curves for three T_G's obtained by Young-Janssen in fig. 3.2-6a.

On fig. 3.2-6b the enthalpy recovery factors, N_{RF}^*, are

plotted against $N_{Ma,G}$. There it is seen that the data separate themselves into two groups: those for dissociation air and those for non-dissociation air. In both groups, however, $N_{Ma,G}$ has only small influences on N^*_{RF} . Furthermore, the effects of main stream temperature on the enthalpy recovery factor are much smaller than the corresponding effects on the temperature recovery factor $N^*_{RF,T}$, as may be verified by comparing the same data of Young and Janssen in both figs. 3.2-6a and 6b.

3.2.3 Effects of injection of different gases

Generally, the injection of any gas into a gas stream has the effect of reducing the local skin-friction or the conductance $(G_u)_G$ and heat-transfer rate or the conductance $(G_h)_G$, as well as $(G_f)_G$ and the recovery factor $N_{RF,T}$. This may be seen from the plots of the exact solutions in figs. 3.2-7a to 3.2-7e for $\beta = 0$, figs. 3.2-8a to 3.2-8f for $\beta = 1/2$ and figs. 3.2-9a to 3.2-9d for $\beta = 1$.

When the gases are inert ones the injection usually acts in two ways. Firstly, the blowing causes the boundary layers to thicken, reducing the skin friction and the heat-transfer rate. Secondly, the added mass may act as a sort of distributed heat sink, which further lowers the heat-transfer rate.

However, if the external flow field is of a highly accelerating type (as, for example, when $\beta = 1$) and the surface temperature is higher than the main stream temperature ($T_S/T_G > 1$), the injection of a light gas into a heavier one might at first cause a slight increase in the skin friction. This can be seen from curves 1A and 1E

in fig. 3.2-9a showing variations of $(G_u)_G$ with B_u for $\beta = 1$. The cause for this has been explained in section 3.2.1.

If a gas of high thermal conductivity (helium, for example) is injected into a gas having comparatively low thermal conductivity (air, for example) the heat-transfer rate may at first increase with the injection rate and then decreases with it steadily. This is due to the fact that at small blowing rates the high thermal conductivity of the injected gas successfully counteracts the comparatively small blowing effect, causing an increase in the heat-transfer rate. At higher injection rates, however, the blowing effect becomes dominant and the heat-transfer rate decreases steadily. A good example of this is provided by curve 7 for helium injection at a two-dimensional stagnation-point in fig. 3.2-9c.

The injection of different gases into an air stream produces different effects. Generally, at a given injection rate and for the same boundary conditions the injection of a lighter gas produces a higher reduction in the conductances g_u, g_h, and g_f. Reference may be made to fig. 3.2-7a showing variations of $(G_u)_G$ with B_u for $\beta = 0$. There it may be seen that curves 5 (I_2-air), 4 (CO_2-air), constant-properties (air-air), 1 (H_2O-air), 2D (He-air) and 3 (H_2-air), all for $T_S/T_G = 1$ and $N_{Ma} \to 0$, lie progressively lower in the above order.

When the effects of thermal diffusion and diffusional conduction in binary mixtures are neglected the qualitative effects of injection of different gases on the temperature recovery factor $N_{RF,T}$ are the same as on the various conductances. This may be seen in diagram (A) of fig. 3.2-7d. Diagram (B) of fig. 3.2-7d is inserted merely to show

the unexpected increase in $N_{RF,T}$ with the injection rate $\dot{m}''/(\mu_G \rho_G u_G/x)^{1/2}$ for He-air and H_2-air (curves 3A, 3B, 4A, 4B and 4C). This is entirely due to the incorrect assumption that the Prandtl number is constant, i.e. independent of both compositiin and temperature.

Fig. 3.2-7e shows the variation of $N_{RF,T}$ with $\dot{m}''/(\mu_G \rho_G u_G/x)^{1/2}$ for the H_2-air mixture for various values of $N_{Ma,G}$ and T_G. Comparison of curves 2C, 2D, 2G and 2J (all for $N_{Ma,G} = 4$) reveals that T_G exerts quite a large influence on the recovery factor.

3.2.4 Effects of thermal diffusion (TD) and diffusional conduction (DT)

Some of the more obvious effects of thermal diffusion and diffusional conduction can be revealed by examining the surface mass-flux and energy-flux expressions, viz.:

$$\dot{m}'' = -\left[\frac{\Gamma_i}{1-m_i}\left(\frac{\partial m_i}{\partial y} + \frac{m_i(1-m_i)\alpha_T}{T}\frac{\partial T}{\partial y}\right)\right]_s \qquad (2.6\text{-}9)$$

and

$$-\dot{q}_s'' = -\left(k\frac{\partial T}{\partial y}\right)_s + \mathcal{R}\left[\frac{(1-m_i)T\alpha_T}{M_i + (M_j - M_i)m_i}\right]_s \dot{m}'' \qquad (2.6\text{-}10)$$

In the absence of any mass addition ($\dot{m}'' = 0$) equation (2.6-9) indicates the existence of a temperature gradient as well as a concentration gradient in the equilibrium state. For an i species of relatively low molecular weight, α_T is negative and an enrichment of the i species takes place at the higher temperature zones.

Equation (2.6-10) shows that whenever there is mass addition ($\dot{m}'' > 0$) the presence of the DT term may produce a finite heat-flux when the surface temperature-gradient vanishes; and a zero heat-flux condition (adiabatic surface) may not be accompanied by a vanishing

temperature gradient. This tends to suggest the important role played by DT in influencing the adiabatic-surface temperature.

To assess the relative importance between the TD and the concentration diffusion terms, and between the DT and the thermal conduction terms, we make use of the ratios formed by the respective, corresponding terms, viz. :

$$R_{TD} \equiv \left[\frac{\alpha_T m_i (1-m_i)\, \partial(\ln T)/\partial y}{\partial m_i/\partial y} \right]_S \qquad (3.2.4\text{-}1)$$

and

$$R_{DT} \equiv \left[\frac{\dot{m}'' \mathcal{R} (1-m_i) T \alpha_T \{M_i + (M_j - M_i) m_i\}}{k\, \partial T/\partial y} \right]_S \qquad (3.2.4\text{-}2)$$

Based on the flat plate solutions obtained for He-air with $\alpha_T = 0$, Baron [S48] evaluated these ratios for a range of the temperature ratio $T_S/T_{S,ad}$. On figs. 3.2-11(a) and 3.2-11(b) are replotted these ratios against $\dot{m}''/(\mu_G \rho_G u_G / x)^{1/2}$, from which some interesting, though necessarily approximate, points may be noted.

Fig. 3.2-11(a) shows that for a given injection rate the effect of thermal diffusion on mass-flux increases with increasing heat-transfer rate or decreasing $T_S/T_{S,ad}$ ratio; it also increases with decreasing injection rate.

Fig. 3.2-11(b) showing the relative importance of the DT term and the heat conduction term suggests that R_{DT} approaches infinity as $T_S/T_{S,ad}$ tends to unity. This underlines the much more pronounced effect of DT on the heat-flux near the adiabatic conditions. On the other hand for a highly cooled surface ($T_S/T_{S,ad}$ small) the heat conduction term dominates.

As can be seen from equations (2.4.1-1, -2, -5, -6, and -7) the interaction of the transports of energy and mass introduces additional complications into the boundary-layer equations. Even in the case of one-dimensional Couette flow the differential equations are still highly coupled. To gain more insight into the effects of TD and DT we shall now revert to examining the solutions obtained with these effects included, so that their influences on $T_{S,ad}$, $\dot{q}''_S$, as well as on the conductances g_h, g_u and g_f may be ascertained.

a) Adiabatic surface temperature, $T_{S,ad}$

Examination of the solutions available reveals that one of the more pronounced effects of TD and DT is the alteration of the adiabatic surface temperature (i.e. surface temperature attained when $\dot{q}''_S = 0$). Without these thermal-diffusional effects the condition $\dot{q}''_S = 0$ can be taken as meaning $(\partial T/\partial y)_S = 0$; when they are present this is no longer true. Instead the much more complicated expression of (2.7.1-22) prevails.

The effect of TD is contained in the last term of the diffusion equation (2.7.1-12); while that of DT is contained in the L.H.S. terms of the energy equation (2.7.1-14). By neglecting appropriate terms it is possible to take into account of only one of these two effects. This was tried by Sparrow et al [S52, S53] . Their results show that the DT effect has by far the stronger influence on the adiabatic surface temperature, $T_{S,ad}$. On figs. 3.2-10(a) and 10(b) are plotted all the available exact solutions for $(T_{S,ad} - T_G)/T_G$ for $\beta = \frac{1}{2}$ and 1.

In both figures the closeness of curves 1A (with DT & TD) and 1B (with DT only) clearly illustrates the dominating influence of DT over that of TD. Although results for He-air only are available to show this, the same is expected to apply for other binary mixtures. Perhaps this could have been deduced from the fact that the DT term is directly involved in the energy equation while the TD term operates via the diffusion equation.

Further examination of figs. 3.2-10(a) and 10(b) shows that the ratio $(T_{S,ad} - T_G)/T_G$ increases with the injection rates; also the temperature level, as characterized by T_G, can exert quite a large influence on $T_{S,ad}$ in certain binary mixtures, e.g. He-air. Another important feature is that when the injectant is lighter than air (the main stream fluid) $T_{S,ad}$ is greater than T_G; when it is heavier, $T_{S,ad}$ is less than T_G. However, the magnitude of these effects cannot be simply related to the molecular weight ratio, M_G/M_T.

b) Surface heat flux, $\dot{q}''_S$

Fig. 3.2-12a shows a plot of $\dot{q}''_S/(\dot{q}''_S)^*$ vs. $\dot{m}''/(\mu_G\rho_G u_G/x)^{1/2}$ with helium injection at a two-dimensional stagnation point for the two cases: $T_G = 520^\circ R$, $T_S/T_G = 1.1$ and $T_G = 5000^\circ R$, $T_S/T_G = 0.2$. For each case three curves were obtained corresponding to: (1) neither DT (diffusional conduction) nor TD (thermal diffusion), (2) with DT and TD and (3) with DT only. It can be seen that for $T_S/T_G = 1.1$ the influences of diffusional conduction on $\dot{q}''_S$ are very significant while that of thermal diffusion is only very small; this is manifested by the closeness of the two curves "with DT and TD" and "with DT only" and the much higher curve for "neither DT nor TD". For the case with a highly cooled wall,

$T_S/T_G = 0.2$, all three curves are quite close together, incicating the much smaller influence on $\dot{q}''_S$ of both TD and DT.

The behaviour observed above may be explained by reference to expression (2.6-10) for $\dot{q}''_S$, which may be re-written as:

$$\frac{-\dot{q}''_S}{T_G} = -\left(k\frac{\partial\theta}{\partial y}\right)_S + \mathcal{R}\left[\frac{(1-m_i)\,\alpha_T}{M_i + (M_j - M_i)m_i}\right]_S \frac{T_S}{T_G}\cdot\dot{m}'' \qquad (3.2.4\text{-}1)$$

In the case when $T_S/T_G = 1.1$, $\left(-k\,\partial\theta/\partial y\right)_S$ is positive. For a helium-air mixture α_T is negative, but $\dot{m}''$ and $(1-m_{i,S})/\left[M_i + (M_j - M_i)\,m_{i,S}\right]$ are positive, hence the DT term, second term of R.H.S. of (3.2.4-1), is negative, i.e. of opposite sign to the conduction term $\left(-k\partial\theta/\partial y\right)_S$. Since T_S/T_G is close to unity the thermal conduction term is of moderate magnitude. At larger values of $\dot{m}''$, the DT term becomes of comparable magnitude. Thus we observe that as $\dot{m}''/(\mu_G\rho_G u_G/x)^{1/2}$ increases the difference between the curves "with neither DT nor TD" and "with DT only" increases (fig. 3.2-12a). In fact, at $\dot{m}''/(\mu_G\rho_G u_G/x)^{1/2}$ larger than about 0.225 the sign of $\dot{q}''_S$ reverses.

For the case of the highly-cooled surface T_S/T_G (=0.2) is much less than unity; the conduction term is of much larger magnitude. With T_S less than T_G $\left(-k\partial\theta/\partial y\right)_S$ is negative and the DT term is also negative as has been seen above; hence these two effects augment each other. However, as the conduction term is now of much larger magnitude, it overshadows the influence of the DT term.

Similar inferences may be made from the data of Baron [S51] for $\beta = \frac{1}{2}$, which are plotted in fig. 3.2-12b for the mixtures of He-air and $CC1F_3$-air, though in these plots the individual effects of TD and

diffusional conduction can not be isolated.

The above findings are in accord with the representation on diagram (b) in fig. 3.2-11. Thus one may summarize [S52] : the influences on the heat-transfer rate of thermal diffusion and diffusional conduction will be large only when T_S/T_G is close to unity (laboratory type situations); whenever these diffusional effects are significant, the dominating one is diffusional conduction rather than thermal diffusion.

c) Enthalpy conductance, g_h

The existence of an adiabatic surface temperature different from the main stream temperature even in the absence of any kinetic heating suggests that the following definition for the enthalpy conductance should be used, irrespective of flow speed:

$$g_h \equiv \frac{\dot{q}''_S}{h_{GS,ad} - h_{GS}} \qquad (3.2.4\text{-}2)$$

Of course, when the effects of TD and DT are neglected and the flow is of negligible kinetic heating, $T_{S,ad} = T_G$, and $h_{GS,ad}$ simply becomes h_G.

From an examination of all the exact solutions collected, the conclusion is reached that the enthalpy conductance g_h as defined in (3.2.4-2) is only slightly affected by TD and DT. This may be readily seen by comparing the corresponding curves for "neither TD nor DT" and for "with TD and DT" in figs. 3.2-8b, 8c, 8d and 8e for β=1/2 and figs. 3.2-9b and 9c for β= 1. There is no solution available for β = 0 with TD and DT taken into account. However, the results of

the one-dimensional analyses made by Twefik et al [G33] and Tewfik [G34] for the binary mixtures of He-air, H_2-air and CO_2-air fully support the above conclusion. We thus expect that the same should apply also to the two-dimensional flat-plate case.

As the great majority of the solutions for the problem under consideration were obtained with these thermal-diffusional effects neglected the above finding allows these solutions to be used without much error, provided g_h is defined as in equation (3.2.4-2).

d) Conductances g_u and g_f

A close study of the solutions available shows that the influence of TD and DT on the skin friction or g_u is very small. Some idea of the magnitude of these effects may be gained by reference to fig. 3.2-8a showing $(G_u)_G$ vs. B_u for β=1/2, from which the results of Baron and Scott for helium injection (cross points) "with neither TD nor DT" may be compared with those of Sparrow et al, curve 2c, for "with TD and DT", both are for T_S/T_G = 0.8 and T_G = 570°R.

The influence of TD and DT on g_f, however, is slightly larger, as may be ascertained from curves 1A - 1D and 4A -4D in fig. 3.2-8c showing $(G_f)_G$ vs. B_f for β= 1/2 with helium and Freon-13 ($CC1F_3$) injections.

CHAPTER 4 CORRELATION OF SOLUTIONS

4.1 The need for a correlation method in engineering applications

Though the number of exact solutions available are quite large, they are still not sufficient to cover adequately the practical ranges of such parameters as T_S/T_G, $(N_{Ma})_G$ or molecular weight ratio M_G/M_T. With the help of modern electronic computers the solving of the differential equations to the problem does not present any unusual difficulties; it nevertheless is still a rather time-consuming task. It is thus desirable to have a correlation method, with which interpolation, and perhaps extrapolation, of the solutions already obtained can be achieved simply and with an accuracy sufficient for engineering applications.

4.2 Correlation methods available

Nearly all the methods available in correlatung the variable-property solutions make use of the concept of a "reference state", at which property values are to be evaluated so that the dimensionless groups of such quantities as, for example, wall shear-stress, may be approximated to the corresponding constant-property value. In the case of zero mass-transfer the reference state becomes merely the "reference temperature"; for a binary boundary layer the reference state may mean a mixture at a certain "reference temperature" and with a certain "reference composition".

The use of a reference temperature was apparently first introduced by Rubesin and Johnson [G25] , who studied the skin-friction

results for a flat plate obtained by Karman and Tsien and Crocco, and recommended:

$$\frac{T_{ref}}{T_G} = 1 + 0.32(N_{Ma,G})^2 + 0.58\left(\frac{T_S}{T_G} - 1\right) \qquad (4.2\text{-}1)$$

Later, Young and Janssen [S15] derived from their own solutions for a flat plate the same expression (4.2-1) for the reference temperature for $N_{Ma,G}$ up to 5, and for $N_{Ma,G}$ between 5 and 10 they recommended:

$$\text{Adiabatic-surface case} - \frac{T_{ref}}{T_G} = 0.0556\left(13\frac{T_{S,ad}}{T_G} + 6\right) \qquad (4.2\text{-}2)$$

$$\text{Heat-transfer case} - \frac{T_{ref}}{T_G} = 0.70 + 0.023(N_{Ma,G})^2 + 0.58\frac{T_S}{T_G} \qquad (4.2\text{-}3)$$

Re-examining Young and Janssen's solutions, Eckert [G7, G8] arrived at the following single reference temperature expression, which is valid for the whole Mach number range as well as for the two cases of $T_S = T_{S,ad}$ and $T_S \neq T_{S,ad}$:

$$\frac{T_{ref}}{T_G} = 0.5\left(1 + \frac{T_S}{T_G}\right) + 0.22\left(\frac{T_{S,ad}}{T_G} - 1\right) \qquad (4.2\text{-}4)$$

Since then this expression has been the most widely used one. For this reason we shall in later discussions refer to this as the representative of the reference temperature formulae.

There are at present two procedures available for the correlation of variable-property laminar-boundary-layer solutions, which can be applied to non-zero mass-transfer case. These are the methods of Eckert/Gross-Hartnett-Masson-Gazley (abbreviated as E/G-H-M-G) and

Knuth. Before proceeding with the discussion of these two methods in greater details we note for the sake of completeness the correlating formula obtained by Young [G35] for the skin friction on a flat plate when there is no mass-transfer and N_{Pr} is constant:

$$\frac{c_f\sqrt{N_{Re}}}{2} = \frac{g_u^*}{\sqrt{\mu_G \rho_G u_G / x}} = 0.332\left[0.45 + 0.55\,\frac{T_S}{T_G} + 0.09(\gamma-1)(N_{Ma})_G^2 (N_{Pr})^{1/2}\right]^{\frac{\omega-1}{2}}$$

where γ is the ratio of specific heats, and ω is the index for the variation of viscosity with temperature: $\mu \propto T^{\omega}$. Because of the rather restricted application of this formula we shall not discuss it any more.

4.2.1 Method of Eckert/Gross-Hartnett-Masson-Gazley, (E/G-H-M-G)

As the name implies this is a composite method consisting of Eckert's method [G7, G8] for zero-mass-transfer and that of Gross, Hartnett, Masson and Gazley [G14] for non-zero mass-transfer; both these methods make use of a reference enthalpy or reference temperature.

For a flat plate ($\beta = 0$) without mass transfer Eckert [G7, G8] recommended the following procedure for calculating the recovery factors, shear conductance g_u or skin friction factor c_f and the enthalpy conductance g_h.

(i) The reference enthalpy or reference temperature is calculated by solving the following pairs of equations:

$$\frac{h_{ref}}{h_G} = \frac{1}{2}\left(1 + \frac{h_S}{h_G}\right) + 0.22\, N_{RF}^* \frac{\gamma_G - 1}{2} (N_{Ma})_G^2 \qquad (4.2.1\text{-}1)$$

and

$$N_{RF}^* = \sqrt{(N_{Pr})_{ref}} \qquad (4.2.1\text{-}2)$$

where the suffix "ref" signifies that the property values are to be evaluated at the reference state;

$$\frac{T_{ref}}{T_G} = \frac{1}{2}\left(1+\frac{T_S}{T_G}\right) + 0.22\, N^*_{RF,T}\,\frac{\gamma_G-1}{2}\,(N_{Ma})^2_G \qquad (4.2.1\text{-}3)$$

and $$N^*_{RF,T} = \sqrt{(N_{Pr})_{ref}} \,. \qquad (4.2.1\text{-}4)$$

The enthalpy expression (4.2.1-1) reduces to the temperature expression (4.2.1-3) when the specific heat is constant; hence expression (4.2.1-3) may be regarded as a particular case of the more general expression (4.2.1-1). Expressions (4.2.1-3) and (4.2.1-4) are inserted as they are required in the method of Gross-Hartnett-Masson-Gazley.

(ii) The skin friction factor and the shear conductance can then be calculated from:

$$\left(\frac{c_f}{2}\sqrt{\frac{u_G x}{\nu}}\right)_{ref} = \frac{g^*_u}{\sqrt{(\mu\rho)_{ref}\,u_G/x}} = 0.332 \,, \qquad (4.2.1\text{-}5)$$

also: $$(G^*_u)_G \equiv \frac{\sqrt{2-\beta}\; g^*_u}{\sqrt{\mu_G \rho_G u_G/x}} = 0.4696\left[\frac{(\mu\rho)_{ref}}{(\mu\rho)_G}\right]^{\frac{1}{2}} \qquad (4.2.1\text{-}6)$$

(iii) The enthalpy conductance is determined from:

$$\frac{g^*_h}{g^*_u} = (N_{Pr})^{-2/3}_{ref} \qquad (4.2.1\text{-}7)$$

In terms of $(G^*_h)_G$ and $(G^*_u)_G$ we have:

$$\frac{(G^*_h)_G}{(G^*_u)_G} = \frac{\sqrt{2-\beta}\;(N_{Pr})^{2/3}_G\; g^*_h/\sqrt{\mu_G\rho_G u_G/x}}{\sqrt{2-\beta}\;\; g^*_u/\sqrt{\mu_G\rho_G u_G/x}} = \left[\frac{(N_{Pr})_G}{(N_{Pr})_{ref}}\right]^{2/3} \qquad (4.2.1\text{-}8)$$

For a flat plate with different gases injected into an air stream, Gross, Hartnett, Masson and Gazley [G14] recommended the

following formula for calulating g_u and the heat-transfer rate $\dot{q}''_S$:

$$\frac{g_u}{g_u^*} = \frac{(G_u)_G}{(G_u^*)_G} = 1 - 2.08\left(\frac{M_G}{M_T}\right)^{1/3} \frac{\dot{m}''}{\sqrt{(\mu\rho)_{G,ref}\, u_G/x}} \qquad (4.2.1\text{-}9)$$

$$\frac{\dot{q}''_S}{(\dot{q}''_S)^*} = 1 - 1.82\left(\frac{M_G}{M_T}\right)^{1/3} \frac{\dot{m}''}{\sqrt{(\mu\rho)_{G,ref}\, u_G/x}} \qquad (4.2.1\text{-}10)$$

The suffix "G,ref" signifies that the properties are evaluated for the fluid with G-state composition but at a reference temperature T_{ref} ; for air as the main stream fluid this means that $(\mu\rho)$ is evaluated for air at the reference temperature T_{ref}. The recommended reference temperature is as given by equation (4.2.1-3).

The surface mass fraction for the injected gas $m_{i.S}$ is to be deduced from a series of curves, $m_{i,S}$ vs. $\dot{m}''/\left[(\mu\rho)_{G,ref} u_G/x\right]^{1/2}$, each curve being valid for a particular mixture. These curves are reproduced in fig. 4.2-1. The temperature recovery factor ratios $N_{RF,T}/N^*_{RF,T}$ are similarly correlated and the corresponding curves are also shown in fig. 4.2-1; as may be seen, the correlation is not very successful with the mixtures of H_2-air and He-air.

The authors also considered correlating the Stanton number ratio, N_{St}/N^*_{St} $\left(N_{St} \equiv \dot{q}''_S/\left[(\rho u c_p)_G\,(T_{S,ad} - T_G)\right]\right)$ in the same way as they treated g_u/g_u^* and $\dot{q}''_S/(\dot{q}''_S)^*$. However, they did not recommend the use of this as it does not yield as good a result as in the case of the heat-transfer rate ratio.

4.2.2 Method of Knuth

This is another method employing the concept of a "reference state". While all the others mentioned so far obtained the reference

state by a purely empirical method, Knuth made use of a much simplified Couette flow model in the derivation of the reference state. The Couette-flow expressions for the reference temperature and composition were then empirically adjusted to give good correlation to boundary-layer solutions. Knuth finally recommended the following reference temperature and reference enthalpy expressions for laminar boundary-layer flows:

$$\frac{T_{ref}}{T_G} = 0.5\left(1+\frac{T_S}{T_G}\right)+0.2\,N^{*}_{RF,T}\,\frac{u_G^2}{2\,c_{p,ref}\,T_G}+0.1\left[E_{h,ref}+\left(E_{h,ref}+E_{m,ref}\right)\frac{c_{p_i}-c_{p_{ref}}}{c_{p\,ref}}\right]\left(\frac{T_S}{T_G}-1\right) \qquad (4.2.2\text{-}1)$$

$$\frac{h_{ref}}{h_G} = 0.5\left(1+\frac{h_S}{h_G}\right)+0.2\,N^{*}_{RF,T}\,\frac{u_G^2}{2h_G}+0.1\left[E_{h,ref}+\left(E_{h,ref}-2E_{m,ref}\right)\frac{c_{p_i}-c_{p_{ref}}}{c_{p\,ref}}\right]\left(\frac{h_S}{h_G}-1\right) \qquad (4.2.2\text{-}2)$$

The E's are defined by:

$$E_{f,ref} \equiv \frac{\dot{m}''/\sqrt{(\mu\rho)_{ref}\,u_G/x}}{0.332} \qquad (4.2.2\text{-}3)$$

$$E_{m,ref} \equiv E_{f,ref}\left(N_{Sc}\right)_{ref}^{0.64}\left[\frac{g_u/\sqrt{(\mu\rho)_{ref}\,u_G/x}}{0.332}\right]^{1/6} \qquad (4.2.2\text{-}4)$$

$$E_{h,ref} \equiv E_{f,ref}\left(N_{Pr}\right)_{ref}^{0.64}\left[\frac{g_u/\sqrt{(\mu\rho)_{ref}\,u_G/x}}{0.332}\right]^{1/6} . \qquad (4.2.2\text{-}5)$$

The reference mixture is given by:

$$m_{i,ref} = 1-\frac{M_j/M_i}{M_j/M_i-1}\,\frac{\ln\left[\frac{M_j}{M_i}+\left(\frac{M_j}{M_i}-1\right)\left(1-m_{i,S}\right)\right]}{\ln\left[\frac{M_j/M_i}{1-m_{i,S}}+\frac{M_j}{M_i}-1\right]} \qquad (4.2.2\text{-}6)$$

With the reference state compllelely defined, Knuth then

recommended two curves, one connecting the conductances with mass-transfer rates and the other connecting the recovery factor and mass-transfer rates. The respective ordinate and abscissa are listed in Table 4.2-1.

As a typical application of the method, we assume that the following data are provided:

T_G, T_S/T_G , u_G, M_j/M_i, T_T, together with details of property-variations. If we regard these quantities and any others that can be computed from these not as variables, Knuth's method may be broken up into the following six functional relationships for the unkowns:

$$m_{i,ref} = f_1 \{ B_f \} \tag{4.2.2-7}$$

$$T_{ref} = f_2 \{ T_{ref}, m_{i,ref}, B_f, g_u, \dot{m}'' \} \tag{4.2.2-8}$$

$$g_u = f_3 \{ \dot{m}'', T_{ref}, m_{i,ref} \} \tag{4.2.2-9}$$

$$g_f = f_4 \{ \dot{m}'', T_{ref}, m_{i,ref}, g_u \} \tag{4.2.2-10}$$

$$g_h = f_5 \{ \dot{m}'', T_{ref}, m_{i,ref}, g_u, N_{RF} \} \tag{4.2.2-11}$$

$$N_{RF} = f_6 \{ \dot{m}'', T_{ref} , m_{i,ref} , g_u \} \tag{4.2.2-12}$$

With the coolant supply conditions known we can make use of the expression for B_h in equation (2.7.4-3a), viz. (when radiation effect is neglected):

$$B_h = (h_{GS,ad} - h_{GS}) / (h_{TS} - h_T)$$
$$= \dot{m}''/g_h$$

This permits us to write, in accordance with the previous stipulations, the additional functional relationship:

$$g_h = f_7 \{ \dot{m}'', N_{RF} \} \qquad (4.2.2\text{-}13)$$

In the seven functional relationships (4.2.2-7) to (4.2.2-13) there are seven independent unknowns (since B_f, $\dot{m}''$ and g_f are connected by $g_f = \dot{m}''/B_f$, only two of these are independent): T_{ref}, $m_{i,ref}$, $\dot{m}''$, g_u, g_h, g_f, and N_{RF}. Hence they may be determined. As the functions are interlinked, the determination of these knowns invariably involves some process of iteration.

4.3 A new correlation procedure

4.3.1 Introduction

Both of the above two methods described suffer from the drawback that detailed knowledge of the fluid properties is required. In this connection the E/G-H-M-G method is better because only the main stream fluid properties are required, while Knuth's method needs all details of the variation of mixture properties with both temperature and composition.

Of the two, the method of E/G-H-M-G is much simpler to use, but it does not give satisfactory correlation oof the surface mass-fraction and the recovery factor, as manifested by the need of using different curves for different binary system in fig. 4.2-1.

Although both the methods are derived for the flat plate case, they have also been recommended for use in flows with pressure gradient, for example, with $\beta = 1/2$ or 1. While this may be successful for the enthalpy conductance g_h, the methods may be greatly in error for the skin friction.

According to the reference enthalpy method, for zero-mass-transfer,

$$\frac{g_u^*}{\sqrt{(\mu\rho)_{ref} u_G/x}} = \left[\frac{g_u^*}{\sqrt{\mu\rho\, u_G/x}}\right]_{c.p.}$$

i.e $$\frac{(G_u^*)_G}{(G_u^*)_{c.p.}} = \sqrt{\frac{(\mu\rho)_{ref}}{(\mu\rho)_G}}$$ irrespective of β values if $(N_{Ma})_G \to 0$.

Similarly, $$\frac{(G_h^*)_G}{(G_h^*)_{c.p.}} = \left[\frac{N_{Pr,ref}}{(N_{Pr})_{c.p.}}\right]^{2/3}$$.

If we consider the case when $N_{Ma,G} \to 0$, then according to the above, for the same T_S/T_G ratio, the ratios $(G_u^*)_G/(G_u^*)_{c.p.}$ and $(G_h^*)_G/(G_h^*)_{c.p.}$ should be constant for all β values. However, reference to figs. 3.2-1, 3.2-2 and 3.2-3 shows that this may not be the case. As may be seen from fig. 3.2-3, for a given T_S/T_G value $(G_h^*)_G/(G_h^*)_{c.p.}$ does not vary very much over the β value range from 0 to 1. However, fig. 3.2-1 clearly shows that for $T_S/T_G = 4$ the ratio $(G_u^*)_G/(G_u^*)_{c.p.}$ varies from 0.9 to over 1.8 when the β value changes from 0 to 1; furthermore, the trends of variation of $(G_u^*)_G$ with T_S/T_G are of opposite nature for $\beta = 0$ and for $\beta = 1/2$ and 1. Thus if the reference state method is successful in accounting for the effect of T_S/T_G on $(G_u^*)_G$ for $\beta = 0$, the same method cannot possibly be successful when applied to the case of $\beta > 0$.

With the goal of overcoming the aforementioned shortcomings of both the methods of E/G-H-M-G and Knuth, the new procedure is developed.

4.3.2 Development of the new procedure

4.3.21 The conductances — $(G_u)_G$, $(G_h)_G$ and $(G_f)_G$

a) Basic functions

From plots of $(G)_G$ vs. B (omission of the subscript to the conductance G means that the discussions following hold for all the three definitions of conductances introduced) it is observed that for a given flow configuration, i.e. for a particular value of β, the curves generally exhibit great regularity with respect to the governing parameters T_S/T_G, $(N_{Ma})_G$ and M_G/M_T. Furthermore, any particular curve can be brought close to the corresponding constant-property one by first multipling the driving force by a constant F_B, and then by multiplying the ordinate by another constant $F_{g,T/N_{Ma}}$. The constant F_B does not vary much for a given binary mixture; and $F_{g,T/N_{Ma}}$ is almost independent of the type of gas injected. This suggests that we can stipulate the following general relationship, rather similar to the parallel case of turbulent boundary layers investigated by Spalding et al [G30] :

$$(G)_G \cdot F_{g,T/N_{Ma}}\left\{\frac{T_S}{T_G},\ N_{Ma,G},\ \beta\right\} = f\left(B \cdot F_B\left\{\frac{T_S}{T_G},\ N_{Ma,G},\ \frac{M_G}{M_T},\ \beta\right\},\ \beta\right) \qquad (4.3.2\text{-}1)$$

As may be seen, this form of correlation removes the need for detailed knowledge of any property variations. The functions $F_{g,T/N_{Ma}}$ and F_B have the following properties:

$$\left.\begin{aligned} F_{g,T/N_{Ma}} &= 1 \text{ for all } \beta \text{ values when } T_S/T_G = 1 \ \&\ (N_{Ma})_G = 0 \\ F_B &= 1 \text{ for all } \beta \text{ values when } T_S/T_G = 1,\ (N_{Ma})_G = 0 \ \&\ M_G/M_T = 1 \end{aligned}\right\} \qquad (4.3.2\text{-}2)$$

Of course, the relationship (4.3.2-1) allows the functions $F_{g,T/N_{Ma}}$ and F_B to vary according to the definition of the conductance, e.g.

$F_{g_u,T/N_{Ma}}$ may differ from $F_{g_h,T/N_{Ma}}$ etc.

In the formulation of (4.3.2-1) it has been implied that the function f is that appropriate for air as the main stream fluid ($N_{Pr/Sc} = 0.7$ assumed). Thus for constant-property case equation (4.3.2-1) reduces simply to :

$$(G)_{c.p.} = f\{B, \beta\} \quad , \tag{4.3.2-3}$$

and when in addition $B = 0$, we have:

$$(G^*)_{c.p.} = f\{\beta\} \quad . \tag{4.3.2-4}$$

The parameter N_{Pr} or N_{Sc} does not explicitly appear. The reason for adopting this lies in the fact that, excluding a few solutions for the zero-mass-transfer case, all the available exact solutions are for air as the main stream fluid; the validity of any correlation procedure derived from these solutions can hardly go beyond this restriction.

As has been remarked, the dependence of F_B on T_S/T_G and $N_{Ma,G}$ is only slight. Thus it seems reasonable to split the function into the following form, so as to facilitate its determination:

$$\boxed{F_B = F_{B,T/N_{Ma}}\left\{\frac{T_S}{T_G}, N_{Ma,G}, \beta\right\} \cdot F_{B,M}\left\{\frac{M_G}{M_T}, \beta\right\}} \tag{4.3.2-5}$$

And $F_{B,T/N_{Ma}}$ and $F_{B,M}$ have the following properties:

$$\left.\begin{aligned} F_{B,T/N_{Ma}} &= 1 \text{ for all } \beta \text{ values when } T_S/T_G = 1 \ \& \ N_{Ma,G} = 0 \\ F_{B,M} &= 1 \text{ for all } \beta \text{ values when } M_G/M_T = 1 \end{aligned}\right\} \tag{4.3.2-6}$$

(b) How the functions may be determined

Here we shall very briefly indicate how the functions $F_{G,T/N_{Ma}}$ $F_{B,T/N_{Ma}}$ and $F_{B,M}$ may be determined from the solutions available. Details of their derivation will be discussed in section 4.3.3.

Relation (4.3.2-1) yields for B = 0:

$$(G^*)_G \cdot F_{g,T/N_{Ma}}\{T_S/T_G,\ N_{Ma,G},\ \beta\} = f\{\beta\} \quad . \qquad (4.3.2\text{-}7)$$

Thus the function $F_{g,T/N_{Ma}}$ can be determined from the zero-mass-transfer data alone. Once this function has been determined the function $F_{B,T/N_{Ma}}$ may then be determined from the data for $M_G/M_T = 1$, i.e. injection of air into an air stream. With these two functions found the third function $F_{B,M}$ can be derived from mass-transfer data other than those for the air-air system.

4.3.22 Recovery factors – flat plate only

(a) Enthalpy recovery factors, N_{RF}

For the zero-mass-transfer case, no noticeable variation of the enthalpy recovery factor N^*_{RF} with main stream Mach number is observed, as may be inferred from fig. 3.2-6b. Nor is there any appreciable influence of the main-stream temperature level observed. However, fairly large differences between the values of N^*_{RF} for air in dissociation equilibrium and those for non-dissociating air. Thus, as a simple approximation, we may take:

$$\left.\begin{aligned} N^*_{RF} &= 0.825 \quad \text{for non-dissociating air with } T_G \text{ between} \\ &\qquad 100 \text{ and } 800^\circ R \text{ and } (N_{Ma})_G \text{ up to } 16; \\ \text{and} \quad N^*_{RF} &= 0.95 \quad \text{for air in dissociation equilibrium with} \\ &\qquad T_G \text{ between } 800 \text{ and } 7000^\circ R \text{ and } (N_{Ma})_G \text{ up to } 17. \end{aligned}\right\} \quad (4.3.2\text{-}8)$$

For the case with gas injections the recovery factors are usually defined in terms of temperatures, and we shall discuss them under heading (b) below.

(b) Temperature recovery factors, $N_{RF,T}$

The recovery factor data are frequently needed so that the recovery temperature, or adiabatic surface temperature, $T_{S,ad}$ may be calculated. For this purpose the temperature recovery factor is more convenient to use than the enthalpy recovery factor; with the latter, variations of enthalpy with temperature are required before $T_{S,ad}$ can be computed. Thus it is useful to be able to determine $N_{RF,T}$ without the need to have any detailed knowledge of property-variations.

Zero-mass-transfer. Examination of fig. 3.2-6a shows that when the Prandtl number N_{Pr} and the specific heat c_p are temperature-dependent, $N^*_{RF,T}$ varies with both $(N_{Ma})_G$ and T_G. However, if we plot $N^*_{RF,T}/(N_{Pr})^{1/2}_G$ vs. $(G^*_u)_G/(G^*_u)_{c.p.}$ the effects of both $(N_{Ma})_G$ and T_G are greatly reduced. Fig. 4.3-1 shows such a plot; the data used are those obtained for non-dissociating air with both the Prandtl number and the specific heat varying with temperature. For constant N_{Pr} and c_p the ratio $N^*_{RF,T}/(N_{Pr})^{1/2}_G$ is close to unity and is almost independent of $(N_{Ma})_G$ and thus of $(G^*_u)_G/(G^*_u)_{c.p.}$; and we shall not here use these data, as the assumption of constant N_{Pr} and c_p does not hold well for air at high Mach numbers.

Fig. 4.3-1 clearly shows that the data can be well represented by:

$$\frac{N^*_{RF,T}}{\sqrt{N_{Pr,G}}} = \left[\frac{(G^*_u)_G}{(G^*_u)_{c.p.}}\right]^p$$

where p is a constant. By the method of least square p was determined to be 0.621. Thus:

$$\frac{N^*_{RF,T}}{\sqrt{(N_{Pr})_G}} = \left[\frac{(G^*_u)_G}{(G^*_u)_{c.p.}}\right]^{0.621} \qquad (4.3.2\text{-}9)$$

The accuracy of equation (4.3.2-9) may be judged by reference to fig. 4.3-2 showing $N^*_{RF,T}/(N_{Pr})^{\frac{1}{2}}_G$ vs. $[(G^*_u)_G/(G^*_u)_{c.p.}]^{0.621}$. In-so-far as can be checked by available data, relation (4.3.2-9) is valid for T_G between 100 and 800°R and for $N_{Ma,G}$ up to 20. The equation is, however, not recommended for use with dissociating air.

With gas injection. In a similar manner the temperature recovery factor data for flat plate with gas injection are plotted in fig. 4.3-3. The only difference from the corresponding zero-mass-transfer plot is in the use of $(N^*_{RF,T})_{c.p.}$ to normalize the recovery factor instead of $(N_{Pr})^{\frac{1}{2}}_G$; this is adopted because when there is mass injection into the boundary layer, even for the constant-property case the recovery factor can no longer be approximated by the square root of the Prandtl number. Thus it is more meaningful to normalize $N_{RF,T}$ with respect to $(N^*_{RF,T})_{c.p.}$.

As may be seen from fig. 4.3-3 all the data lie above the mean zero-mass-transfer line. This suggests that the injection process reduces the value of $(G_u)_G$ far more than that of $N_{RF,T}$. The plot does not show significant influence of the type of gas injected. Instead the data tend to separate themselves into groups according to the main stream temperature T_G. We shall therefore ignore the influence of the type of gas injected and account only for the effect of the temperature

level T_G, according to the form (T_G in °R):

$$\frac{N_{RF,T}}{(N^*_{RF,T})_{c.p.}} = \left[\frac{(G_u)_G}{(G^*_u)_{c.p.}}\right]^{p_1\cdot(T_G/400^\circ)} .$$

By the method of least square fitting, p_1 was found to be 0.0936. Thus:

$$\boxed{\frac{N_{RF,T}}{(N^*_{RF,T})_{c.p.}} = \left[\frac{(G_u)_G}{(G^*_u)_{c.p.}}\right]^{0.0936(T_G/400^\circ)}} \qquad (4.3.2\text{-}10)$$

Equation (4.3.2-10) is valid for all binary systems with air as the main stream fluid and for T_G between 392 and 2000°R and $(N_{Ma})_G$ up to 12. Fig. 4.3-4 shows a plot of $N_{RF,T}/(N^*_{RF,T})_{c.p.}$ vs. $[(G_u)_G/(G^*_u)_{c.p.}]^{.0936(T_G/400^\circ)}$, from which the accuracy of equation (4.3.2-10) may be ascertained.

From equation (4.3.2-9) and (4.3.2-10) it appears that the recovery factor approaches zero as the skin friction tends to vanish.

4.3.3 Determination of the functions $F_{g,T/N_{Ma}}$, $F_{B,T/N_{Ma}}$ and $F_{B,M}$

The functions were determined from the exact solutions collected in this work. After suitable forms for the functions had been ascertained the various constants were then deduced by the method of least square from the relevant solutions. As the number of the solutions available are quite numerous, all the computations were performed with the help of the Atlas Computer of London University.

As have been discussed earlier, the effects of TD and DT on the conductances $(G_h)_G$ and $(G_u)_G$ are small, their effects on $(G_f)_G$ are somewhat larger. However, in the derivation of the various

functions we shall use indiscriminately both the solutions with neither TD nor DT included and those with TD and DT included. This procedure is adpoted because the available solutions with TD and DT included neither are sufficiently large in number nor cover wide enough ranges of such parameters as T_S/T_G, $(N_{Ma})_G$, M_G/M_T and B. In fact for the case of flat plate no solution at all is available. It is, nevertheless, expected that the correlation procedure thus derived will be reliable over the whole ranges of the parameters considered even when the effects of thermal diffusion and diffusional conduction are not negligible. This statement can of course be checked when more solutions with TD and DT become available.

(a) The function $F_{g,T/N_{Ma}}$

Relation (4.3.2-1) yields for B = 0, i.e. zero-mass-transfer:

$$(G^*)_G \cdot F_{g,T/N_{Ma}}\left\{T_S/T_G,\ N_{Ma,G},\ \beta\right\} = f\{\beta\} \qquad (4.3.3\text{-}1)$$

Thus for a given β value, we simply have:

$$\boxed{(G^*)_G \cdot F_{g,T/N_{Ma}} = (G^*)_{c.p.}} \qquad (4.3.3\text{-}2)$$

The above shows that for zero mass-transfer the multiplication of the variable-property value of $(G^*)_G$ by the function $F_{g,T/N_{Ma}}$ should give a quantity equal to the corresponding constant-property value. $F_{g,T/N_{Ma}}$ can thus be deduced from the zero-mass-transfer data. Since $(G^*)_G$ is often the quantity to be determined, the relation (4.3.3-2) suggests that it is more convenient to have an expression of $1/F_{g,T/N_{Ma}}$ rather than $F_{g,T/N_{Ma}}$ itself. For this reason, we shall seek the formulation for $1/F_{g,T/N_{Ma}}$.

On examining the $(G_u^*)_G$ data for a flat plate ($\beta = 0$), it emerges that the effects of T_S/T_G and $N_{Ma,G}$ on this conductance can be satisfactorily accounted for, if the function $F_{g_u,T/N_{Ma}}$ takes the form of :

$$1/F_{g_u,T/N_{Ma}} = (T_S/T_G)^{a_1} + a_2 (T_S/T_G)^{a_3} (N_{Ma,G})^{a_4} \qquad (4.3.3\text{-}3)$$

where the a's are constants. This form also proves to be satisfactory for $(G_h^*)_G$. We shall, however, generalize the above form to read:

$$\boxed{1/F_{g,T/N_{Ma}} = f_1\{T_S/T_G\} \cdot \left[1+a\,(T_S/T_G)^b\,(N_{Ma})_G^c\right]} \qquad (4.3.3\text{-}4)$$

where a, b and c are constants. When $N_{Ma,G} = 0$, we simply have:

$$1/F_{g,T/N_{Ma}} = f_1\{T_S/T_G\} = 1/F_{g,T} \quad . \qquad (4.3.3\text{-}5)$$

For this case $F_{g,T/N_{Ma}}$ is a function of T_S/T_G only, and we have adopted the symbol $F_{g,T}$, with the subscript T indicating this. For flows with $\beta > 0$, $(N_{Ma})_G = 0$ is always the case; hence for these flows $F_{g,T}$ will be the appropriate function. Nevertheless, $F_{g,T}$ may be regarded as a particular variation of the function collectively known as $F_{g,T/N_{Ma}}$.

Combination of equations (4.3.3-5) and (4.3.3.2) then yields:

$$\frac{1}{f_1\{T_S/T_G\}} = \frac{(G^*)_G}{(G^*)_{c.p.}} \qquad (4.3.3\text{-}6)$$

Thus the function f_1 may be found from the zero-mass-transfer data for $N_{Ma,G} = 0$ by plotting $(G^*)_G/(G^*)_{c.p.}$ vs. T_S/T_G. This has been done and the plots for $\beta = 0$, 1/2 and 1 are shown in fig. 3.2-1 for G_u^* and in fig. 3.2-3 for G_h^*. The sources and main-stream temperature information of the data used are also listed in the figures. The

curves through the points represent $1/f_1\{T_S/T_G\}$, and were determined by least square fitting after suitable forms had been chosen. In the case of G_h^* for $\beta = 1/2$ (fig. 3.2-3), some data for air in dissociation equilibrium have been included; and in accordance with established practice we use for these dissociation data the enthalpy ratio h_S/h_G in place of the temperature ratio T_S/T_G as the suitable parameter. In the case of G_u^*, it is found unnecessary to use the enthalpy ratios even for dissociation data.

No G_f^* data are available for determining the corresponding f_1 function. However, since the variation of G_f^* with T_S/T_G is expected to be more like that for G_h^* than G_u^*, the function f_1 for G_h^* is assumed to apply also to G_f^*.

With the function f_1 known, the constants a,b and c can then be determined by considering the zero-mass-transfer data for $N_{Ma,G} > 0$. Combining equations (4.3.3-2) and (4.3.3-4) now yields:

$$a(T_S/T_G)^b(N_{Ma,G})^c = 1/\left[(G^*)_G \cdot f_1\{T_S/T_G\}/(G^*)_{c.p.}\right] - 1 \qquad (4.3.3\text{-}7)$$

All the quantities on the R.H.S. of equation (4.3.3-7) are known, thus the best value for the constants a, b and c can be readily determined by the method of least square. The results may be found in the summary in Table 4.3-1. The data used for evaluating these constants are those displayed in figs. 3.2-4a and 4b for G_u^* and figs. 3.2-5a and 5b for G_h^*. Again, the enthalpy ratio was used for the dissociation data for G_h^*. The sources and main-stream temperature information of the data are also contained in the figures.

No data are available for G_f^*. However, with hydrogen injection quite a number of solutions covering a comprehensive range of both T_S/T_G and $N_{Ma,G}$ are available. These data were used in the determination of the constants a, b and c. The method used is similar to that described above except that equation (4.3.3-7) was modified to read:

$$a\left(\frac{T_S}{T_G}\right)^b \left(N_{Ma,G}\right)^c = \frac{1}{\left[\dfrac{(G_f)_G}{(G_f)_{T_S/T_G=1,\,N_{Ma}\to 0}}\right]_{\text{Same}B_f} \cdot f_1\left(\dfrac{T_S}{T_G}\right)} - 1 \qquad (4.3.3\text{-}7a)$$

(b) The function $F_{B,T/N_{Ma}}$

This function may be determined from data with air injection. For this system M_G/M_T is unity, hence combination of equations (4.3.2-1) and (4.3.2-5) gives:

$$(G)_G \cdot F_{g,T/N_{Ma}} = f\{B \cdot F_{B,T/N_{Ma}},\ \beta\} \qquad (4.3.3\text{-}8)$$

Graphically, this implies that for a given β value the curves of $(G)_G \cdot F_{g,T/N_{Ma}}$ vs. $B.F_{B,T/N_{Ma}}$ should coincide with, or lie close to, the corresponding curve for constant-properties. If the function $F_{B,T/N_{Ma}}$ is significant, then the same data plotted with $(G)_G \cdot F_{g,T/N_{Ma}}$ vs. B will show two distinct curves, the amount of separation depending on the magnitude of $F_{B,T/N_{Ma}}$. Thus by evaluating the ratio $(G)_{c.p.}/[(G)_G \cdot F_{g,T/N_{Ma}}]$ for the same B value the magnitude of the function $F_{B,T/N_{Ma}}$ may be ascertained.

Fig. 4.3-5 shows such a plot for both G_u and G_h and for $\beta = 0$, 1/2 and 1. From this it is seen that the function $F_{B,T/N_{Ma}}$ is close to unity. Also no systematic influence of both T_S/T_G and $N_{Ma,G}$ on the

ratio $(G)_{c.p.}/[(G)_G \cdot F_{g,T/N_{Ma}}]$ was detected. On this evidence we shall adopt for all three types of driving forces:

$$\boxed{F_{B,T/N_{Ma}} = 1} \quad . \qquad (4.3.3\text{-}9)$$

(c) The function $F_{B,M}$

With $F_{B,T/N_{Ma}} = 1$, the relationship (4.3.2-1) becomes:

$$\boxed{(G)_G \cdot F_{g,T/N_{Ma}}\left(\frac{T_S}{T_G},\ N_{Ma,G},\ \beta\right) = f\left[B \cdot F_{B,M}\left(\frac{M_G}{M_T},\ \beta\right),\ \beta\right]} \qquad (4.3.3\text{-}10)$$

This implies that the function $F_{g,T/N_{Ma}}$ accounts entirely for the effects of T_S/T_G and $N_{Ma,G}$, while the function $F_{B,M}$ accounts solely for the effects of injecting different gases into the air stream.

For a given flow configuration (or β value) and a particular binary system, $F_{B,M}$ is merely a constant number. We shall first determine such constants for each system, i.e. without stipulating any functional relationship between these constants and the molecular weight ratios M_G/M_T . The procedure adopted for the determination of these constants is outlined below.

For a particular β value (e.g. $\beta = 0$) and a particular system (e.g. H_2-air) the collected solutions for $B > 0$, $(G_u)_G \sim B_u$, for example, will be used. For a given data point the conductance is multiplied by the corresponding value of $F_{g_u,T/N_{Ma}}$ to yield $(G_u)_G \cdot F_{g_u,T/N_{Ma}}$. Next, a value of the corresponding constant-property driving force, $(B_u)_{c.p.}$, is found such that the constant-property conductance $(G_u)_{c.p.}$ is given by:

$$(G_u)_{c.p.} = (G_u)_G \cdot F_{g_u,T/N_{Ma}} \quad .$$

This is graphically illustrated in fig. 4.3-6. $F_{B_u,M}$ as determined from this data point is given by:

$$F_{B_u,M} = (B_u)_{c.p.} / B_u \quad .$$

The procedure is repeated for all the data point and an arithmetic mean value of $F_{B,M}$ is found. This mean value may not be the value giving the best results. To obtain the best value, the mean value is varied, usually by steps of 5%, over the range of between 0.5 and 2 times the mean value, and the best value of $F_{B,M}$ is picked out as the one that gives the smallest overall root-mean-square value of the deviation

$$\left\{ \left[(G_u)_{c.p.} / F_{g_u,T/N_{Ma}} \right] - (G_u)_G \right\} / (G_u)_G \quad ,$$

where $(G_u)_{c.p.}$ is the constant-property conductance corresponding to a driving force $(B_u)_{c.p.}$ given by:

$$(B_u)_{c.p.} = B_u \cdot F_{B_u,M} \quad .$$

The functions $F_{B_u,M}$ and $F_{B_h,M}$ so found for the various systems for the three cases of β = 0 , 1/2 and 1 are listed in Table 4.3-2. They are also plotted against M_G/M_T in fig. 4.3-7, from which it can be seen that for both B_u and B_h the simple relationship

$$\boxed{F_{B_{u/h},M} = (M_G/M_T)^{1.3}} \qquad (4.3.3\text{-}11)$$

gives a fairly good representation of these functions for most of

the systems considered.

For $(G_f)_G \sim B_f$, it was found that for a particular β value, with $F_{B_f,M}$ as a function of M_G/M_T alone the accuracy of the correlation tends to drop with increasing value of B_f. This dependence on B_f can be largely taken into account by incorporating B_f into the function $F_{B_f,M}$ in the following form:

$$F_{B_f,M} = \frac{A\left\{\frac{M_G}{M_T}, \beta\right\} + e\,B_f}{1 + e\,B_f} \qquad (4.3.3-12)$$

where $A = A\{M_G/M_T, \beta\}$ and e is a constant. The function A has the value of unity for all values of β when M_G/M_T is equal to unity; so that $F_{B_f,M}$ still assumes the value of unity for $M_G/M_T = 1$.

Once the constant e is known A can be determined in exactly the same way as $F_{B_{h/u},M}$ were determined. To find the best value for e, we first assigned different values to it. For each value, the best values of A were determined and the overall root-mean-square deviation calculated; the procedure was then repeated for all the other values of e assigned. The value of e giving the lowest root-mean-square deviation was then chosen. In this way e was found to be 0.03. Thus we have:

$$\boxed{F_{B_f,M} = \frac{A + 0.03\,B_f}{1 + 0.03\,B_f}} \qquad (4.3.3-13)$$

With e known the function A was determined and the results are listed in Table 4.3-2. They are also plotted against M_G/M_T in fig. 4.3-8; as may be seen there, for the three cases of $\beta = 0$, 1/2 and 1

$$\boxed{A = M_G/M_T} \qquad (4.3.3-14)$$

gives a good approximation for most of the systems considered.

(d) Constant-property solutions

In the derivation of the above functions the constant-property solutions were frequently required. To facilitate the use of the computer to perform the calculations, the constant-property solutions were calculated from an interpolation formula of the form:

$$\ln(G/G^*) = \ln(g/g^*) = c_1 \ln(1 + B) + c_2 [\ln(1 + B)]^2 \quad . \quad (4.3.3\text{-}15)$$

The constants c_1 and c_2 were determined by least square fitting of the exact solutions extracted from references [G10, G11, G29, G31]. In this way equation (4.3.3-15) can be readily used to give constant-property solutions with a maximum deviation of less than 0.5% for driving force B between the range of 0 and 120. Table 4.3-3 contains these constants for the various conductances for β values of 0, 1/2 and 1. For a given ratio of g/g^*, B can be found from:

$$\ln(1 + B) = \frac{-c_1 - \sqrt{c_1^2 + 4\, c_2\, (\ln g/g^*)}}{2\, c_2} \quad . \quad (4.3.3\text{-}16)$$

(e) Discussions

Although the functions are derived from the solutions themselves, success of the proposed procedure in correlating these solutions can only be assured if the various assumptions involved in the formulation of the functions are justified. To validate these assumptions we shall provide assessment to see the extent the present method is successful in correlating the solutions.

Zero-mass-transfer. For a given β value we simply have:

$$(G^*)_G/(G^*)_{c.p.} = 1/F_{g,T/N_{Ma}} \quad (4.3.3\text{-}2)$$

Thus by plotting $(G^*)_G/(G^*)_{c.p.}$ vs. $1/F_{g,T/N_{Ma}}$ the accuracy of the correlation may be easily judged. These plots are displayed in figs. 4.3-9 and 4.3-10 for $\beta = 0$ and in fig. 4.3-11 for $\beta = 1/2$ and 1.

For each data point the percentage deviation, d, was calculated, where

$$d \equiv \left[\frac{(G^*)_{pre'd}}{(G^*)_G} - 1 \right] \cdot 100\% \quad .$$

And the root-mean-square (RMS) value of these deviations was evaluated for each case according to :

$$\text{RMS deviation} = \sqrt{\frac{\sum^{n} d^2}{n}} \quad ,$$

where n is the number of data points. These RMS values are also shown on the respective figures.

In the above, $(G^*)_{pre'd}$ is the predicted value of $(G^*)_G$ from the given values of T_S/T_G and, where applicable, $N_{Ma,G}$. As may be seen from equation (4.3.3-2), for a given β value,

$$(G^*)_{pre'd} = (G^*)_{c.p.} / F_{g,T/N_{Ma}} \quad .$$

The overall RMS deviation for all these data concerned (some 653 points) is 5.8%, which is considered a satisfactory figure.

With gas injection. With $F_{B,T/N_{Ma}} = 1$, reducing the variable-property data, $(G)_G \sim B$, to the form: $(G)_G \cdot F_{g,T/N_{Ma}} \sim B.F_{B,M}$ should bring the data close to the corresponding constant-property curve.

These plots have been made and are displayed in figs. 4.3-12a to 4.3-14c. The values of $F_{B,M}$ used are those taken from Table 4.3-2. The success of the correlation may be judged visually by the degree of scatter of the points around the constant-property curve. It should, however, be noted that many data points are so close together that some have been omitted from the graphs to preserve clarity.

To provide a more precise measure of the accuracy of the procedure, the RMS values for the percentage deviation:

$$\left[(G)_{pre'd}/(G)_G - 1\right] \cdot 100\%$$

have again been computed for each case and are also displayed in the respective figures. Here $(G)_{pre'd}$ is the value of $(G)_G$ for the given value of the driving force B predicted from the corresponding constant-property solutions together with the appropriate functions $F_{g,T/N_{Ma}}$ and $F_{B,M}$: for a given variable-property data point $[B, (G)_G]$, we first computed the constant-property value $(G)_{c.p.}$ for a driving force of $B \cdot F_{B,M}$, $(G)_{pre'd}$ was then given by:

$$(G)_{pre'd} = (G)_{c.p.}/F_{g,T/N_{Ma}} .$$

As can be seen, for the case when the surface is not at the adiabatic temperature the RMS values for the deviation vary between 5.1% and 10.4%. The overall RMS value is 7.3% for a total of some 1539 points; this is again considered a satisfactory figure.

For the adiabatic surface, the RMS deviation is 14.1% for $(G_u)_G$ and 10.3% for $(G_f)_G$. The total RMS deviation for these data is 12.0% for a total of some 210 points.

The total RMS deviation for all the data points, both with and without mass transfer, is 7.5%; this figure speaks favourably for the present method.

In Table 4.3-1 it may be seen that $F_{g_h,T}$ for $\beta = 1$ is 1. This is recommended on examining a rather limited number of solutions. When more data become available it may be necessary to re-determine this function. The function $F_{g_f,T}$ for $\beta = 1$ was assumed to be equal to $F_{g_h,T}$.

The functions $F_{B,M}$ are tabulated in Table 4.3-2 for each pair of gases. It may be noted from figs. 4.3-7 and 4.3-8 that for a particular β value the variations of $F_{B_u,M}$, $F_{B_h,M}$ and A with M_G/M_T are not "smooth". This lack of "smoothness" may be due to the fact that some of these fucntions were derived from relatively few solutions. It is, however, reassuring to note that no exceptionally large change in these functions for any two adjacent values of the M_G/M_T ratio considered. In view of this a linear interpolation between two suitable values of M_G/M_T is possible. This procedure is expected to be more reliable than the simple approximations suggested earlier, viz. :

$$F_{B_{u/h},M} = (M_G/M_T)^{1.3} \qquad (4.3.3\text{-}11)$$

and

$$A = M_G/M_T \quad . \qquad (4.3.3\text{-}14)$$

4.4 Comparison of the correlation methods

4.4.1 Introduction

Because of the lack of detailed information on the property-variations for most of the solutions collected, the methods of E/G-H-M-G and Knuth can not be checked against all the solutions. Even when sufficient information is available from the source reference containing the solutions, invariably the property-values had to be scaled of rather small graphs, with consequent poor representations of the properties. It is thus impossible to make a precise comparison of the methods. Without the need for this property-information the present method can be readily checked against the solutions collected; this has been discussed under "Discussions" in section 4.3.3.

However, we shall try to improvise a comparison under the headings of : simplicity of use; accuracy and range of applicability.

4.4.2 Simplicity of use

Without the need for details of any property-variations, the present procedure is simpler to use than either the E/G-H-M-G method or Knuth's. The fact that the present procedure requires knowledge of the constant-property solutions does not reduce this attraction, as the relevant constant-property values can be readily and accurately obtained from the algebraic formulae (4.3.3-15) and (4.3.3-16).

Of the other two methods, that of E/G-H-M-G is simpler to use than Knuth's. As may be seen in section 4.2.2, in normal applications Knuth's method may require the determination of seven quantities

simultaneously from seven functional relationships by an iterative process.

4.4.3 Accuracy and ranges of applicability

As bas been emphasized many times, in using the methods of E/G-H-M-G and Knuth, details of property-variations are required. Unfortunately, as so often the case when theoretical solutions are reported in the literature, the fluid-property variations used to obtain the solutions are seldom given in sufficient details; consequently it is quite impossible to make any direct quantitative comparison of the accuracy of the methods by checking them against all the collected solutions. However, some suitable solutions are available, and computations have been made to provide a comparison, which, though not conclusive, will at least give some indications of the relative accuracy of the three methods.

All the computations were again performed with the help of the Atlas computer. Before using the methods of E/G-H-M-G and Knuth, the variations with temperature of pure component gases, which were invariably scaled off small graphs in the source reference with consequent poor accuracy, were first fitted in polynomial forms. These, together with the given expressions for the mixture property variations with composition, provide the required details for the property values. The correlation methods were then used to predict the solutions, e.g. $(G_u)_G$, with the same boundary conditions and, in the case with

mass transfer, with the same mass-transfer rate as those for the theoretical solutions obtained for the same set of property-variations. The deviations between the predicted value and the theoretical value, e.g. $\left[(G_u)_{pre'd}/(G_u)_G - 1\right]$, for each correlation method were determined and the corresponding RMS values of these deviations evaluated. These RMS values then provide the basis for comparing the relative accuracy of the methods. Since the data used in this comparison are only a small percentage of the solutions collected, we shall just give, for each set of solutions, the RMS values for each set of solutions, and shall not try to provide an overall RMS value, which might be rather misleading.

Furthermore, as the methods of E/G-H-M-G and Knuth were not explicitly derived for use in flows with pressure gradients, this quantitative comparison will be confined to the flat plate case, i.e. $\beta = 0$.

a) Zero-mass-transfer. For this case, both the methods of Eckert/Gross-Hartnett-Masson-Gazley and Knuth are essentially the same; the only difference is in the use of a slightly different reference state. Since, however, Eckert's reference-enthalpy formula has been much more widely used, we shall try to compare the present procedure with this one only.

As the present method is valid only for air as the main stream fluid, we shall choose the solutions for air obtained with "actual" property-variations. The RMS deviations for the various sets of

solutions are listed in Table 4.4.1. From there it can be inferred that Eckert's reference enthalpy method is generally more accurate than the present procedure, especially for the enthalpy conductance $(G_h^*)_G$ when the air is in dissociation equilibrium. For the skin friction or the conductance $(G_u^*)_G$, the present method gives a rather satisfactory performance; and in the case of dissociated air, the present simpler method gives a smaller RMS value than Eckert's method. This contrasts the poorer performance in the case of $(G_h^*)_G$; and reflects the relative insensitivity of $(G_u^*)_G$ to property variations. On the whole, Eckert's method still scores higher, but the difference is not large, and the present method is sufficiently accurate for engineering calculations. It may be noted that for zero-mass-transfer the present method is especially simple to use.

As has been pointed out in section 4.3.1 the reference enthalpy method will give erroneous predictions on the skin friction for $\beta = 1/2$ and $\beta = 1$; the present method gives quite reliable predictions for these cases, as may be seen from fig. 4.3-11.

As far as can be checked, the present method is valid for: T_G between 100 and 7000°R; T_S/T_G between 0.25 and about 20 for $\beta = 0$, 0.01 and 4 for $\beta = 1/2$, and 0.25 and 4 for $\beta = 1$; $N_{Ma,G}$ up to about 20. Eckert's reference enthalpy method also covers roughly the same ranges for $\beta = 0$.

b) <u>With gas injections</u>. In this case, the flat-plate solutions of Sziklas and Banas [S32] and those of Eckert et al [S37, S44] in

Tables 3.2-22 and 3.2-25 respectively are used for the purpose of comparison. These solutions are chosen because the property-variations are given in sufficient details in the source references; also the solutions of Sziklas and Banas cover a wide range of mixtures: H_2-air, He-air, air-air and H_2O-air, while those of Eckert et al (for H_2-air only) cover a wide range of the parameters T_G, T_S/T_G and $N_{Ma,G}$.

In using the correlation method of Gross-Hartnett-Masson-Gazley for $(G_u)_G$ and $(G_h)_G$, the actual correlation curves for g_u/g_u^* and $\dot{q}_S''/(\dot{q}_S'')^*$ in reference [G14] were used instead of the quoted formulae (4.2.1-9) and (4.2.1-10); the use of the formulae will greatly lower the accuracy. The same method has not been used for the recovery factors as the correlation in this case is not unique; however, some recovery factors have been plotted in fig. 4.4-1 in the form used by Gross et al. This figure may be compared with fig. 4.3-3 on which are plotted the same data in our form; the comparison clearly favours the present method.

The RMS values for the various sets of solutions are listed in Table 4.4-2. From there it is seen that in general the present procedure is better than either the method of E/G-H-M-G or Knuth. Once again we remark that the property values used were not precisely those used to obtain the exact solutions and the comparison must not be viewed as an exact one.

The methods of E/G-H-M-G and Knuth were not derived for use with pressure gradients. In the case of zero-mass-transfer we have

seen that the reference enthalpy method gives erroneous predictions for the skin friction for $\beta = 1/2$ and $\beta = 1$. The satisfactory results obtained by the present method for these cases for $B = 0$ as well as for $B > 0$ suggests that the reference state method may also give erroneous predictions for the skin friction when $B > 0$.

All the three methods are inaccurate at very low main-stream temperature ($\approx 123^{\circ}R$). As far as can be checked, the present method gives satisfactory results for: T_G between 390 and $2000^{\circ}R$; T_S/T_G between 0.5 about 15 for $\beta = 0$ and between 0.25 and 4 for $\beta = 1/2$ and $\beta = 1$; $N_{Ma,G}$ up to 12. The other two methods cover roughly the same ranges for $\beta = 0$.

4.5 Summary of recommended method of calculation

(I) Zero-mass-transfer

For given values of T_G, T_S/T_G, $N_{Ma,G}$ and β the conductances can be calculated from equations (4.3.3-2), viz.:

$$(G^*)_G = (G^*)_{c.p.} / F_{g,T/N_{Ma}} \qquad (4.3.3\text{-}2)$$

Definitions of the conductances are given in (2.7.4-7) to (2.7.4-10); appropriate values of the constant-property conductance $(G^*)_{c.p.}$ may be found from Table 4.3-3 (p.295) and of the function $1/F_{g,T/N_{Ma}}$ from Table 4.3-1 (p.293).

The temperature recovery factor $N^*_{RF,T}$ for $\beta = 0$ when the air is non-dissociating can be estimated from equation (4.3.2-9), viz.:

$$N^*_{RF,T} = \sqrt{N_{Pr,G}} \left[\frac{(G^*_u)_G}{(G^*_u)_{c.p.}} \right]^{0.621} \qquad (4.3.2\text{-}9)$$

Or the simple approximations (4.3.2-8) may be used to estimate the enthalpy recovery factor N^*_{RF} :

$$\left.\begin{aligned} N^*_{RF} &= 0.825 \qquad \text{for non-dissociating air;} \\ &= 0.95 \qquad \text{for air in dissociation equilibrium.} \end{aligned}\right\} \quad (4.3.2\text{-}8)$$

Definitions of the recovery factors are given in (2.7.4-14) and (2.7.4-15).

(II) With gas injection

In most cases of mass-transfer cooling the problem is specified as follows:

Main-stream conditions: T_G, $N_{Ma,G}$ or u_G, β ;

Maximum surface temperature: T_S, hence T_S/T_G;

Coolant supply conditions: T_T, M_T hence M_G/M_T.

It is required to find the coolant flow rate $\dot{m}''$ which is needed at each point of the surface to keep the temperature there to the specified value. The procedure of solving this problem by the use of the present method may be summarized as follows:

1) The driving force B_h is calculated by inserting the data of the problem into equation (2.7.4-3a), viz.:

$$B_h = (h_{GS,ad} - h_{GS})/(h_{TS} - h_T - \dot{q}''_{rad}/\dot{m}'') \ . \qquad (2.7.4\text{-}3a)$$

The adiabatic-surface temperature needed to evaluate $h_{GS,ad}$ may be obtained from equation (4.3.2-10) for $\beta = 0$ when the effects of thermal diffusion and the coupling between diffusion and heat conduction can be neglected:

$$N_{RF,T} = 0.8477 \left[\frac{(G_u)_G}{(G^*_u)_{c.p.}}\right]^{0.0936(T_G/400^\circ R)} \qquad (4.3.2\text{-}10)$$

or from fig. 3.2-10 for $\beta = 1/2$ and $\beta = 1$ when the thermal-diffusional effects are taken into account.

2) The conductance $(G)_G$ can then be calculated from equation (4.3.3-2), viz.:

$$(G)_G = (G)_{c.p.} / F_{g,T/N_{Ma}} \quad . \qquad (4.3.3\text{-}2)$$

Definitions of the conductances are given in (2.7.4-7) to (2.7.4-10); the constant-property conductance $(G)_{c.p.}$ can be obtained from equation (4.3.3-15) with $(B \cdot F_{B,M})$ as the driving force inserted there. The functions $1/F_{g,T/N_{Ma}}$ and $F_{B,M}$ can be obtained from Tables 4.3-1 (p.293) and 4.3-2 (p.294) respectively. Functions $F_{B,M}$ can also be approximated by equations (4.3.3-11), (4.3.3-13) and (4.3.3-14).

3) Evaluate g and obtain $\dot{m}''$ from:

$$\dot{m}'' = g \cdot B \quad .$$

CHAPTER 5 CONCLUSIONS ABOUT THEORETICAL SOLUTIONS

Many exact solutions are available for laminar boundary-layer flows with non-uniform properties. They have been collected from the literature and are tabulated in Tables 3.1-1 to 3.1-28. It is a great pity that most of these had to be scaled off graphs from the source references. Although the solutions collected are quite numerous, the large number of parameters precludes an adequate coverage of all the ranges of interest.

Most of the zero-mass-transfer solutions were explicitly obtained for air, and all the solutions for binary boundary-layers are for air as the main stream fluid. The flat plate ($\beta = 0$) solutions predominate; and solutions for flows with pressure gradients are mainly confined to $\beta = \frac{1}{2}$ and $\beta = 1$.

For binary boundary-layers most of the solutions were obtained with the reciprocal effects of thermal diffusion and diffusional conduction ignored. Those with these effects included are all for either $\beta = \frac{1}{2}$ or $\beta = 1$.

Examination of the solutions shows that the interaction of energy and mass transport phenomena does not have significant effects on the conductances g_u, g_f or g_h provided g_h is defined as in equation (3.2.4-2), irrespective of flow speeds. Its main effect is in altering the adiabatic wall temperature $T_{S,ad}$, which can no longer be taken as equal to the main-stream stagnation temperature, even in the absence of any aerodynamic heating. Generally, $T_{S,ad}$ is greater than the main-stream temperature for injection of a lighter gas; it is less

than the main-stream temperature for injection of a heavier gas. The difference between the adiabatic wall temperature and the main-stream temperature is most marked for an H_2-air boundary layer. As a very rough guide the magnitude of this temperature difference may be taken as proportional to the molecular weight ratio M_G/M_T. However, the temperature level in the boundary layer also exerts some influence on $T_{S,ad}$.

The surface heat-flux is affected strongly by the coupling between diffusion and heat conduction and only slightly by thermal diffusion when the surface temperature T_S is close to the adiabatic temperature $T_{S,ad}$; when the surface is highly cooled both these effects have only slight influence on the surface heat-flux.

A new procedure has been developed empirically to correlate the theoretical solutions. Without the need for details of fluid-property variations this method is easier to use than the two methods available at present, viz. those of Eckert/Gross-Hartnett-Masson-Gazley and Knuth. The extent to which the present method is successful in correlating the solutions may be judged from figs. 4.3-2, 4.3-4 and 4.3-9 to 4.3-14c. Checked against the solutions the method gives a total RMS deviation of 7.5%; it is thus of sufficient accuracy for engineering calculations.

For flows over a flat plate with zero mass-transfer the present method tends to give a slightly lower accuracy than Eckert's reference enthalpy method. But the reference enthalpy method can give gross errors in predicting the skin friction for flows with high pressure-

gradiends, e.g. $\beta = \frac{1}{2}$ or $\beta = 1$; the present method gives much more reliable performence for these cases. For the case with gas injections the present method seems to be more accurate than the other two methods. A precise comparison with all the solutions was hampered by the lack of detailed information on fluid-properties for most of the solutions.

CHAPTER 6 EXPERIMENTS

6.1 Introduction

6.1.1 Purpose of present experiments

Recently the hitherto neglected effects of thermal diffusion and diffusional conduction on the heat and mass transfer characteristics of a binary boundary layer have been fully recognized [S48, E38] and new theoretical analyses for laminar boundary layers have been made to include these effects [S51, S52, S53] . Accurate experimental data are required for comparison with the analyses as well as with some engineering correlation methods.

As has been discussed in section 3.2.4, one of the main effects of thermal diffusion and diffusional conduction is in affecting the adiabatic surface temperature. Since the adiabatic surface temperature is also influenced by the free stream Mach number, in order that these two effects may be separated it is desirable to use a low-speed free stream flow, for which the effect of kinetic heating is negligible.

As will be seen in section 6.1.3, some experimental data for supersonic free stream Mach numbers with foreign gas injections are available; most of these are, however, of rather poor accuracy. Low-speed data are more accurate but are very scarce. The present experiments provide a comprehensive range of low-speed data with injection into an air stream of the following gases: hydrogen, helium, nitrogen, air, carbon-dioxide and "Arcton-13" ($CClF_3$). It appears that the experiments with hydrogen injection have not been reported in the literature before.

6.1.2 Description and characteristics of the experimental flow configuration

The experiments described in this chapter were carried out for a laminar boundary layer with gas injection in an axi-symmetric stagnation-point-flow region.

The axi-symmetric stagnation-point-flow is characterised by an external flow velocity (outside the boundary layer) directly proportional to the radial distance from the stagnation point, i.e. u_G = constant.x . As far as the present experiments are concerned this particular flow offers the following two advantages:

1) The external flow is of the accelerating type, with an inherent high favourable pressure gradient. The presence of a favourable pressure gradient is known to stabilize the boundary layer; hence under ordinary circumstances the attendant boundary layer for this type of flow will invariably be laminar.

2) According to theoretical analysis, the linear variation of the main stream velocity u_G with the distance from the stagnation-point x gives rise to a boundary layer of uniform thickness, allowing an isothermal surface to be obtained with uniform mass-flux through the surface. This means that in experiments a porous plate of uniform thickness need be used to achieve a uniform surface temperature. A uniform surface temperature is desirable because in nearly all the theoretical analyses this is one of the conditions stipulated.

From potential flow theory, it may be deduced that the chosen configuration can be conveniently realized by impinging a circular jet against a flat plate held normal to the jet axis. However, it is

necessary to check that the conditions of a stagnation-point-flow are satisfied with this arrangement for a real jet (air jet in the present case). For although many experiments (these will be reviewed in section 6.1.3) have been carried out with this jet-on-plate system, measurements on the velocity distributions outside the boundary layer are almost non-existent.

6.1.3 Related experiments carried out by others

Experimental heat transfer results for laminar boundary layers with gas injection are not numerous. Broadly, these results may be classified into two groups. The first group consists of those for zero pressure gradient; these were invariably obtained for cylindrical cones at supersonic free stream Mach numbers [S32, E23, E32, E13, E28]. The second group encompasses those for non-zero pressure gradients; apart from the two low-speed cylinder experiments [E18, E40], all the results were obtained for hemispheres [E1, E14, E15]. Since in the small but finite region surrounding the stagnation-point of a hemisphere, the flow may, for all practical purposes, be regarded as an axi-symmetric stagnation-point flow, the hemisphere results in this region are thus particularly relevant to the present experiments. As may be seen from the summary in Table 6.1-1 all these results were again obtained at supersonic free stream Mach numbers.

In both groups early investigators [S32, E23, E1] were puzzled by the results with helium injection which showed that the temperature recovery factors might increase with mass injection rates. This was in contrary to the trend predicted by the theorectical analyses

available at that time. It was later pointed out by Baron [S48] that the unecpected behaviour may be explained if the coupling effects of heat and mass transfer, which had up to then been neglected in the analyses, are taken into account.

More recently Tewfik et al [E41] and Sparrow et al [E37] reported experimental results for binary free-convection boundary layers. These results also confirmed the practical significance of the thermal-diffusional effects.

As has been mentioned, the present experiments were carried out with an air jet impinging on a flat plate held normal to the jet axis. This jet-on-plate system has been employed by many investigators: in experiments of "pure" heat-transfer [E11, E12, E16, E29, E34, E43] ; sublimation [E7, E35] ; and dissolution (liquid jets) [E31, E30] . With the exception of Christie [E7] all the investigators presented their results in terms of the jet velocities; hence it was not necessary for them to know the main stream velocity distribution ($u_G \sim x$). In the present experiments this knowledge is required for the correlation of the results.

6.1.4 Outline of present chapter

Although the main purpose of the present experiments was to obtain results with simultaneous heat and mass transfer, it was also desirable to obtain with the same rig results with heat-transfer only, as these represent a convenient limit of the blowing rate range. In view of the findings of Kestin et al [E20] on the large influence of main stream turbulence intensity on local heat-transfer rates at

a two-dimensional stagnation-point-flow region, these "pure" heat-transfer results would also serve to establish whether such a large influence is present in an axi-symmetric stagnation-point flow.

The experiments may be conveniently separated into two stages. The first may be called the proving stage during which the main stream velocity distributions ($u_G \propto x$), the turbulence intensities in the main stream and the heat-transfer rates when there was no mass-transfer were measured. The second stage was then entirely concerned with tests with gas injection.

For convenience of presentation, all the apparatus are described in section 6.2 and details of the various tests may be found in section 6.3. In section 6.4 the method of reducing the various data is outlined; the final results are presented and comparison with appropriate theoretical analyses and correlation method made; discussions of the various results are also included. Final conclusions based on the experiment results appear in section 7.

6.2 Apparatus

6.2.1 The air jet

The general arrangement of the air jet system is schematically shown in fig. 6.2-1; it may also be seen in the photograph of fig. 6.2-2.

Air drawn through the filter box by a centrifugal blower was delivered along a 5" diameter brass pipe with two right-angled bends to a 5"/2" diameter copper-spun nozzle and was then discharged to the atmosphere.

The blower was belt driven by a 3/4 h.p., constant speed induction motor. The pipe work was supported through a steel plate welded to the exit end of the nozzle by a frame integral with the base for the whole assembly. To avoid vibration the plate on which the jet impinged was supported by a separate frame resting on the laboratory floor directly.

The air flow rate could be measured by a 2" diameter B.S. orifice plate placed some 7 pipe diameters from the blower outlet. The temperature of the jet could be raised by a 5 kw electric heater consisting of five 1 kw elements situated in the first right-angled bend. The heater power supply could be varied between zero and 240 volts.

Immediately after the second right-angled bend was a 6" long section of aluminium honey comb. This straightened the flow through it and reduced the turbulence of the discharging jet.

6.2.2 Measurement of velocity distributions outside the boundary layer

The set up for the measurement of the velocity profiles outside the boundary layer is shown in fig. 6.2-3. The equipment used that require any discription are the rotating static-pressure plate and the micro-manometer.

a) The rotating static-pressure plate

The velocity profiles were obtained from dynamic-pressure distributions, which were measured with the help of this static-pressure plate.

The plate was made of clear perspex, 9" square and ½" thick,

in which were drilled 5 static-pressure holes, each 0.015" diameter with the edge slightly chamfered. One of the holes was approximately at the centre of the plate and the other four were accurately positioned on a pitch circle of 1¼ inches radius from the first hole and equally spaced from each other. These four holes were used to locate the stagnation point when the circular jet impinged on the plate.

The plate was mounted, through a channel steel section, on a tool maker's dividing table, the centre hole being 1.976" from the axis of rotation of the dividing table.

b) The micro-manometer

As the velocities to be measured were small, a sensitive micro-manometer was needed. The one used was a modified version of that designed by Spalding [E36] . Fig. 6.2-4 is a schematic diagram of the complete manometer. The only difference between this one and that of [E36] is the addition of the syringe system.

With the inclusion of the syringe system the manometer can be used either as a null-reading or a direct-reading one. The former was adopted in favour of the latter which requires careful calibration.

With reference to fig. 6.2-4, when P1 and P2 are equal the light beam appears at the "zero" position of the scale. When P1 is greater than P2 the light beam will move to another position on the scale. However, by adjusting the syringe micrometer the light beam can be brought back to its original position. This in effect restores the liquid level in cylinder 2 to its orginal height. The net amount x moved by the syringe plunger, as deduced from the micrometer readings, bears a simple, fixed relationship with the pressure difference, or,

more accurately, with the difference in liquid levels of the two cylinders, h . If A_3 and A_1 are respectively the cross-sectional area of the syringe and of cylinder 1, then:

$$h = (A_3/A_1) \cdot x \qquad (6.2\text{-}1)$$

In the manometer used, $A_3/A_1 = (0.824)^2/(2.0)^2$, hence:

$$h = 0.170\ x \qquad (6.2\text{-}2)$$

In common with most other micro-manometers, it is necessary to check from time to time the zero reading of the manometer. In the present one this checking was facilitated by the use of a simple quick-action valve similar to the one described by Spalding [E36] , which communicated the two cylinders to the atmosphere at the same time without disconnecting any pressure line.

6.2.3 Test plate and instrumentation for tests with heat-transfer only

As will be seen later in section 6.4.1 the useful region (i.e. where u_G is directly proportional to x) produced by the 2" diameter jet on the plate was just over 1" diameter; the heat transferring area must therefore be less than this. For easy fabrication of the test plate a transient method was used to measure the heat-transfer rates.

Two solid copper discs of different sizes were used. One, designated Disc 1, was 0.986" diameter and 0.233" thick; the other, designated Disc 2, was 0.50" diameter and 0.158" thick. Each disc was buried flush in the middle of a 9" diameter, ½" thick perspex plate as shown in fig. 6.2-5.

An iron-constantan thermocouple was soldered to the middle of

each copper disc to measure the disc temperature T, and another was held above the perspex plate to measure the main stream temperature T_G. Calibration of the iron-constantan thermocouple is described in section 6.2.42.

A Honeywell multipoint "Electronik" indicating and recording potentiometer was used to record the emf-time history of the disc thermocouple, which had as its other junction the thermocouple in the main stream. Hence the emf output was that corresponding to $(T_G - T)$. By using a double pole switch the main stream thermocouple could be connected to a cold junction immersed in an ice bath as shown in fig. 6.2-5; thus the absolute value of the main stream temperature T_G could also be measured.

The stagnation pressure of the jet was measured by the pitot tube fixed on the perspex plate and connected to one limb of a 36-limb, paraffin-filled inclined manometer, the reservoir of which was open to the atmoshpere. From this pressure measurement the maximum velocity of the jet, $U_{jet,max}$, could be calculated and u_G/x deduced from the graph of $U_{jet,max}$ vs. u_G/x in fig. 6.4-3.

The four concentric and equally spaced static-pressure tappings in the perspex plate were used to locate the copper disc centrally with respect to the jet. They were also connected to the 36-limb inclined manometer.

6.2.4 Heat and mass transfer experiments

6.2.41 Test plug assembly

A sectional view of the porous plug assembly is shown in fig.

6.2-6, and a photograph if it may be seen in fig. 6.2-6a.

The plug was made of porous bronze#, 0.997" diameter and 0.25" thick. It was surrounded by a 5" outside diameter brass disc, which in turn was surrounded by a 9" diameter perspex plate. The porous plug was tightly fitted to, and flush on the top side with, the brass plate, which was 0.06" thick. The protruding lower portion of the plug was fitted over by a 0.06" thick perspex sleeve, which was positioned to leave a gap of about 0.1" between its end and the bottom surface of the brass disc. The gap was later filled with Araldite epoxy, holding the brass disc, the plug and the perspex sleeve firmly together, at the same time providing a gas tight seal. The outside of the sleeve was then well wrapped with fibre glass heat-insulating material.

At a radius of 1¼" from the centre of the porous plug four 0.035" diameter static-pressure holes, equally spaced, were drilled in the brass plate. These were used to locate the plug cnetral with respect to the jet. During tests in measuring the velocity distributions outside the boundary layer it was found that by this method the stagnation-point could be located to within 0.010" of the centre of the plug. A deviation of this magnitude was not important because the whole plug would still be inside the stagnation-point flow region, which encompassed an area of about 1.2" diameter.

Two concentric channels were machined on the underside of the brass disc. In one an electric heating coil was cemented by Autostik

---

Of "grade C" pore size and supplied by Sintered Products Ltd., Sutton-in-Ashfield, England.

(a high temperature adhesive) to it and served as a guard heater to the plug. The heater voltage could be varied between zero and 240 volts.

The other channel was closed by soldering a brass ring to its open side and served as a guard cooler. Four openings in the ring provided two pairs of inlet and outlet for the cooling water. Cooling water was drawn directly from a constant pressure main and could be accurately regulated by a fine globe valve.

The need of the use of guard heater and/or cooler to eliminate any radial conduction heat-transfer between the plug and its surrounding plate was revealed from preliminary tests, which showed that even when the plate surrounding the porous plug was a perspex one, the conduction heat-transfer could amount to as much as 35% of the total heat transferred through the plug.

6.2.42 Thermocouple installation and calibration, and temperature measurement

Installation. Six 0.005" diameter, iron-constantan, fibre glass insulated thermocouples were attached to the porous plug; they are designated T1 to T6 in fig. 6.2-6. Also in fig. 6.2-6 is a sketch showing how the thermocouples were attached to the plug: a 0.020" diameter hole was first carefully drilled in the plug and the beaded, shellac insulated thermocouple wires were inserted into the hole, the hole was then filled with Technical "G" copper cement[#] and allowed to set. The procedure adopted was essentially that recommended by

---

[#] A cement which is an electric insulating material having good thermal dconduction properties.

reference [E2].

All the thermocouples in the plug were installed in such a way that a thin layer of the top portion of the porous material was left free from any drilling or other mechanical operations. This ensured that the top layer of the randomly formed pores would distribute the flow through it uniformly.

Thermocouples T4, T5 and T6 were positioned along a line perpendicular to the plug surface and led out parallel to the surface, while T1, T2 and T3 were led out penpendicular to the surface. T6 was 0.035" below the top surface, T5 was 0.130" from the top surface and T4 was in the bottom surface. T1, T2 and T3, which were positioned along one diameter of the plug, provided information on the temperature gradient across the plug surface; T4, T5 and T6 yielded temperature profiles in the thickness of the plug, from which the surface temperature could be extrapolated.

The shielded thermocouples T9 and T10 measured the temperature of the gas before it reached the plug. T9 was placed directly under, and 0.18" below, T4; T10 was 1/2" from the porous discs used to even out the gas temperature.

T7 and T8 were attached to the perspex sleeve to measure the temperature gradient along it.

T11, T12, T13 and T14 were soldered to the under side of the brass plate. These provided a means of checking the temperature gradient across the contacting circle with the porous plug. In the experiments the guard heater and/or the guard cooler were adjusted to give a zero gradient.

The main stream temperature T_G was measured by T15, which was held 3/16 inch above the top-surface, pointing towards the centre and just outside the rim of the plug.

One thermocouple was taped to the plate supporting the nozzle to measure the plate temperature for radiation correction, and another placed just behind the "porous-plate flow meter" measured the gas temperature there for mass flow rate calculations.

Calibration. The thermocouples were not individually calibrated. Instead, two portions, one from each end, of the particular small batch of wires were calibrated at the same time against a standard thermometer with $0.1^{\circ}F$ graduations. The results of the calibration showed that the wires were of very consistent quality. In fact the two calibration curves coincided, the root-mean-square deviation of all the calibrated points about the mean curve being less than 0.5%. On the basis of this, it seemed justified in using this calibration curve as "the" curve for the whole small batch of wires used. The calibration curve is shown in fig. 6.2-7; it is a linear one in the range of temperature considered.

Temperature measurement. The thermocouple circuit diagram is shown in fig. 6.2-8. Since all the thermocouples used were of the same type, viz. iron-constantan, only one cold junction was needed. This junction was immersed in oil in a 1/4 inch diameter glass tube, which was in turn immersed in a mixture of water and crushed ice contained in a thermos flask. Each thermocouple was connected to the cold junction via a multi-point thermocouple selector. The emf output from the thermocouples was measured by a Tinsley variable-resistance

type potentiometer together with a sensitvie Pye Scalamp galvanometer. The smallest emf that could be measured by the potentiometer set-up was 1 μv.

6.2.43 Coolant flow system

a) General arrangement

By coolant here means the injected gas, regardless of whether its temperature is higher than that of the main stream fluid.

The flow circuit may be traced in fig. 6.2-9. The coolant gas under high pressure from cylinders passed a pressure-reducing regulating valve, through a 6" diameter, very fine porous-plate filter, a coarser porous plate (5/8 inch diameter and 1/8 inch thick grade "C" porous bronze) used as a "flow-meter", an electric heater, two porous discs to even out the gas temperature, and, finally, through the porous test plug to the adjacent boundary layer.

The upstream pressure of the "porous-plate flow meter" was maintained constant to within 0.25 mm of water by a bleed tube immersed in a water column. The pressure could be adjusted by varying the length of immersion of the bleeding tube. By this means the flow rate could be automatically maintained constant for a long period.

b) Coolant flow rate measurements

For small flow rates the pressure drop across a porous plate had been found to be directly proportional to the volume flow rate [E25]. Hence this is a convenient means of measuring small flow rates.

The porous disc used was 5/8 inch diameter, 1/8 inch thick having moderate porosity (grade C). As it was anticipated that dirt in

the flow might, after long use, change the characteristics of the porous plate, a very fine filter with small pressure drop was installed before the flow meter. This filter was later proved to be extremely effective.

The porous-plate flow meter was calibrated for each gas against a positive-displacement, wet-type gas meter in conjunction with a 1/20 second stop watch. The calibration curves, volume flow rate vs. pressure drop across the porous plate, for various gases are shown in figs. 6.2-10a and 6.2-10b; the data are also contained in Table 6.4-1. In the case of carbon-dioxide, which dissolves in water, care was taken to saturate the water in the gas meter with the gas before it was used.

6.3 Tests

6.3.1 Measurement of velocity distribution outside the boundary layer

Purpose. Although the flow configuration produced by an air jet impinging on a flat plate held normal to the jet axis had been frequently used in experiments [E11, E12, E16, E29, E35, E43] , in none of these had the velocity distribution outsude the boundary layer, $u_G(x)$, in the impinging region been measured. If, however, experimental results are to be compared with the theoretical calculations, it is necessary to have knowledge of this.

Procedure. In the present experiments, the velocity distributions were measured for a fixed distance between the nozzle exit plane and the plate of 2-21/32 inches. This distance is a little in excess of the minimum distance of 2.4 times the radius of the jet

beyond which (measured from the plate surface) the flow field of the arriving jet will not be disturbed by the presence of the plate : this has been theoretically determined by LeClerc for a potential flow [E24] and experimentally verified for an air jet by Jakob and Kezios [E11] (see the "Discussion" of [E35]). It was hoped that by keeping this distance a minimum the flow close to the plate would have a lower turbulence level.

Before measurements were taken, the rotating static-pressure plate (see section 6.2.2(a)) was first positioned by eye-sight so that the central pressure hole was roughly central with respect to the nozzle. The air jet was then turned on and the plate position was further adjusted until the four concentric, equally spaced static-pressure tappings gave the same readings, or as nearly the same readings as possible, on the multi-limb inclined manometer. The hydrodynamic axis of the jet was then assumed to be normal to the plate; and the stagnation point either coincided with the central hole in the plate or was in its close vicinity. Generally, a deviation of about 5% between the four pressure readings was unavoidable.

From some preliminary tests it had been established that the stagnation pressure of the jet was essentially the same as that of the radial flow within about 1" radius from the jet axis and a short distance above the plate. As a consequence of this observation, a pitot tube of 0.020" diameter was fixed in space, pointing towards the jet axis and 0.6" from it, and 1/32 inch above the plate, to measure the stagnation pressure of the jet. This pitot tube was connected to one limb of the multi-limb inclined manometer as well as to one of the

two cylinders of the micro-manometer; the central static-pressure tapping was connected to the other cylinder of the micro-manometer, as shown in fig. 6.2-3. By measuring the difference between the stagnation pressure and the static pressure, or the dynamic pressure, directly the fluctuations in the pressure lines caused by the jet velocity fluctuations tended to cancel each other out. However, in order to get a reasonably steady reading on the micro-manometer it was still necessary to include a 3" long piece of fine capillary tube in each pressure line. This lengthened the responsetime of the micro-manometer to about four minutes.

In the near-symmetrical position as located by the four static pressure readings the static pressure from the central hole was usually one to two thousandths of an inch water lower than the stagnation pressure from the pitot tube. This suggested that the stagnation point did not coincide with the central hole. The procedure used to locate the true stagnation point is outlined in the following paragraph.

From the position shown in fig. 6.2-3 the plate was rotated a known angle and the pressure difference between the central hole and the fixed pitot tube noted, this was the dynamic pressure at that location. By repeating the procedure at different locations, and on the other side of the initial position, -x in fig. 6.2-3, a plot of dynamic pressure, Δp, versus x was obtained. From the Δp-x plot the point of symmetry could be located, and this was taken as the true stagnation point. The curve was then shifted so that this point of the curve coincided with the orgin (0,0), ensuring that at the

stagnation point the dynamic pressure was always zero.

6.3.2 Main stream turbulence intensity measurement#

Purpose. Kestin et al [E20] reported that the influence of main stream turbulence on the local heat-transfer rates when a high pressure gradient exists may be quite considerable. In view of this it was thought necessary to have some idea of the turbulence level of the flow, particularly in regions close to the plate.

Method. A DISA hot wire anemometer set of the constant temperature type was used to measure the turbulence intensity. A brief description of how this was measured may be found in Appendix 6.1.

As the quantitative relationship between the turbulence intensity in the main stream and the change in the local heat-transfer rates is not known, a very thorough measurement was thought to be unnecessary for the present project. It was therefore decided to measure the turbulence intensities along the jet axis only.

The solid plate used to measure the velocity distributions was again fixed at 2-21/32 inches from the nozzle and the hot wire probe was traversed along the jet axis between the nozzle exit and points as close to the plate as possible. Traverses were made for three different jet velocities.

The help rendered by Dr. A.J. Taylor-Russel in connection with these measurements is gratefully acknowledged.

6.3.3 Heat transfer tests

Purpose. The turbulence intensity in the main stream had been found to be of the order of 4%. According to Kestin et al [E20] , this, coupled with the high pressure gradient encountered in the stagnation-point-flow region, might affect the heat-transfer rates (and probably also the mass-transfer rates) quite considerably. As the findings of reference [E20] were derived from experiments on a two-dimensional body, it is not certain whether the same applies to the axi-symmetric stagnation-point flow considered here. In order to settle this point some experiments were carried out with heat transfer only.

Procedure. The solid test plate and instrumentation has been described in Section 6.2.3.

Reference is made to fig. 6.2-5. By means of the four concentric pressure tappings the plate was shifted until the copper disc was central with respect to the jet; and the jet temperature was raised to between 50 to 60°F above the ambient temperature and allowed to attain steady conditions. The jet, however, was prevented from striking the disc by a baffle plate held between the nozzle and the disc; hence the initial temperature of the disc was approximately the prevailing ambient temperature. When the jet had attained steady conditions, the deflecting plate was quickly withdrawn to allow the jet to strike on the disc. At the same time the automatic emf recorder was started. The following data were also noted: main stream temperature T_G, atmospheric pressure, pressure drop across the 2" orifice plate, and the stagnation pressure of the jet as registered by the pitot tube.

6.3.4. Heat and mass transfer tests

6.3.41 Coolant temperature, T_T

As mentioned earlier in section 6.2.42, two shielded thermocouples T9 and T10, fig. 6.2-6, were available to measure the coolant temperature before it reached the porous plug. T9 was situated 0.18" below the bottom surface, and T10 was ½" from the porous disc used to even out the gas temperature and was about 1-¾ inches from the bottom surface of the plug. During runs when the coolant was not heated and $T_S > T_T$, the difference between T9 and T10 was between 0 and 0.3°F, T9 being always the higher. However, when the coolant was heated and $T_T > T_S$, T10 might be some 10°F higher than T9, depending on the mass flow rate. This cast some doubt as to which of these two temperatures should be taken as the coolant temperature. In order to throw some light on this, tests were made in which both T10 and T4 (i.e. bottom surface of the plug) were maintained constant by adjusting the coolant heater and the guard heater or guard cooler respectively, while the mass flow rate and hence the velocity of the flow in the chamber was varied, and the temperature registered by T9 were recorded. On plotting (T10 - T9) versus flow velocity in the chamber (fig. 6.3-1 shows a typical one) it was apparent that (T10 - T9) gradually increased with decreasing flow velocity. On the evidence of this it was thought that the difference between the temperatures measured by T9 and T10 was mainly due to the free convection effect inside the chamber. It may be remarked that similar phenomenon was also experienced by Gollnick [E14] .

By keeping the flow rate and the coolant heater input constant but varying the bottom surface temperature of the plug, it was found that while T9 changed T10 remained constant throughout.

On the basis of these tests, it was concluded that T10 and not T9 should be taken as T_T .

6.3.42 Variation of mass-flux across the plug surface

Experiments using sintered porous material by Libby et al [E25] and by Bartle [E3] showed that if the pressures on both sides of the porous plate were uniform the distributions of mass-flux across the plate was constant within the accuracy of the measurement. It was assumed that the same applied here.

However, in the present experiments the side of the porous plug on which the air jet impinged experienced a pressure gradient, the pressure decreasing radially from the centre of the plug. Since this pressure distribution had been measured, it is possible to estimate the likely variation of mass-flux across the plug. This has been done in Appendix 6.2, using Forscheimer's formulation. It shows that even with the maximum pressure variation on the surface the variation of the mass-flux between the centre and the edge of the plug was not more than 3%. This was considered small enough to be neglected.

6.3.43 Measurement and distribution of the plug surface temperature

From the temperature profiles across the thickness of the porous plug (some typical ones are shown in fig. 6.3-2), it is

inferred that in nearly all the cases the temperature as measured by the thermocouple T6 (fig. 6.2-6) could be accurately taken as the surface temperature of the plug. As may be seen in fig. 6.3-2 the difference between the temperature measured by T6 (located 0.035" below the surface) and the extrapolated surface temperature was, in nearly all the cases, only 1 μv, corresponding to less than 0.04°F. Even in the worst case the difference was not more than 3 μv (about 0.1°F). In view of the fact that the smallest emf that could be measured by the potentiometer used was 1 μv, the use of T6 as the surface temperature was amply justified.

It may be remarked that the above finding is in accord with the experimental investigation of Bartle [E3] and the analytical results of Bernicker [E4] .

Fig. 6.3-3 shows the results of plotting (T - T2) for many tests in the locations of T1, T2 and T3, which were situated along a diameter of the porous plug. From the plot it may be inferred that the maximum temperature gradient present was 0.36°F/in, i.e. the maximum temperature difference between one end of a diameter and the other end was 0.36°F. However, most of the tests showed a gradient much less than this maximum. Since T6 was situated at a radius of 0.25", i.e. midway between the centre and the edge, it would register a temperature somewhere between the maximum and the minimum. In the light of all these considerations it was justified to assume that T6 registered a temperature which could be taken as "the" surface temperature of the porous plug, T_S.

The following are possible causes for the existence of a

temperature gradient on the surface:

1) slightly non-uniform temperature in the brass plate surrounding the plug;

and 2) the three thermocouples T1, T2 and T3 might not be exactly in the same plane as they were supposed to be (it was quite impossible to check this accurately).

6.3.44 Procedure of tests

The general procedure of a test was as follows:

The coolant flow was first set for a particular rate by adjusting the immersion length of the bleed tube. The air jet was then turned on and the jet heater and coolant heater adjusted to give the desired level of the main stream temperature T_G and the coolant temperature T_T. For the first run of a day, usually 1½ hours were required for the jet temperature to get steady; for later runs with gradual temperature changes, half an hour sufficed for it to attain steady conditions. When the coolant heater was used, about 1½ hours were invariably required for the coolant temperature to become steady.

The surface temperature of the porous plug and the temperatures of the brass plate surrounding it were frequently monitored and the guard heater and/or guard cooler adjusted to eliminate any temperature difference across the contacting circle. When conditions became steady the following data were taken: atmospheric pressure, atmospheric temperature, pressure drop across the 2" diameter orifice, pressure drop across the "porous flow meter", stagnation pressure of the jet as registered by the pitot tube and the emf's from the 17 thermocouples.

6.4 Results and discussions

6.4.1 Velocity distributions outside the boundary layer

Results. From the dynamic pressure profiles (figs. 6.4-1a and 6.4-1b; also Table 6.4-2) the velocity distributions outside the boundary layer were deduced using the Bernoulli equation for incompressibe flow:

$$u_G = \sqrt{2g_o(p_{stagn} - p_G)/\rho_G} = \sqrt{2g_o \Delta p/\rho_G}$$

which may be written as:

$$u_G = C_{pressure \rightarrow velocity} (\Delta p)^{1/2} \qquad (6.4\text{-}1)$$

The quantity $C_{pressure \rightarrow velocity}$ depends on the temperature and pressure of the flow fluid and also on the property of the manometer fluid used. It is, however, constant for each profile, since each profile was taken at constant temperature and practically constant absolute pressure p_G.

The velocity profiles obtained are shown in figs. 6.4-2a to 6.4-2c and Table 6.4-2 for eight jet velocities, covering jet temperatures from 67 to 160°F. The velocity distribution in fig. 6.4-2a shows that u_G was directly proportional to x only for a region of just over 0.5" radius; the change of velocity gradient with x occured at about the same value of x for all the jet velocities. For this reason it was necessary to restrict the test area in later heat and mass transfer tests to within this limit; actually, a round figure of 1" diameter was decided upon.

From each of the velocity profiles the velocity gradient was deduced and plotted against $U_{jet,mean}$ and $U_{jet,max}$; the results are

displayed in fig. 6.4-3. $U_{jet,mean}$ was the mean velocity of the jet as calculated from the pressure drop across the 2" diameter orifice in the 5" diameter pipe; calculating procedure used was that of BS 1042 [E5]. $U_{jet,max}$ was the maximum velocity of the jet as measured by the fixed pitot tube, the static pressure being assumed to be that of the prevailing atmosphere.

Discussion. The limit of the accuracy of the micro-manometer used (section 6.2.2(b)) was set by the optical lever chosen. It was estimated that the smallest pressure that could be detected corresponded to a change of water level of 0.00004". Thus, the accuracy of the velocity measurement was of the order of 0.5 ft/s.

The plots of the velocity profiles show that within this accuracy the profiles were linear.

From fig. 6.4-3 it is seen that the straight line correlation between u_G/x and $U_{jet,max}$ is slightly better than that between u_G/x and $U_{jet,mean}$. As $U_{jet,max}$ was also easier to calculate from measurements this was used to obtain u_G/x in later experiments.

Compared with the simple relationship given by LeClerc [E24],

$$u_G/x = U_{jet}/d \quad , \qquad (6.4\text{-}2)$$

d being the diameter of the nozzle, the mean curve of $U_{jet,mean}$ vs. u_G/x is some 4% lower. The discrepancy might be due to the departure from a truly flat jet-velocity-profile assumed in [E24].

6.4.2 Main stream turbulence intensities

The results of the measurement of turbulence intensities along

the jet axis are shown in fig. 6.4-4; they are also contained in Table 6.4-3. Inspection of these results shows that near the plate the turbulence intensity increased as the plate was approached. Similar phenomenon was reported by Kueth et al [E22] on the measurement of turbulence near the stagnation point of a blunt body. Close to the plate turbulence intensity varied between 3.5 to 4.7% depending on the jet velocity. Generally, lower jet velocity produced higher turbulence, and vice versa. This may be due to the fact that the lower jet velocity was obtained by blocking a larger part of the blower inlet with a sluice-gate type plate, which tended to produce a "rougher" flow.

It may not be unreasonable to believe that when the plate is a porous one with gas blown through it to the main stream the corresponding turbulence level might be higher in regions close to the plate.

6.4.3 Heat-transfer without mass-transfer

6.4.31 Analysis of the transient method

For an axi-symmetric stagnation-point flow the main stream velocity is directly proportional to the radial distance, i.e. $u_G \propto x$, and the theoretical dimensionless conductance $g_h^*/(\mu_G \rho_G u_G/x)^{\frac{1}{2}}$ for zero mass-transfer is constant. Hence in the region of constant u_G/x and with constant fluid properties the temperature throughout the heat transferring area will be the same, so is the heat transfer coefficient α. In the case of a good conductor like the copper discs described in section 6.2.3, it may be assumed that the temperature throughout the whole thickness of the disc is also uniform.

From Newton's law of cooling we have:

$$\alpha A (T_G - T) = M_d c \frac{dT}{d\tau} \qquad (6.4\text{-}3)$$

where α = heat-transfer coefficient $\equiv \dot{q}''_S/(T_G - T)$, Btu/ft^{2}h degF;

$\dot{q}''_S$ = heat-flux from the main stream to the surface, Btu/ft^{2}h;

A = area of the disc, ft^2;

M_d = mass of the copper disc, lb$_m$;

c = specific heat of the disc material, Btu/lb$_m$degF;

T = temperature of the disc at time τ, $^\circ$R;

T_G = main stream temperature, $^\circ$R;

τ = time, h.

Integrating equation (6.4-3), we obtain:

$$\frac{\alpha A}{M_d c} \tau = \ln \frac{T_G - T_0}{T_G - T} \qquad (6.4\text{-}4)$$

where T_0 is the temperature of the heat transferring disc at $\tau = 0$.

Now, the iron-constantan thermocouple used had a linear relationship between emf and temperature in the temperature range met in the experiments (see calibration curve in fig. 6.2-7). Thus equation (6.4-4) may be written as:

$$\ln \frac{(\text{emf})_G - (\text{emf})_{\tau=0}}{(\text{emf})_G - (\text{emf})_{\tau=\tau}} = \frac{\alpha A}{M_d c} \tau \quad . \qquad (6.4\text{-}5)$$

Since A, M_d and c are known quantities, α may be deduced from the slope φ of a plot of $\ln\{[(\text{emf})_G - (\text{emf})_{\tau=0}]/[(\text{emf})_G - (\text{emf})_{\tau=\tau}]\}$ vs. τ.

In terms of g_h^*, φ and the characteristics of the disc,

equation (6.4-5) may be written as:

$$g_h^* = \left(\frac{c_{disc}}{c_{p,G}} \cdot \rho_{disc} \cdot t\right) \cdot \varphi \qquad (6.4\text{-}6)$$

where ρ is the density, lb_m/ft^3 and t is the thickness of the disc, ft.

6.4.32 Results and disccusion

From the emf-time chart obtained from the automatic recorder, plots of $\ln \left\{ [(emf)_G - (emf)_{\tau=0}] / [(emf)_G - (emf)_{\tau=\tau}] \right\}$ vs. τ were made and are shown in fig. 6.4-5, from which values of g_h^* were evaluated according to equation (6.4-6). Table 6.4-4 shows the calculated results and other relevant data for the four runs made.

The mean value of $g_h^*/(\mu_G \rho_G u_G/x)^{1/2}$ for the four runs was 0.919, which is some 5% lower than the theoretical value# of 0.959 obtained by Howe and Mersman [S30] for a zero turbulence-intensity situation. The good agreement was obtained in spite of the rather high turbulence intensity (about 4%) present in the main stream flow. This contrasts with the findings of Kestin et al [E20] , who reported that a turbulence intensity of 3% in the main stream flow sufficed to effect an increase of some 80% in the heat-transfer rates at a two-dimensional stagnation region. Partly, this may well be due to the fact that a smaller pressure gradient is associated with an axi-symmetric stagnation flow

---

The theoretical value was transformed from a suitable two-dimensional value to the one applicable to the axi-symmetric stagnation-point flow, using Mangler's transformation (see section 2.7.5).

than with a two-dimensional stagnation flow.

The present results, however, are roughly in accord with the findings of Buyuktur et al [E6] , who experimented with an accelerating flow along a flat plate with various main stream turbulence-intensities.

On the strength of the above comparison it may be inferred that: 1) the flow was a laminar one, and

2) for a main stream turbulence intensity of less than about 4% the turbulence level has, if any, only slight influence on the heat-transfer rate for an axi-symmetric stagnation-point flow.

The satisfactory agreement obtained also lends confidence to the performance of the jet system as a whole.

6.4.4 Heat ans mass transfer results

6.4.41 Evaluation of $g_h/(\mu_G \rho_G u_G/x)^{1/2}$ and B_h

a) Analysis

By considering the heat balance for the control volume embracing the porous plug and the coolant chamber (see sketch), we have for a well insulated chamber:

$$\dot{q}_S + \dot{q}_{rad} + \dot{q}_{cond} = \dot{q}_{out} - \dot{q}_{in} \qquad (6.4\text{-}7)$$

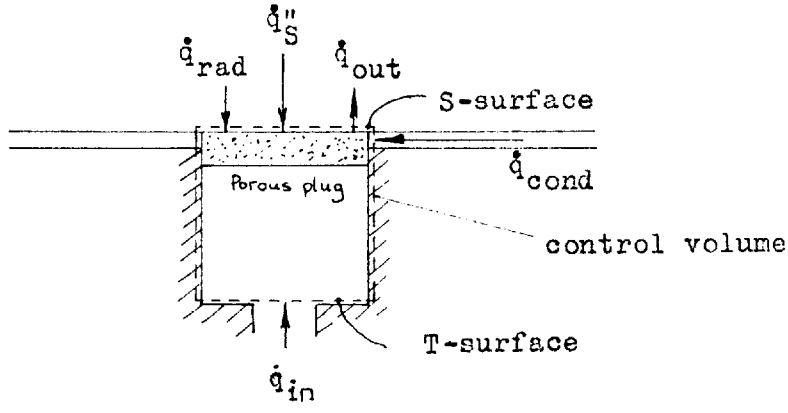

where $\dot{q}_S$ = rate of heat transferred from stream to surface, Btu/h;

$\dot{q}_{rad}$ = rate of heat radiated to the surface, Btu/h;

$\dot{q}_{cond}$ = rate of heat conducted to the plug, Btu/h;

$\dot{q}_{in}$ = rate of heat carried in by the coolant, Btu/h;

$\dot{q}_{out}$ = rate of heat carried out by the coolant, Btu/h.

We assume:

1) that no main stream fluid (air) got into the coolant chamber, i.e. the chamber contains pure injectant, (cf. section 2.6),

and 2) that as the injected gas emerged from the porous plug it acquired a temperature equal to the surface temperature of the plug, T_S.

Then clearly:

$$\dot{q}_{out} - \dot{q}_{in} = \dot{m} (h_{TS} - h_T),$$

where $\dot{m}$ = the rate at which the gas is injected through the porous plug, lb_m/h;

h_{TS} = specific enthalpy of the transferred substance (injected gas) at the surface temperature T_S;

h_T = specific enthalpy of the transferred substance just before entering the control volume.

Now, the design of the apparatus was such that radial conduction through the plug rim could be eliminated, thus $\dot{q}_{cond} = 0$. And equation (6.4-7) for unit area of test region becomes:

$$\dot{q}''_S = \dot{m}'' (h_{TS} - h_T) - \dot{q}''_{rad} \quad . \qquad (6.4\text{-}8)$$

In the temperature range considered the specific enthalpy

difference for all the gases used may be quite accurately represented by $\Delta h = \bar{c}_p \cdot \Delta T$, hence we may write:

$$\dot{q}''_S = (\bar{c}_p)_T(T_S - T_T)\dot{m}'' - \dot{q}''_{rad} \quad . \qquad (6.4\text{-}8a)$$

And the driving force B_h becomes:

$$B_h = \frac{(\bar{c}_p)_G(T_{S,ad} - T_S)\ \dot{m}''}{(\bar{c}_p)_T(T_S - T_T)\ \dot{m}'' - \dot{q}''_{rad}} \quad . \qquad (6.4\text{-}9)$$

As can be seen, all the quantities appearing on the r.h.s. were either known or could be measured or calculated. The radiation heat-flux $\dot{q}''_{rad}$ was calculated according to the formulation in Appendix 6.3.

The conductance is then given by:

$$g_h/(\mu_G\rho_G u_G/x)^{1/2} = \left[\ \dot{m}''/(\mu_G\rho_G u_G/x)^{1/2}\ \right] / B_h \qquad (6.4\text{-}10)$$

b) <u>The velocity gradient u_G/x</u>

In section 6.4.1 the velocity distributions outside the boundary layer of the jet impinging on a smooth solid surface were obtained. From selected checks on the static pressure distributions, it was established that for the same jet velocity the velocity distribution on the porous plate , $u_G(x)$, was, within the accuracy of the measurement, the same as that for the smooth plate. Furthermore, within the range of mass blowing rates used , the velocity profiles outside the boundary layer were not affected by the blowing.

On this basis, the velocity distributions, and hence u_G/x, obtained for the smooth solid plate could be confidently used in the case of the porous plug with gas injection.

It may be noted that similar conclusion was reached by Tewfik et al [E40] in the case of a plane stagnation-flow region.

c) Adiabatic surface temperature

Recent publications [S48, S51, E15, S52, S53, E38, E39, E40] have underlined the importance of the role played by the hitherto neglected coupling effects of heat and mass transfer in binary boundary layers. In the absence of aerodynamic heating but in the presence of these coupling effects the surface temperature for an adiabatic wall condition may considerably exceed the main stream stagnation temperature. Hence, in experiments involving binary boundary layers the adiabatic surface temperature should be measured and cannot be simply assumed to be that of the free stream stagnation temperature.

In the present tests, for a fixed mass-transfer rate the adiabatic surface temperature was deduced from plots of $\dot{q}''_S$ versus $(T_G - T_S)$; where the curve cuts the $\dot{q}''_S = 0$ line gives $(T_G - T_{S,ad})$. For a given constant mass-transfer rate $\dot{q}''_S$ may be changed by varying the stream temperature T_G and/or the coolant (injected gas) temperature T_T.

d) Properties of gases

The fluid properties required for the reduction of experimental results are the viscosity, density, and the specific enthalpy.

For air the viscosity data were taken from reference [E42]. Fig. 6.4-6 shows its variation with temperature.

The operating temperature range was between 530 and 600°R. In

this range, for all gases used it can be assumed that:

$$\Delta h = \bar{c}_p \cdot \Delta T \quad .$$

The values of $\bar{c}_p$ for the different gases are contained in the following table.

Gas	Molecular weight M	$\bar{c}_p$ Btu/lb$_m$degF	Reference
air	28.96	0.240	[E42]
nitrogen	28.02	0.248	[E19]; see fig.6.4-7a
carbon-dioxide	44.01	0.203	[E19]; see fig.6.4-7b
helium	4.00	1.242	[E8]
hydrogen	2.016	3.425	[E19]; see fig.6.4-7c
"Arcton-13" ($CClF_3$)	104.47	0.157	[E9]; see fig.6.4-7d

Density of the gases was calculated from the perfect gas law:

$$\rho = p\, M / (\mathcal{R}\, T) \quad ,$$

where M is the molecular weight of the gas; the universal gas constant $\mathcal{R}$ was taken as 1545.4 ft-lb$_f$/mole ^{o}F. For "Arcton-13" in the temperature and pressure ranges considered, the density calculated from the above relationship agrees within 0.5% with those tabulated in ref. [E9] .

6.4.42 Air injection

Some plots of $\dot{q}''_S$ versus $(T_G - T_S)$ for air injection runs are shown in fig. 6.4-8. As can be seen there $\dot{q}''_S$ varies linearly with $(T_G - T_S)$; furthermore, all the curves pass through the origin (0,0), indicating that an adiabatic-surface condition ($\dot{q}''_S = 0$) was achieved when $T_G = T_S$. This was expected: there was essentially no aerodynamic heating; and since the boundary layer was a single-component one the question of thermal diffusion and diffusional conduction did not arise. Hence for these runs, $T_{S,ad} = T_G$.

As the equality of $T_{S,ad}$ and T_G holds for all the mass-transfer rates, the driving force B_h (equation (6.4-9)) may be evaluated from measurements of one single test, i.e. it is not necessary to obtain first the full $\dot{q}''_S \sim (T_G - T_S)$ curve for each mass-transfer rate. Fig. 6.4-9 shows the results of $g_h/(\mu_G \rho_G u_G/x)^{1/2}$ versus B_h; these results covered jet velocities between 70 and 90 ft/s, mass-transfer rate $\dot{m}''$ between 17.6 and 11.91 lb_m/ft^2h, and $(T_G - T_S)$ between -40 and 42°F. As may be seen from fig. 6.4-9 the experimental data cluster around the theoretical constant-property curve for Prandtl number of 0.7, which may be taken as the value for air in the temperature range considered here. The agreement between the measurements and the theoretical prediction is, for the great majority of cases, within 10%.

Further examination of the results leads us to the following deductions.

1) Since the theoretical curve is valid for flows with a zero main-stream turbulence-intensity, the rather satisfactory agreement

between measurements and theory seems to support the conclusion reached in section 6.4.32: for a main-stream turbulence-intensity of less than about 5% the turbulence level has but little effect on the heat-transfer rates in an axi-symmetric stagnation-point region.

2) In spite of the not-very-smooth surface of the porous plug the boundary layer on it was essentially a laminar one. Also, no sudden increase of the conductance g_h was observed in the whole range of driving force realized (0 to 7), indicating that the transition point had not been reached. Though blowing is known to be destabilizing, the characteristically high favourable pressure-gradient of the stagnation-point flow must have helped to stabilize the boundary layer and maintained the flow laminar.

3) The independently obtained results for $B_h = 0$ blend well with the mass-transfer results. This lends support to the technique of measurement as a whole.

6.4.43 Nitrogen injection

Typical curves of $\dot{q}''_S$ versus $(T_G - T_S)$ for nitrogen injection are displayed in figs. 6.4-10a and 6.4-10b. All the curves pass the origin (0,0), again indicating the absence of any coupling effects. This was expected as the transport properties of nitrogen are only very slightly different from those of air.

In fig. 6.4-11 are plotted results of $g_h/(\mu_G \rho_G u_G/x)^{1/2}$ vs. B_h,

again the data agree, within 10%, with the constant-property theoretical curve. These results support the validity of the general remarks made on the air injection results in Section 6.4.42.

6.4.44 Helium and hydrogen injections

For experiments with hydrogen injection precautions were taken to ensure that both the operating temperature and the hydrogen concentration were well below the limit, beyond which chemical reactions may occur. Thus, as far as the present measurements are concerned hydrogen may be considered as an inert gas.

In the tests, for a fixed mass transfer rate the main stream temperature was varied to obtain variation of $\dot{q}''_S$. Of course, the variation of $\dot{q}''_S$ could also be attained by raising the coolant temperature T_T with the heater installed. In the case of helium injection this was done for two runs only, because it necessitated an unpractically high rate of helium consumption, owing to the much longer time required for steady conditions to be reached. In the case of hydrogen injection, for safety reason it was necessary to restrict the time for each test to a minimum; this ruled out the possibility of varying the coolant temperature to obtain variation of $\dot{q}''_S$.

The range of main stream temperature was generally between 530° and 590°R; and the temperature difference across the boundary layer was about 50°F. As the only effect of main stream temperature on the results is through its influence on the thermal properties of the fluids, the small range encountered here is not expected to affect the results much; i.e. for a given mass transfer rate the

$\dot{q}''_S \sim (T_G - T_S)$ curve, obtained through a small range of main stream temperatures, may be assumed, for comparison purposes, to be also valid for the mean stream temperature.

Adiabatic surface temperature

Plots of $\dot{q}''_S$ versus $(T_G - T_S)$ for several mass flow rates are displayed in figs. 6.4-12a and 6.4-12b for helium injection, and in figs. 6.413a and 6.4-13b for hydrogen injection. Unlike similar plots for air or nitrogen injection the curves do not pass the origin (0,0). Actually, all the curve cut the $\dot{q}''_S = 0$ line at $(T_G - T_S) < 0$. When $\dot{q}''_S = 0$ the surface temperature of the porous plug is $T_{S,ad}$, hence we see that for helium and hydrogen injection, $T_{S,ad} > T_G$. As the jet velocities were not high enough to cause any appreciable aerodynamic heating, such a large difference between $T_{S,ad}$ and T_G (up to 73°F for helium injection and up to 102°F for hydrogen injection) could only be caused by some other mechanism.

Anslyses made by Baron [S48] and by Sparrow et al [S52, 353] indicate that in the absence of any aerodynamic heating, thermal diffusional effects (both thermal diffusion and diffusional conduction) in the laminar binary boundary layer of helium-air and hydrogen-air can cause appreciable difference between the adiabatic surface temperature and the main stream temperature. To ascertain whether these thermal diffusional effects were really responsible for the large differences noted, $(T_{S,ad} - T_G)$ are plotted against the non-dimensional mass-transfer rate $\dot{m}''/(\mu_G \rho_G u_G / x)^{1/2}$ and compared with the above analyses on fig. 6.4-14 for helium injection and on fig. 6.4-15 for hydrogen injection. The results are also contained in Table 6.4-6.

The values of $(T_{S,ad} - T_G)$ were obtained by extrapolating the mean curve through the experimental points on plots of $\dot{q}''_S$ vs. $(T_G - T_S)$ in figs. 6.4-12 and 6.4-13. Where the curve cuts the $\dot{q}''_S = 0$ line gives the $(T_G - T_{S,ad})$ value. Generally, the scatter of the points is not large enough to cause an uncertainty in $(T_{S,ad} - T_G)$ larger than $1^{\circ}F$ for helium injection or $3^{\circ}F$ for hydrogen injection. The likely uncertainty in the extrapolating procedure for both cases is thus less than about 3%.

Inspection of figs. 6.4-14 and 6.4-15 shows that the experimental results of $(T_{S,ad} - T_G)$ for both helium and hydrogen injections agree well with the corresponding analyses of Baron [S48] and Sparrow et al [S52, S53] . For helium injection the slight difference between the analyses of Baron and Sparrow et al is mainly due to the different choice of the fluid properties. As all these theoretical analyses include the coupling effects of energy and mass transfer, but not aerodynamic heating, the rather satisfactory agreement between measurements and theories points out that these thermal diffusional effects were indeed largely, if not entirely, responsible for the large differences between $T_{S,ad}$ and T_G observed.

If mean values of T_G are used, the experimental result may be replotted in the dimensionless form of $(T_{S,ad} - T_G)/T_G$ versus $\dot{m}''/(\mu_G \rho_G u_G / x)^{1/2}$; these are shown in fig. 6.4-16 for helium injection and in fig. 6.4-17 for hydrogen injection.

Heat-transfer results

Reference to the $\dot{q}''_S$ versus $(T_G - T_S)$ curves in figs. 6.4-12a to

6.4-13b suggests that in evaluating the conductance g_h given by

$$g_h = \dot{q}''_S / [c_{p,G}(T_{S,ad} - T_S)]$$

$T_{S,ad}$ must not be substituted by T_G even though no aerodynamic heating was present; otherwise g_h may assume not only both positive and negative values but also infinity.

The heat-transfer results plotted in the form of the dimensionless conductance $g_h/(\mu_G \rho_G u_G/x)^{1/2}$ against the driving force B_h are presented in fig. 6.4-18 for helium injection and in fig. 6.4-19 for hydrogen injection. It may be noted that in the case of helium injection the heat-transfer results for the range of mass-transfer rates represented by the full $\dot{q}''_S \sim (T_G - T_S)$ curves in figs. 6.4-12a and 6.4-12b covered values of the driving force B_h up to 0.6 only. The results for higher driving-force were obtained from measurements for single runs with the corresponding $(T_{S,ad} - T_G)$ values exptrapolated from the mean curve of $(T_{S,ad} - T_G)$ versus $\dot{m}''/(\mu_G \rho_G u_G/x)^{1/2}$ in fig. 6.4-14. This procedure was necessary because it was not possible to ensure supply of helium gas in large enough quantities to enable full $\dot{q}''_S \sim (T_G - T_S)$ curves to be obtained for high mass-transfer rates. It is, however, believed that the extrapolated values of $(T_{S,ad} - T_G)$ were reliable.

<u>With helium injection.</u> Reference to fig. 6.4-18 reveals that where comparison is permitted the results agree well, within 10%, with the theoretical prediction of Sparrow et al [S52], which has taken into account the full thermal diffusional effects. For small blowing rates (B_h small) the conductance g_h tends to remain constant for increasing B_h. This may be due to the relatively high thermal conductivity of helium (approximately 6.5 times that of air), which,

at small blowing rates, successfully counteracts the blowing effects, as has been discussed in section 3.2.3. At large blowing rates, however, the blowing-effect overpowers this and the conductance is seen to decrease fairly rapidly with increasing B_h. Generally, the experimental results cluster around a curve distinctly separated from the constant-property one. It may also be noticed that good agreement exists for the whole range between the experimental results and the theoretical analysis of Baron-Scott [S41] , which does not include any coupling effects. The temperature ratios, T_S/T_G, for the present measurements ranged from 0.97 to 1.09 whereas the theories are for $T_S/T_G = 0.8$. However, according to the correlation method developed in section 4.3, for axi-symmetric flows $g_h/(\mu_G\rho_G u_G/x)^{\frac{1}{2}} \propto (T_S/T_G)^{-.034}$; and for the same driving force B_h the difference between the value of $g_h/(\mu_G\rho_G u_G/x)^{\frac{1}{2}}$ for $T_S/T_G = 1.09$ and that for $T_S/T_G = 0.8$ amounts to less than 1%. Hence the comparison is valid. It is interesting to know that similarly good agreement was also obtained between the experimental results of Tewfik et al [E40] and the theoretical prediction of Baron and Scott [S41] for helium injection into an air stream at a plane stagnation region. If the analyses of Sparrow et al [S52] may be used as a guide, then when the reciprocal effects of thermal diffusion and diffusional conduction were taken into account the curve of Baron and Scott would lie somewhat (a few percent) below their corresponding curve for no thermal diffusional effects. Even so, the agreement would still be quite satisfactory.

With hydrogen injection. Inspection of fig. 6.4-19 shows that all the experimental points lie some 10% above the analysis of

Sparrow et al [S53] , which has taken into account the full thermal diffusional effects. At small blowing rates the experimental results seem to indicate a slight tendency for g_h to increase with B_h. This may again be due to the high thermal conductivity of hydrogen (approximately 7 times that of air) as has been explained in the last paragraph in connection with helium-injection results. At large blowing rates $g_h/(\mu_G \rho_G u_G/x)^{1/2}$ decreases with increasing B_h; the rate of decrease is more rapid than that for helium injection. Once again somewhat better agreement is observed between the experimental data and the theoretical analysis that does not take into account the coupling effects.

From the foregoing comparison it appears that the use of $(T_{S,ad} - T_S)$ in the definition of g_h is quite successful in accounting for the effects on the conductance g_h of thermal diffusion and the coupling between diffusion and heat conduction.

6.4.45 Carbon-dioxide and "Arcton-13" ($CClF_3$) injections

The results with injection of light gases (helium and hydrogen) have been presented and discussed in section 6.4.44. In this section the results for injection of the heavier gases, viz. carbon-dioxide and "Arcton-13" (commonly known as "Freon-13" in the U.S.A.) are presented. It may perhaps be helpful in later discussions to bear in mind that the thermal diffusion factor α_T for both He-air and H_2-air mixtures are negative; and those for CO_2-air and $CClF_3$-air are both positive but are much smaller in magnitude than those for the He-air and H_2-air mixtures. Reference may be made to fig. 2.7-1

for more information on α_T for the various mixtures.

Adiabatic surface temperature

Plots of $\dot{q}''_S$ versus $(T_G - T_S)$ are displayed in figs. 6.4-20a to 6.4-20d for carbon-dioxide injection and in fig. 6.4-21 for "Arcton-13" injection. As may be seen, in both cases the mean curves through the experimental points cut the $\dot{q}''_S = 0$ line at points on the right hand side of the origin (0,0). Thus for these binary boundary-layers the adiabatic surface temperature $T_{S,ad}$ is less than the main stream temperature T_G; this contrasts with helium and hydrogen injection, in which $T_{S,ad}$ is greater than T_G.

Values of $(T_{S,ad} - T_G)$ and corresponding values of $\dot{m}''/(\mu_G \rho_G u_G / x)^{1/2}$ are contained in Table 6.4-6 and plotted in fig. 6.4-22 for carbon-dioxide injection and in fig. 6.4-23 for "Arcton-13" injection. The values of $(T_{S,ad} - T_G)$ are obtained from interpolation of the $\dot{q}''_S \sim (T_G - T_S)$ curves in figs. 6.4-20 and 6.4-21, where it is seen that the scatter of the CO_2 injection results is quite large compared with the difference between $T_{S,ad}$ and T_G; for "Arcton-13" the scatter is slightly smaller.

In the case of carbon-dioxide injection, values of $(T_{S,ad} - T_G)$ are of the same order of magnitude as the uncertainty in the interpolation procedure. Hence it is not altogether surprising that no definite trend of the variation of $(T_{S,ad} - T_G)$ with $\dot{m}''/(\mu_G \rho_G u_G / x)^{1/2}$ can be detected in fig. 6.4-22. However, it should be borne in mind that $(T_{S,ad} - T_G)$ was only in the order of 1% of the main-stream absolute temperature; this may be seen more clearly from a plot of $-(T_{S,ad} - T_G)/T_G$ versus $\dot{m}''/(\mu_G \rho_G u_G / x)^{1/2}$ in fig. 6.4-24. The value of

T_G in the denominator used was the mean value for each mass-transfer rate and was approximately 560°R. Compared with the theoretical curve of Sparrow et al [S53] for a T_G of 535°R the experimental data tend to lie below it; however, they definitely show the same order of magnitude and the same sign in the deviation of $T_{S,ad}$ from T_G, as predicted by Sparrow et al. On this basis the agreement between measurements and the theory is satisfactory.

For "Arcton-13" injection the only theoretical analysis available is that of Baron [S51] for T_G = 1360°R. In the present measurements the mean value of T_G was 557°R. Thus it is not unexpected that plotted in the form of $-(T_{S,ad} - T_G)$ vs. $\dot{m}''/(\mu_G \rho_G u_G/x)^{1/2}$, fig. 6.4-23, Baron's curve lies well above the experimental data. Plotted in the dimensionless form of $-(T_{S,ad} - T_G)/T_G$ versus $\dot{m}''/(\mu_G \rho_G u_G/x)^{1/2}$ in fig. 6.4-25, the discrepancy is somewhat smaller; this is expected as in this form the influence of T_G is smaller. Though the measurements show roughly the same trend in the variation of $-(T_{S,ad} - T_G)/T_G$ with $\dot{m}''/(\mu_G \rho_G u_G/x)^{1/2}$ as Baron's prediction, no satisfactory quantitative agreement is obtained. Gollnick [E15] experimented with "Freon-13" injection in a small region around the stagnation point of a hemisphere in a flow with free-stream Mach number 8.07, and obtained results of $-(T_{S,ad} - T_G)/T_G$ under conditions closely resembling those used in Baron's analysis; the agreement between his measurements and Baron's prediction was good. This seems to suggest that the deviation between Baron's analysis and the present measurements is due to the difference in main stream temperature level.

Heat-transfer results

The heat-transfer results in the form of $g_h/(\mu_G \rho_G u_G/x)^{1/2}$ versus B_h are plotted in fig. 6.4-26 for carbon-dioxide injection and in fig. 6.4-27 for "Arcton-13" injection. For comparison purposes the corresponding theoretical curves as well as the constant-property one are also plotted on the graphs.

For carbon-dioxide injection, it can be seen in fig. 6.4-26 that the theoretical curves for constant-properties and carbon-dioxide injection are close together. At large values of B_h the CO_2 curve tends to lie above the constant-property one. With the exception of one, all the experimental points lie above the constant-property curve. The small range of the theoretical CO_2 curve does not allow detailed comparison with the measurements; it appears that at large B_h values the agreement is fairly good. However, the scatter of the experimental results is quite large; this is undoubtedly a reflection of the relative inaccuracy in the determination of the $(T_{S,ad} - T_G)$ quantity. For though the "measured" value of $T_{S,ad}$ was only between 0 and 5°F lower than the mean stream temperature T_G, an error of the order of 1 or 2°F will be proportionally transferred to g_h through the quantity $(T_{S,ad} - T_S)$; this may be seen from equation (6.4-9). In spite of the fairly large scatter, inspection of fig. 6.4-26 shows that the mean curve through the experimental points lies somewhat above the constant-property curve; and that the conductance g_h decreases with increasing blowing rates, i.e. increasing B_h, the rate of decrease being about the same as that for the constant-property case.

The results for "Arcton-13" injection are displayed in fig.

6.4-27. Compared with Baron's analysis the experimental results show satisfactory agreement. This contrasts with the poor agreement in the results for the adiabatic surface temperature; this is due to the relatively small influence of T_G on $g_h/(\mu_G\rho_G u_G/x)^{1/2}$.

6.4.46 General discussions of the results

Inspection of plots of $g_h/(\mu_G\rho_G u_G/x)^{1/2}$ vs. B_h for the various gas injections in figs. 6.4-9, -11, -18, -19, -26 and -27 shows that for all cases the conductance g_h decreases with increasing B_h; the rate of decrease is the highest with hydrogen injection.

Analyses which do not include thermal diffusion and diffusional conduction suggest that compared with air hydrogen and helium are by far the better coolant; this is mainly because of their relatively high specific heat (about 5 times that of air for helium and about 14 times that of air for hydrogen). However, the thermal diffusional effects in an actual hydrogen-air or helium-air boundary layer may "reduce" the attractiveness of either hydrogen or helium as a transpiration-coolant. This may be demonstrated below.

The plot of $g_h/(\mu_G\rho_G u_G/x)^{1/2}$ vs. B_h for hydrogen injection in fig. 6.4-19 or helium injection in fig. 6.4-18 shows that the conductance g_h is only slightly affected by the thermal diffusional effects; that is, the slopes of the curves $\dot{q}''_S$ vs. $(T_G - T_S)$ for the same mass-transfer rate are approximately equal as shown in the sketch below. The

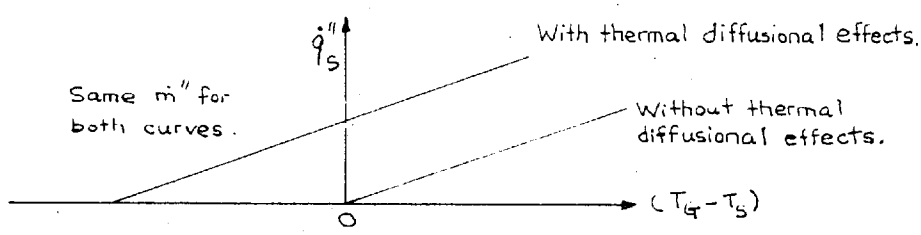

difference between the curves for the two situations is a shift to the left for the one with thermal diffusional effects. It is easily seen that for the same mass-transfer rate and the same "thermal potential" $(T_G - T_S)$ the thermal diffusional effects cause an increase in the heat-flux to the surface, with a corresponding decrease in the effectiveness of the gas as a coolant.

Actual variations of $\dot{q}''_S$ with $(T_G - T_S)$ are plotted in fig. 6.4-28 for the same mass blowing rate of $\dot{m}''/(\mu_G \rho_G u_G / x)^{\frac{1}{2}} = 0.35$ with injections of hydrogen, helium, air and carbon-dioxide; the solid part of the curves are obtained from interpolation of the experimental results, and the dashed parts are extrapolations from the solid curves. The figure shows clearly that in the range of small $(T_G - T_S)$, i.e. T_S/T_G close to unity, for the same thermal potential $(T_G - T_S)$ both air and carbon-dioxide injections result in lower heat-transfer rates than hydrogen or helium injection. However, as $(T_G - T_S)$ increases, ie. T_S/T_G decreases, both the curves for hydrogen and helium injection tend to lie below those of air and carbon-dioxide injections. In fact, at this particular mass injection rate the hydrogen curve and helium curve cross the air curve respectively at $(T_G - T_S) \approx 145^{\circ}F$ or $T_S/T_G \approx 0.72$ or $T_S/T_{S,ad} \approx 0.62$ and $(T_G - T_s) \approx 180^{\circ}F$ or $T_S/T_G \approx 0.48$ or $T_S/T_{S,ad} \approx 0.42$.

These confirm the deductions in section 3.2.4 that when $T_S/T_{S,ad}$ is close to unity the thermal diffusion and diffusional conduction have particularly strong influence on the surface heat-flux $\dot{q}''_S$; and that when the surface is highly cooled their influences are proportionally smaller and both hydrogen and helium are still

effective transpiration-coolants.

To test the correlation method developed in section 4.3, in fig. 6.4-29 are plotted all the experimental heat-transfer results in the form of $[g_h/(\mu_G \rho_G u_G/x)^{1/2}] \cdot F_{g_h,T}$ vs. $B_h \cdot F_{B_h,M}$; the appropriate values of $F_{g_h,T}$ and $F_{B_h,M}$ are those for $\beta = 1/2$ in Tables 4.3-1 and 4.3-2. As can be seen all the data cluster around the constant-property curve, confirming the reliability of the correlation.

CHAPTER 7 CONCLUSIONS BASED ON EXPERIMENTAL RESULTS

An axi-symmetric stagnation-flow was satisfactorily created by impinging an air jet onto a flat plate held normal to the jet axis. Although a turbulence intensity of some 5% was measured in the main stream flow near the stagnation point, the heat-transfer measurements on a solid plate by a transient method confirmed the existence of a laminar boundary layer over the stagnation-flow region. The measured heat-transfer rates there agree well, within 7%, with the theoretical value for zero turbulence intensity, suggesting the slight influence of main stream turbulence on the heat-transfer rates; this is roughly in accord with the findings of Buyuktur et al [E6] , but strongly disagree with those expected from the findings of Kestin et al [E20].

The heat-transfer measurements with injection into the air stream of : hydrogen, helium, air, nitrogen, carbon-dioxide and "Arcton-13", agree well with theoretical predictions. It is seen that reduction in heat-transfer rates can be achieved by mass injection.

Large differences (up to $+102^{\circ}F$) between the adiabatic-surface temperature and the stagnation temperature of the main stream with hydrogen and helium injections were observed. The corresponding differences for carbon-dioxide and "Arcton-13" injections are very much smaller (maximum $-20.5^{\circ}F$) and are of opposite nature to those for hydrogen and helium injections.

A temperature difference of up to $102^{\circ}F$ could not possibly be due to errors in measurements, nor could it be attributed to aerodynamic heating as the maximum jet Mach number was only about 0.1. It must

therefore be actuated by some other mechanism. The close agreement between the measured adiabatic wall temperatures and those predicted when the reciprocal effects of thermal diffusion and the coupling between diffusion nnd heat conduction are taken into account points out that these effects are responsible for the observed temperature differences. These temperature differences are seen to increase with mass injection rates.

Good agreement bwtween the experimental results and theories which do not take into account of any coupling effects confirms the small influence of these thermal-diffusional effects on the enthalpy conductance g_h defined in equation (3.2.4-2). However, the results emphasize their importance in experimental measurements close to the adiabatic surface temperature; under these conditions, a light gas with high specific heat (e.g. helium or hydrogen) may not be a more effective transpiration-coolant than a heavier gas with lower specific heat (e.g. carbon-di oxide). Nevertheless, it is expected that for a highly cooled surface the light gas is still the more effective coolant.

The experimental data also confirm the reliability of the correlation method developed earlier in the present work.

CHAPTER 8 SUGGESTIONS FOR FUTURE WORK

(I) From the survey of the theoretical solutions it is clear that there is a need for more theoretical solutions with the effects of thermal diffusion and the coupling between diffusion and heat conduction included, especially for the flat plate case.

Some values of $F_{B,M}(M_G/M_T, \beta)$ have been determined from a rather limited number of solutions; when more solutions become availabee , these may have to be re-determined.

Flows over objects of arbitrary shape can usually be treated as a series of "equivalent wedge" flows. For these calculations it is necessary to have "similar" solutions for a comprehensive range of the pressure gradient parameter β . So far, all the solutions for $B>0$ are for β values of 0, 1/2 and 1. It will be useful to obtain soltuions for β values other than these, so that the present correlation method can be extended.

(II) The jet-on-plate system has been proved to be a simple and reliable means of creating an axi-symmetric stagnation-flow. This arrangement should be fully exploited to obtain more experimental data. At present, few experimental data with combution in the boundary layer are availabe, and studies in this drrection will be of great importance. For this purpose, it appears that the jet-on-plate system is an ideal arrangement.